EPA-650/4-75-026

June 1975

Environmental Monitoring Series

MATHEMATICAL MODELING OF SIMULATED PHOTOCHEMICAL SMOG

EPA-650/4-75-026

MATHEMATICAL MODELING OF SIMULATED PHOTOCHEMICAL SMOG

by

Paul A. Durbin, Thomas A. Hecht, and Gary Z. Whitten

Systems Applications, Inc.
950 Northgate Drive
San Rafael, California 94903

Contract No. 68-02-0580
ROAP No. 21AKC - 23
Program Element No. 1A1008

EPA Project Officer: Marcia C. Dodge

Chemistry and Physics Laboratory
National Environmental Research Center
Research Triangle Park, North Carolina 27711

Prepared for

U.S. ENVIRONMENTAL PROTECTION AGENCY
Office of Research and Development
Washington, D. C. 20460

June 1975

EPA REVIEW NOTICE

This report has been reviewed by the National Environmental Research Center - Research Triangle Park, Office of Research and Development, EPA, and approved for publication. Approval does not signify that the contents necessarily reflect the views and policies of the Environmental Protection Agency, nor does mention of trade names or commercial products constitute endorsement or recommendation for use.

RESEARCH REPORTING SERIES

Research reports of the Office of Research and Development, U.S. Environmental Protection Agency, have been grouped into series. These broad categories were established to facilitate further development and application of environmental technology. Elimination of traditional grouping was consciously planned to foster technology transfer and maximum interface in related fields. These series are:

1. ENVIRONMENTAL HEALTH EFFECTS RESEARCH
2. ENVIRONMENTAL PROTECTION TECHNOLOGY
3. ECOLOGICAL RESEARCH
4. ENVIRONMENTAL MONITORING
5. SOCIOECONOMIC ENVIRONMENTAL STUDIES
6. SCIENTIFIC AND TECHNICAL ASSESSMENT REPORTS
9. MISCELLANEOUS

This report has been assigned to the ENVIRONMENTAL MONITORING series. This series describes research conducted to develop new or improved methods and instrumentation for the identification and quantification of environmental pollutants at the lowest conceivably significant concentrations. It also includes studies to determine the ambient concentrations of pollutants in the environment and/or the variance of pollutants as a function of time or meteorological factors.

This document is available to the public for sale through the National Technical Information Service, Springfield, Virginia 22161.

Publication No. EPA-650/4-75-026

PREFACE

As part of its program to clarify the roles of organic compounds and oxides of nitrogen in the production of photochemical smog, the U.S. Environmental Protection Agency (EPA) is supporting the study of irradiation-induced air pollution in environmental chambers and the determination of the rate constants and mechanisms of elementary reactions thought to be important in smog formation. To complement this experimental effort, the EPA is sponsoring SAI's work on the development of a chemical kinetic mechanism for photochemical smog formation. This mechanism, incorporating experimentally measured rate constants, is presently being compared with data obtained from smog chamber experiments. Ultimately, the mechanism should be capable of predicting the kinetics of the chemical transformations that take place in photochemical smog. Our initial efforts to formulate and evaluate a kinetic mechanism for photochemical smog formation were summarized in a detailed planning document (Seinfeld et al., 1973), in a 1973 final report (Hecht et al., 1973), and in a 1974 final report (Hecht et al., 1974a).

ABSTRACT

This report deals with the continued development and testing of a kinetic mechanism for photochemical smog formation. An "explicit" mechanism is developed and validated on smog chamber data taken at the University of California at Riverside, Battelle, and the National Air Pollution Control Association. After critical review of recent observations of reactions believed to occur in photochemical smog, a mechanism is developed for each of the following systems: propylene-NO_x, butane-NO_x, propylene-SO_2-NO_x, and toluene-NO_x. In addition, the report demonstrates that some chamber effects, such as photolysis and surface reactions, potentially play a critical role in smog chamber experiments. Finally, the report discusses the application of kinetic simulation to a study of hydrocarbon reactivity and ozone production in smog systems.

CONTENTS

ILLUSTRATIONS

TABLES

I INTRODUCTION

The problem of photochemical air pollution has received considerable attention from scientists, legislators, and the public during the past two decades. Although the problem was originally manifested in Los Angeles, it has become increasingly evident in other urban and even nonurban areas and is worthy of widespread concern. As its name indicates, a fundamental characteristic of photochemical air pollution is the role played by sunlight-initiated chemical transformations. Primary pollutants are often hazardous themselves; however, these secondary chemical processes greatly exacerbate the problem. They lead to the production of phytotoxicants, lacrymators, and carcinogens.

The present document reports on the continuation of an ongoing research effort to isolate and model the complex chemical reactions that occur in polluted atmospheres. This effort is aimed at producing a photochemical kinetic mechanism for smog formation having sufficiently accurate kinetics to provide realistic predictions of pollution production while, at the same time, being simple enough for practical use in large computer models of urban airsheds. Past efforts (Hecht et al., 1973; Hecht et al., 1974a) toward these ends have resulted in the development of a "generalized" kinetic mechanism. The generalized mechanism has proved to have great utility, making urban airshed modeling feasible (Reynolds et al., 1974). However, in the present report, a digression from the generalized approach has been made. To take full advantage of smog chamber data and kinetic studies, we employed an "explicit" mechanism. The explicit approach and the reasons for its incorporation are discussed below, after a review of some background information. A final topic, the application of the kinetic mechanism to an investigation of hydrocarbon reactivity, is discussed at the end of this introduction.

A. SMOG CHAMBER SIMULATIONS AND ELEMENTARY REACTION KINETICS

Smog chamber investigations and elementary kinetics studies provide the basic inputs to the present kinetic mechanism. In smog chamber studies, clean air and pollutants (usually NO, NO_2, and a hydrocarbon) are irradiated in a reactor. Measurements of reactant and product concentrations as a function of time provide smog profiles, which the kinetic mechanism should reproduce. These profiles constitute quantitative and qualitative descriptions of the macroscopic features of smog. Thus, the conversion of NO to NO_2, the oxidation of hydrocarbons, and the production of oxidants, as observed in the atmosphere, are reproduced in a controlled laboratory environment. But smog chamber studies cannot provide a knowledge of the microscopic features of smog formation. Independently, kineticists study elementary reactions that could be important in this process.

Kinetics studies are performed to elucidate the rates and mechanisms of particular reactions that occur within the overall process of smog formation. These studies differ from smog chamber studies in that the reactants and other conditions are carefully chosen to isolate or emphasize the reactions of interest. The observed variations in reactant and product concentrations with time are used to formulate rate equations and rate constants. If complicating reactions are absent or well characterized, these rate equations and constants have universal validity. Mechanistic information comes from the rate expression as well as from observed reaction products.

Ideally, a kinetic mechanism would be simply the assemblage of results from kinetic studies of all reactions that occur. In reality, not all of the reactions that could occur have been studied, and often orders of magnitude of uncertainty may be associated with those that have been studied. In addition, the number of possible reactions in smog is very large. Hence, a complete mechanism is neither practical, because it would include an enormous number of reactions, nor feasible, because the needed kinetic information is unavailable. The best one can do to obtain a closed system of chemical equations and rate constants is to use available kinetic information and methods

for estimating other information, to draw analogies, and to make other simplifying assumptions. The kinetic mechanism that results may be a fairly accurate, albeit simplified, description of reality. The system of equations constituting the current mechanism has largely been discussed previously (Hecht and Seinfeld, 1972; Hecht et al., 1974b). However, several changes and additions have been made since last year's report. These new features, and the kinetic studies supporting them, are reviewed in Chapter II of the present report.

In addition to the reactions characterized by universal kinetic expressions, there are processes, both physical and chemical, occurring in smog chambers that are peculiar to a given chamber. These chamber effects include surface-catalyzed reactions, adsorption and desorption of chemicals, dilution due to sampling, inhomogeneous concentrations, and spatial and spectral variability of light sources. Of the surface reactions, probably the most important is the heterogeneous formation of nitrous and nitric acid. The heterogeneous production of HNO_x is investigated in Chapter II. A possible spectral variation of the light source used in smog chamber simulations done at the University of California at Riverside is also considered from a theoretical standpoint. The results show the critical influence of surface and light properties on smog profiles and point to a need for more detailed characterizations of smog chambers.

In Chapter III, predictions of smog profiles made by numerical simulation are compared with experimental data. To model the smog chamber results completely, we had to incorporate some of the chamber effects mentioned above. The techniques for doing so are described in Chapter III.

B. EXPLICIT MECHANISTIC APPROACH

The most straightforward approach to formulating a kinetic mechanism is to assemble the most important reactions that occur. The mechanism's complexity is then dictated by the criterion for "important." A technique described by Hecht et al. (1974b) even further simplifies the formulation. In this technique, groups of reactions are "lumped" into single reactions; these reactions are then combined to form a generalized mechanism. But the lumping

approach introduces nonphysical lumped rate constants, stoichiometric coefficients, and chemical species. Because of this last feature, the prediction of detailed product yields is not feasible, and because of the first two, kinetic information cannot be used directly. Thus, we used the classical, explicit approach instead, to take advantage of recent kinetic studies and the full range of product measurements available.

Formulating the explicit mechanism involves simply expanding the lumped reactions of the generalized mechanism. Conversely, reformulation of a generalized mechanism involves contracting the explicit mechanism. Thus, in the present approach, uncertainties associated with the lumping procedure have been eliminated, while a kinship with the generalized mechanism has been retained. After validation, the explicit mechanism can then serve as a basis for rederiving a generalized mechanism and for checking the accuracy of lumping techniques. We should emphasize that the explicit approach is an interim step. We hope that it will serve to further clarify smog kinetics and thus to lay the groundwork for the more practical generalized approach.

A review of the reactions and rate constants used in the mechanisms contained herein appears in Tables 1 and 2. The lumped format (i.e., use of the R group) was used to represent a class of reactions, which appear explicitly in the later mechanisms (Chapter III).

C. HYDROCARBON REACTIVITY

Pollution control strategists must know the reactivity of various hydrocarbons to predict the potential impact of different emissions sources. The conceptualization of reactivity can, however, take various forms. Correspondingly, there are many ways of quantifying reactivity in smog systems. Probably the most obvious and commonplace measure of reactivity is the time required for NO_2 to reach its peak concentration, because the NO_2 peak is a distinctive feature of smog profiles. Many other measures have appeared in

Table 1

SUMMARY OF REACTIONS

I. Inorganic H-N-O Compound Chemistry

A. The NO_2-NO-O_3 Cycle

1. $NO_2 + h\nu \rightarrow NO + O$
2. $O + O_2 + M \rightarrow O_3 + M$
3. $O_3 + NO \rightarrow NO_2 + O_2$

B. Other NO_x Chemistry

4. $NO_2 + O \rightarrow NO + O_2$
5. $NO_2 + O_3 \rightarrow NO_3 + O_2$
6. $NO_3 + NO \rightarrow 2NO_2$
7. $NO_3 + NO_2 \rightarrow N_2O_5$
8. $N_2O_5 \xrightarrow{M} NO_3 + NO_2$
9. $H_2O + N_2O_5 \xrightarrow{\text{surface}} 2HNO_3$

C. HNO_2 Chemistry

10. $NO + NO_2 + 2H_2O \xrightarrow{\text{surface}} 2HNO_2 + H_2O$
11. $2HNO_2 \xrightarrow{\text{surface}} NO + NO_2 + H_2O$
12. $HNO_2 + h\nu \rightarrow NO + OH\cdot$

D. $OH\cdot$ and $HO_2\cdot$ Reactions with NO_x

13. $OH\cdot + NO \xrightarrow{M} HNO_2$
14. $OH\cdot + NO_2 \xrightarrow{M} HNO_3$
15. $HO_2\cdot + NO \rightarrow NO_2 + OH\cdot$

II. O_3 Inorganic Chemistry

16. $O_3 + h\nu \rightarrow O_2 + O(^3P)$
17. $O_3 + h\nu \rightarrow O_2 + O(^1D)$

18. $O(^1D) + M \rightarrow O(^3P)$

19. $O(^1D) + H_2O \rightarrow 2OH\cdot$

20. $O_3 + OH\cdot \rightarrow HO_2\cdot + O_2$

21. $O_3 + HO_2\cdot \rightarrow OH\cdot + 2O_2$

22. $O_3 \xrightarrow{\text{surface}}$ products

III. Organic Oxidation Reactions

A. Butane

23. $C_4H_{10} + O \xrightarrow{O_2} RO_2\cdot + OH\cdot$

24. $C_4H_{10} + OH\cdot \xrightarrow{O_2} n\text{-}RO_2\cdot + H_2O$

25. $C_4H_{10} + OH\cdot \xrightarrow{O_2} s\text{-}RO_2\cdot + H_2O$

B. Propylene

26. $C_3H_6 + OH\cdot \rightarrow n\text{-}RO\cdot$

27. $C_3H_6 + OH\cdot \rightarrow s\text{-}RO\cdot$

28. $C_3H_6 + O_3 \xrightarrow{O_2} CH_3CHO + HO_2\cdot + OH\cdot + CO$

29. $C_3H_6 + O_3 \xrightarrow{O_2} H_2CO + CH_3C(O)O_2\cdot + OH\cdot$

30. $C_3H_6 + O \xrightarrow{O_2} RO_2\cdot + RC(O)O_2\cdot$

31. $C_3H_6 + O \xrightarrow{O_2} RO_2\cdot + HO_2\cdot + CO$

C. Aldehydes

32. $RCHO + OH\cdot \xrightarrow{O_2} RC(O)O_2\cdot + H_2O$

D. Toluene

33. $C_6H_5CH_3 + OH\cdot \xrightarrow{O_2} C_6H_5CH_2O_2\cdot + H_2O$

34. $C_6H_5CH_3 + OH\cdot \xrightarrow{O_2} C_6H_4(CH_3)(OH) + HO_2\cdot$

34a. $C_6H_5CH_3 + OH\cdot \xrightarrow{O_2} C_6H_5OH + CH_3O_2\cdot$

E. Organic Radicals

35. $RO\cdot \xrightarrow{O_2} RO_2\cdot + H_2CO$

36. $RO\cdot + O_2 \longrightarrow ALD + HO_2\cdot$

IV. Other Photolysis Reactions

37. $H_2O_2 + h\nu \rightarrow 2OH\cdot$

38. $RCHO + h\nu \xrightarrow{O_2} RO_2\cdot + CO + HO_2\cdot$

39. $RCHO + h\nu \rightarrow \text{paraffin} + CO$

40. $H_2CO + h\nu \xrightarrow{2O_2} CO + 2HO_2\cdot$

41. $H_2CO + h\nu \rightarrow H_2 + CO$

V. Reactions of Organic Free Radicals with NO_x

A. NO Oxidation

42. $RO_2\cdot + NO \rightarrow RO\cdot + NO_2$

43. $RC(O)O_2\cdot + NO \xrightarrow{O_2} RO_2\cdot + CO_2 + NO_2$

B. PAN Chemistry

44. $RC(O)O_2\cdot + NO_2 \rightarrow RC(O)O_2NO_2$ (PAN)

45. $PAN \xrightarrow[O_2]{M} NO_3 + CO_2 + RO_2\cdot$

VI. Radical-radical Recombination Reactions

46. $HO_2\cdot + HO_2\cdot \rightarrow H_2O_2 + O_2$

47. $HO_2\cdot + RO_2\cdot \rightarrow RO_2H + O_2$

48. $RC(O)O_2\cdot + HO_2\cdot \rightarrow RC(O)O_2H$

VII. SO_2 Chemistry

A. SO_2 Oxidation

49. $NO_3 + SO_2 \rightarrow SO_3 + NO_2$

50. $HO_2\cdot + SO_2 \rightarrow SO_3 + OH\cdot$

51. $RO_2\cdot + SO_2 \rightarrow SO_3 + RO\cdot$

52. $RC(O)O_2\cdot + SO_2 \xrightarrow{O_2} SO_3 + CO_2 + RO_2\cdot$

53. $SO_2 + OH\cdot \xrightarrow{O_2} HSO_5\cdot$

54. $HSO_5\cdot + NO \rightarrow HSO_4\cdot + NO_2$

55. $HSO_4\cdot + HO_2\cdot \rightarrow H_2SO_4 + O_2$

56. $HSO_4\cdot + NO_2 \xrightarrow{H_2O} H_2SO_4 + HNO_3$

Table 2

SUMMARY OF RATE CONSTANTS
(ppm^{-1} min^{-1} unless noted)

Reaction Number	Rate Constant			
	Garvin and Hampson (1974)	Uncertainty Factor	This Study[a]	Others
1			Experimental	
2 (ppm^{-2} min^{-1})	2.08×10^{-5}	1.2	2.08×10^{-5}	2.04×10^{-5} (Wu and Niki, 1975)
3	25.2	1.3	25.2	27.0 (Wu and Niki, 1975)
4	1.34×10^{4}	1.2	1.34×10^{4}	1.39×10^{4} (Wu and Niki, 1975)
5	5.0×10^{-2}	1.3	5.0×10^{-2}	6.8×10^{-2} (Wu and Niki, 1975)
6	1.3×10^{4}	5.0	1.3×10^{4}	1.5×10^{4} (Wu and Niki, 1975)
7	5.6×10^{3}	2.5	5.6×10^{3}	4.5×10^{3} (Wu and Niki, 1975)
8 (min^{-1})	21.9	2.0	24.0	$k_8/k_9 = 4.2 \times 10^{-3}$ (Benson, 1968)[b]
9	$< 1.5 \times 10^{-5}$[c]		5.0×10^{-6}	
10 (ppm^{-3} min^{-3})	$< 10^{-13}$[c]		1.3×10^{-11}	$10^{-10} - 10^{-12}$ (Noch et al., 1974)
11			2.6×10^{-1}	$k_{10}\,H_2O/k_{11} = 9.7 \times 10^{-7}$ (Demerjian et al., 1974)
12			Experimental	
13	2.95×10^{3}	2.0	3.0×10^{3}	8.9×10^{3} (Cox, 1974)
14	1.2×10^{4}	2.5	1.0×10^{4}	
15	2.95×10^{2}	3.2	8.0×10^{2}	$\sim 1.2 \times 10^{3}$ (Mabey and Hendry, 1974)
16			Experimental	
17			Experimental	

Reaction Number	Rate Constant			
	Garvin and Hampson (1974)	Uncertainty Factor	This Study[a]	Others
18	8.6×10^4[d]	1.4	8.6×10^4	
19	5.17×10^5	1.3	5.1×10^5	
20	8.71×10^6	2.0	8.7×10^1	
21	2.4	2.0	2.4	
22			Experimental	
23			64.0	12.6 (Johnson et al., 1970)
24, 25	3.47×10^3	1.2	3.4×10^3	
26, 27	2.14×10^4	1.2	2.5×10^4	2.5×10^4 (Morris et al., 1971)
28, 29	0.02		0.02	0.026 (Becker et al., 1974)
30, 31	5.3×10^3	1.2	5.3×10^3	
32 RCHO; R=0,1			2.1×10^4	2.3×10^4 (Morris and Niki, 1971; Morris et al., 1971)
RCHO; R=2,3			4.5×10^4	4.6×10^4 (Morris and Niki, 1971)
33,34			9.2×10^3	9.0×10^3 (Davis, 1974)
35 (min^{-1})			$0.6 - 1.3 \times 10^4$[e]	$0.8 - 12.0 \times 10^4$ (Batt et al., 1974)
36	$\sim 4.4 \times 10^{-3}$		$0.04 - 0.2$[e]	~ 0.8 (Mendenhall et al., 1974)[f]
37-41			Experimental	
42, 43			10^3 (estimate)	
44			3×10^2 (estimate)	
45			3×10^{-3}	
46	8.5×10^3	2.0	6.0×10^3	
47, 48			3×10^3 ($1/2\ k_{44}$)	
49			14.0	< 14.7 (Davis, 1974)

Reaction Number	Rate Constant			
	Garvin and Hampson (1974)	Uncertainty Factor	This Study[a]	Others
50			1.3	1.35 (Davis, 1974)
51, 52			1.5 (estimate)	
53			9×10^2	1.35×10^3 (Davis, 1974)
54			8×10^2 (estimate)	
55			9×10^3 (3/2 k_{44})	
56			1×10^4 (estimate)	

[a] At 303°K

[b] Calculated using $K_{eq} \sim \exp(-\Delta G_{298}/RT)$, ΔG from Benson (1968)

[c] Surface-dependent

[d] Combination of values for M = O_2 and M = N_2

[e] Depends on carbon skeleton

[f] Combination of BuO· and MeO· data

the literature. A review of these reactivity indices and an evaluation of the properties of some of them appear in Chapter IV of this report.

Ultimately, reactivity should be related to the production of harmful components of photochemical air pollution. For this reason, we investigated the relationship between reactivity measures and ozone production. In this report, ozone yield is shown to be relatively insensitive to reactivity for a group of olefins, though it does depend on initial NO_x and hydrocarbon concentrations.

An important aspect of photochemical smog production in the atmosphere is its dynamic behavior. An understanding of the interaction of the time scales for reaction, transport, and dispersion is necessary to master the pollution problem. The dynamics of smog formation are, to a significant extent, determined by the time required for NO_2 to reach its peak. Chapter IV investigates this interrelationship.

II CHEMICAL KINETICS

A. INORGANIC CHEMISTRY

An excellent review of inorganic (and some organic) reactions occurring in the stratosphere has been prepared by Garvin and Hampson (1974). A majority of the inorganic reactions thought to occur in polluted atmospheres can also be found in that review. The rate constant recommendations made by Garvin and Hampson have generally been adhered to in the present study. The few exceptions to this rule are cases where the results of more recent studies have become available or where the reactions are surface dependent. The latter set of reactions is considered below because of their possible significance (and elusiveness) in smog chamber simulations.

1. Heterogeneous HNO_2 Chemistry

Of the reactions that can take place on smog chamber walls, perhaps the most significant is the heterogeneous formation of HNO_2:

$$2H_2O + NO + NO_2 \xrightarrow{\text{surface}} 2HNO_2 + H_2O \qquad (10)^*$$

The occurrence of this reaction following the introduction of NO_x reactants could produce significant amounts of HNO_2. OH radicals produced by HNO_2 photolysis play a major role early in the reaction. Thus, the occurrence of Reaction (10) can have a profound effect on the length of the induction period. It is important to note that Reaction (10) is a thermal reaction and that it can occur in the approximately 45 minute dark mixing time allowed at the beginning of Riverside experiments. During this time, Reaction (10) will compete with Reaction (11):

* This report uses two numbering systems. Chemical reactions used in modeling have simple Arabic numbers taken from Table 1 and previous work (Hecht et al., 1974b). Other chemical reactions and mathematical equations are numbered sequentially within each chapter, e.g., (II-1), (II-2).

$$2HNO_2 \xrightarrow{\text{surface}} H_2O + NO + NO_2 \quad . \qquad (11)$$

A solution of the rate expression derived from Reactions (10) and (11) for the concentration of HNO_2 at time t is

$$[HNO_2]_t = \frac{1}{A + \frac{1}{B \tanh\left(\frac{t}{\tau'}\right)}} \qquad (II\text{-}1)$$

$$\approx [HNO_2]_{eq} \tanh\left(\frac{t}{\tau}\right) \quad ,$$

where

$$A = \frac{1}{4}\left(\frac{1}{[NO]_0} + \frac{1}{[NO_2]_0}\right) \quad ,$$

$$B = [HNO_2]_{eq}\left[1 + \left[\frac{k_{10}[H_2O]^2\left([NO]_0 - [NO_2]_0\right)^2}{16 k_{11}[NO]_0[NO_2]_0}\right]\right]^{1/2} \quad ,$$

$$\tau = \frac{(k_{eq})^{1/2}}{\left(2[NO]_0[NO_2]_0\right)^{1/2} k_{10}[H_2O]^2} \quad ,$$

$$\tau' = \left[\frac{\left([NO] - [NO_2]\right)^2\left(k_{10}[H_2O]^2\right)^2}{4} + \frac{1}{\tau^2}\right]^{-1/2} \quad ,$$

$$[HNO_2]_{eq} = \left(k_{eq}[NO]_0[NO_2]_0\right)^{1/2} \quad ,$$

$$k_{eq} = \frac{k_{10}[H_2O]^2}{k_{11}} \quad .$$

Taking $[NO]_0$ = 1.0 ppm, $[NO_2]_0$ = 0.1 ppm, $[H_2O]$ = 2 x 10^4 ppm, and k_{eq} = 1.9 x 10^{-2} gives

$$[HNO_2]_{eq} = 4.4 \times 10^{-2} \text{ ppm}$$

In their study, Noeh et al. (1974) found $k_{10} \approx 10^{-12}$ ppm^{-3} min^{-1} (we have adjusted their third-order results to fourth-order kinetics) in a quartz cylinder and $k_{10} \approx 10^{-10}$ with metal present. Garvin and Hampson report $k_{10} < 10^{-13}$ for gas phase reactions.

Taking k_{10} = 10^{-13}, 10^{-12}, 10^{-11}, and 10^{-10} ppm^{-3} min^{-1} as a representation of this range gives the following respective values of τ: τ = 5500, 550, 55, and 5.5 minutes. Thus, at t = 45 minutes, $[HNO_2]/[HNO_2]_{eq}$ = 0.008, 0.08, 0.67 and 1.0, respectively. Depending on k_{10}, the dark reaction will produce from 0.8 to 100 percent of the equilibrium concentration of HNO_2 in 45 minutes. The rate constant listed for "this study" in Table 2 leads to a time scale (τ) of 41.9 minutes (or approximately 1 hour), and to an HNO_2 concentration of 79 percent of the equilibrium value in 45 minutes. Naturally, these results depend on $[NO]_0$, $[NO_2]_0$, and the dark mixing time. In interpreting the conclusions for large k_{10}, one should realize that the approximation used in Eq. (II-1) may break down when t is on the order of τ.

Figure 1 illustrates the effect of setting k_{10} at 10^{-13}, 10^{-12}, and 10^{-10} ppm^{-3} min^{-1} (and varying k_{11} to keep k_{eq} constant) on the propylene-NO_x system. The shortening of the induction period is readily visible in the NO_2 curves. Figure 2 shows the results of setting k_{10} equal to 10^{-13} ppm^{-3} min^{-1} and introducing 0, 10, or 100 percent of the equilibrium amount of HNO_2 as an initial condition. Again, HNO_2 shortens the induction period. For both sets of figures, the experimental conditions were identical, except for the variable being studied.

It is conceivable that all the HNO_2 formed at the reactor walls does not vaporize. Inadequate cleaning of chamber walls might then allow a "memory effect" on subsequent experiments. Jaffee and Smith (1974) have experimentally demonstrated the effects of inadequate cleaning, as well as other chamber effects. The anomalous OH source observed recently in the

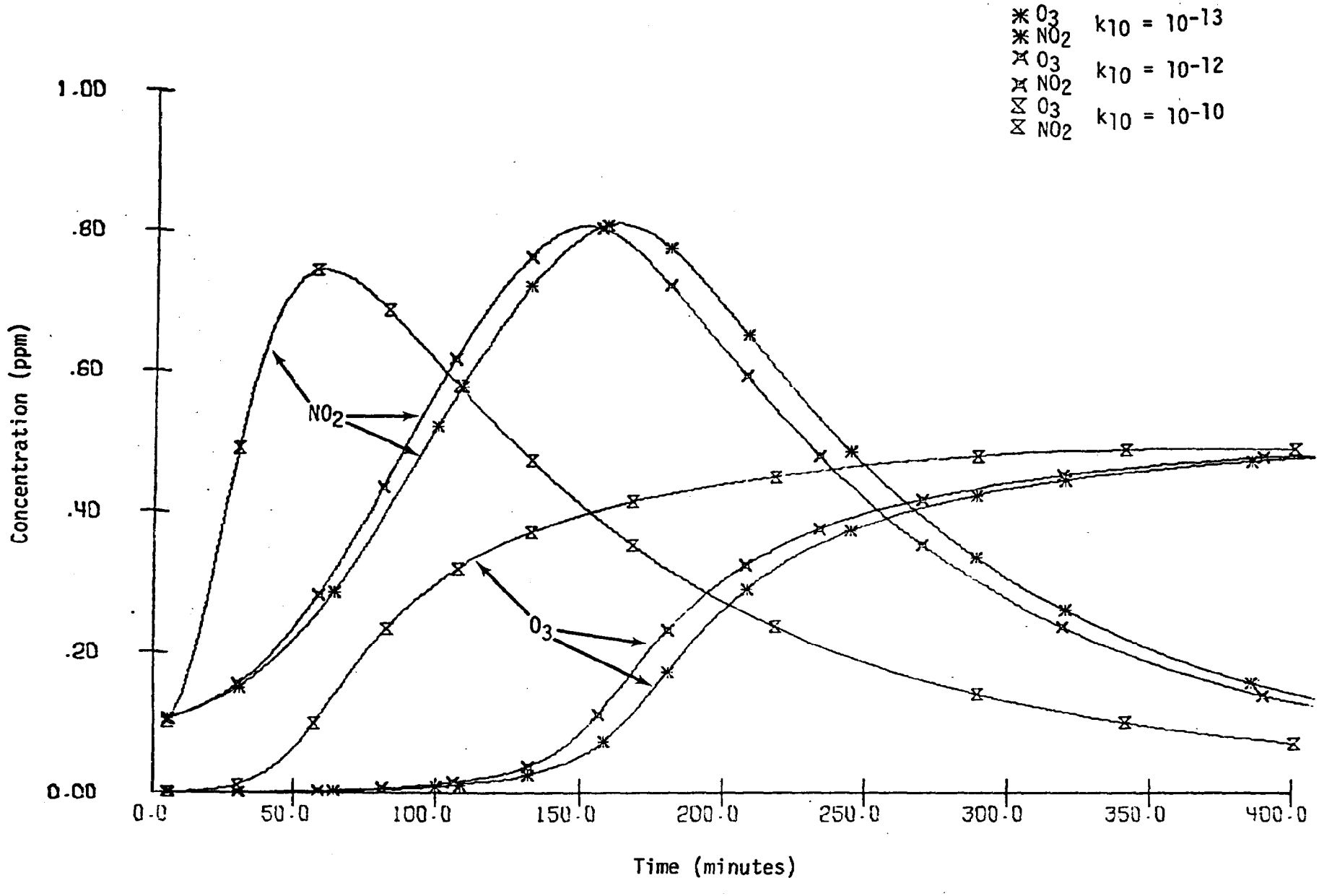

FIGURE 1. SMOG PROFILES FOR DIFFERENT VALUES OF k_{10}, THE RATE CONSTANT FOR THE REACTION $2H_2O + NO + NO_2 \rightarrow 2HNO_2 + H_2O$

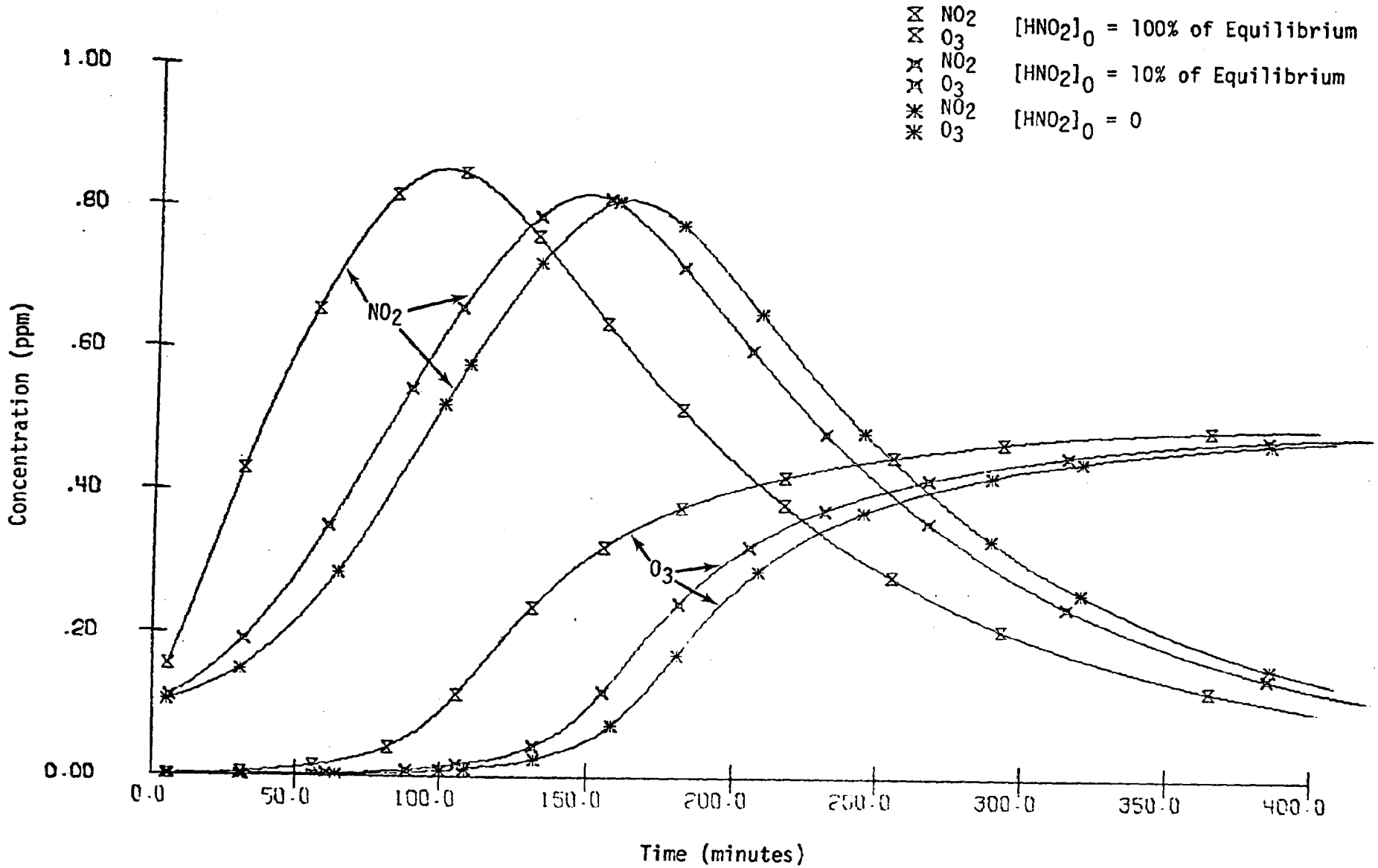

FIGURE 2. SMOG PROFILES FOR DIFFERENT INITIAL CONCENTRATIONS OF HNO_2

Riverside chamber (Winer, 1975) could be due to HNO_2 retention by the chamber walls (see Chapter III).

2. Heterogeneous HNO_3 Formation

Morris and Niki (1973) found that, for the reaction

$$N_2O_5 + H_2O \xrightarrow{\text{surface}} 2HNO_3 \qquad (9)$$

the upper limit of the rate, k_9, is 1.5×10^{-5} ppm^{-1} min^{-1} in the gas phase. They also showed that this reaction has both homogeneous and heterogeneous components. Spicer and Miller (1974) have presented evidence that the primary mode of HNO_3 production in their chamber is the heterogeneous reaction. They achieved nearly a 100 percent nitrogen balance in the gas phase and thus concluded that HNO_3 vaporizes after formation.

Because the sequence of reactions

$$NO_2 + O_3 \rightarrow NO_3 + O_2 \qquad (5)$$

$$NO_3 + NO_2 \leftrightharpoons N_2O_5 \qquad (7\text{-}8)$$

will result in the highest N_2O_5 concentrations only after significant O_3 has formed, Reaction (9) is important primarily after the NO_2 peak. Figure 3 shows the effect of this reaction. For the two sets of profiles in Figure 3, k_9 was taken to be 1.5×10^{-3} ppm^{-1} min^{-1} (Jaffee and Ford's value, 1967) and 5×10^{-6} ppm^{-1} min^{-1}. The higher value results in a markedly greater consumption of NO_2 and correspondingly lower production of O_3.

This theoretical evaluation of heterogeneous HNO_x formation has shown its potential significance. Obviously, the extent of these reactions depends on surface type as well as on surface-to-volume ratio. The need for experimental evaluation of k_9 and k_{10} in individual smog chambers is evident.

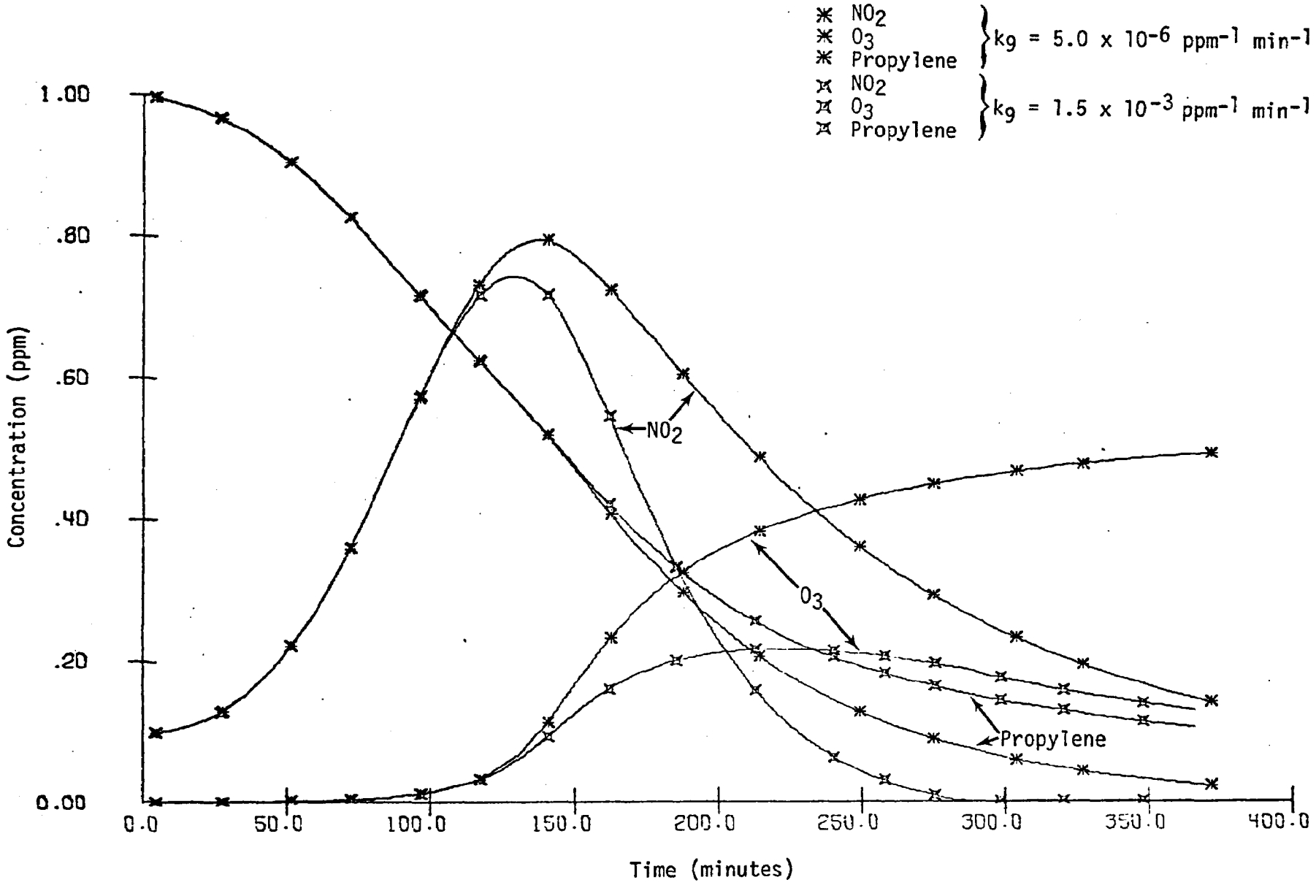

FIGURE 3. SMOG PROFILES FOR DIFFERENT VALUES OF kg, THE RATE CONSTANT FOR THE HETEROGENEOUS FORMATION OF HNO_3, $N_2O_5 + H_2O \rightarrow 2HNO_3$

3. O_3 Decay

The rate of O_3 destruction on chamber walls [Reaction (22), Table 1] used in the calculations in Chapter III was obtained from O_3 half-lives observed in each smog chamber. Decay rates were exponential; first-order decay was assumed.

B. ORGANIC CHEMISTRY

The oxidation of organic molecules in polluted air has been described previously (Demerjian et al., 1974a; Hecht et al., 1974a). In the following sections, we discuss recent studies in this area in relation to the development of the kinetic mechanism. Those reactions not dealt with here are described in the above references.

1. Propylene + OH·

Early investigators of the olefin-NO_x-air photochemical reactions discovered that, in addition to ozone and oxygen atoms, an unknown oxidant was participating strongly in smog formation (see Leighton, 1961). Several speculations were made as to the identity of this reactant, and it now appears (e.g., Demerjian et al., 1974a or Hecht et al., 1974a) that the OH radical is the most likely of these possibilities. In fact, OH is probably the most important olefin oxidant in smog, accounting for well over 50 percent of the olefin disappearance rate (Calvert and McQuigg, 1975). Hence, the success of a kinetic mechanism rests heavily on its representation of the OH-olefin (or, in general, OH-organic) reaction (including the ensuing chain).

There are two likely alternatives for the initial step in the OH-propylene reaction:

- Abstraction of an allylic hydrogen
- Addition of OH to the carbon-carbon double bond.

Slagle et al. (1974) studied the propylene-OH reaction in their crossed molecular beam reactor. Product analysis by photoionization mass spectrometry yielded a dominant ion signal corresponding to the abstraction product. Hence, they suggested that the propylene-OH reaction proceeds primarily by abstraction of an allylic hydrogen. In our simulations, this reaction was assumed to be followed immediately by the addition of O_2 to the allyl radical.

$$OH\cdot + CH_2{=}CHCH_3 \rightarrow H_2O + CH_2{=}CHCH_2^{\cdot} \xrightarrow{O_2} CH_2{=}CHCH_2O_2^{\cdot} \quad . \qquad \text{(II-2)}$$

This could be followed by NO oxidation to form NO_2 and acrolein:

$$CH_2{=}CHCH_2O_2^{\cdot} + NO \rightarrow CH_2{=}CHCH_2O\cdot + NO_2 \quad , \qquad \text{(II-3)}$$

$$CH_2{=}CHCH_2O\cdot + O_2 \rightarrow CH_2{=}CHCHO + HO_2^{\cdot} \quad , \qquad \text{(II-4)}$$

but the large production of acrolein that would result from this reaction is contrary to the observed products.

Another speculative reaction pathway was considered, in which 2 O_2 molecules add to the allyl radical to form a five membered cyclic peroxy radical.

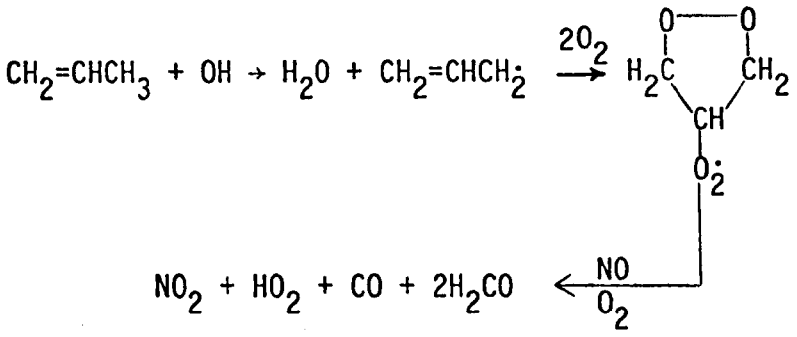

(II-5)

However, this formulation could not match the rapid reaction process that was observed in the UCR chamber, nor could it account for the large acetaldehyde product yield. Unless further experimental evidence arises to indicate

that the abstraction mechanism is important in smog, we shall assume that the OH-propylene reaction proceeds by addition.

Morris et al. (1971) investigated the OH-propylene reaction in a flow-discharge reactor coupled to a time-of-flight mass spectrometer. Adduct peaks were observed. It was concluded that OH adds to propylene and that the adduct is collisionally stabilized. In the C_3D_6 + OH reaction, they observed that H was retained in the final aldehyde product, while D was lost. Furthermore, acetaldehyde was a major product of OH + C_2H_4, and propionaldehyde was observed in the reaction of OH + C_3H_6. These results indicate that addition followed by hydride shift is a principal mechanism for the elementary OH-olefin reaction:

$$CH_3CH{=}CH_2 + OH \rightarrow CH_3\dot{C}HCH_2OH \rightarrow CH_3CH_2CH_2O\cdot \quad , \qquad (26)$$

$$CH_3CH{=}CH_2 + OH \rightarrow CH_3\overset{OH}{\overset{|}{C}}HCH_2\cdot \rightarrow CH_3\overset{O\cdot}{\overset{|}{C}}HCH_3 \qquad (27)$$

Reaction (26) corresponds to terminal addition, and Reaction (27) to internal addition. Preliminary results obtained by Slagle et al. (1974) also indicate that, to the extent that OH addition products were observed, the hydroxyl hydrogen is retained in the product. However, both these studies were done in the absence of O_2. For Reactions (26) and (27) to occur in air, the hydride shift must be so fast that it precludes the addition of O_2. By incorporating these reactions in our mechanism as presented above, we have implicitly assumed that this is true.

Although the experiments cited above provide mechanistic insights, they do not indicate the relative importance of Reactions (26) and (27). One would expect terminal addition to dominate because it yields the thermodynamically favored secondary radical. The best agreement between model predictions and the data was obtained with a terminal/internal ratio of 4. The present OH-propylene mechanism predicts the formation of propionaldehyde and minor amounts of acetone in accord with the UCR product measurements.

2. Unimolecular Decomposition of Alkoxyl Radicals

Carbonyl product yields are determined to a significant extent by the mode of reaction of alkoxyl radicals, short-lived intermediate products of hydrocarbon oxidation. In addition to Reactions (26) and (27), these species are formed from alkylperoxy radicals in reactions with NO or SO_2 [Reactions (42) and (51) in Table 1]. The fates of alkoxyl radicals that have been considered are decomposition [Reaction (35)], reaction with O_2 [Reaction (36)], and reactions with NO or NO_2. The last two reactions were summarily investigated and found to be relatively unimportant. Yields of nitrites and nitrates were very small,* and so RO· + NO_x reactions are not considered here. In this section and the next, the first two modes of reaction are discussed.

Recent experiments by Batt et al. (1974) have resulted in the first absolute measurement of rate constants for alkoxyl radical unimolecular decomposition at high pressure. By thermally decomposing alkyl nitrates, monitoring fractionation products, and using their own rate constants for RO + NO reactions, they were able to determine rate constants for RO decomposition. They did not estimate the accuracy of these rate constants. But, considering other figures they reported, we believe that an uncertainty factor of 8 is reasonable. Even with this uncertainty, their new values are several orders of magnitude higher than most previous estimates (reviewed in Batt et al., 1974).

Batt et al. (1974) obtained rate constants only for the decomposition of i-C_3H_5O·, s-C_4H_9O·, and t-C_4H_9O·, whereas other isomers of these species and shorter alkoxyl radicals appear in the mechanisms of Chapter III. We estimated additional rate constants when necessary by using smog chamber data and noting that, in Batt et al.'s results, the unimolecular decomposition rate decreases with decreasing numbers of skeletal carbon atoms.

---

* Alkyl nitrates have been detected at UCR by Fourier interferometry, but available literature (e.g., Spicer and Miller, 1974; Kopczynski et al., 1974) leads us to believe that quantitative yields are indeed low. An unknown oxidant peak observed during butane-NO_x experiments at UCR was attributed to butyl nitrate, but the estimated 6-hour concentration was on the order of 1 pphm, which corresponds to only about 1 percent of the reacted butane.

3. Alkoxyl Radical--O_2 Reactions

The individual rates of Reactions (35) and (36) are of little concern in developing a smog mechanism. But their ratio determines the course of the overall reaction. Unfortunately, no such ratio measurements are available. Those used in the present formulation were determined largely from UCR product distributions.

Available rate constants for the reaction

$$CH_3O\cdot + O_2 \rightarrow H_2CO + HO_2 \qquad (36.1)$$

vary over two orders of magnitude. Garvin and Hampson (1974) have recommended that $k_{36.1} \approx 4.5 \times 10^{-3}$ ppm^{-1} min^{-1}, whereas Mendenhall et al. (1974) have estimated that $k_{36.1} \approx 0.8$ ppm^{-1} min^{-1}. In the latter study, $k_{36.1}$ was determined from measurements of t-butylnitrate pyrolysis and a (very uncertain) rate constant ratio for the reactions of O_2 and NO with $CH_3O\cdot$. The authors concluded that a more direct measurement of $k_{36.1}$ was desirable. Therefore, while Mendenhall et al.'s value serves as a guideline, considerable freedom has been taken in the present study in adjusting rate constants for the $RO\cdot + O_2$ reactions. For smog modeling, the need for rate ratio measurements is even greater.

4. Propylene + O_3

As noted in Subsection 1, the importance of the O_3-olefin reaction in photochemical smog has long been recognized. Consequently, a large number of kinetic studies have been performed, and reasonable agreement on the rate constant for propylene + O_3 has been reached (Becker et al., 1974; Stedman et al., 1973; Garvin and Hampson, 1974). The mechanism for this reaction is in a greater state of flux. However, there is much evidence in favor of a recent mechanism postulated by O'Neal and Blumstein (O-B) (O'Neal and Blumstein, 1973; Finlayson et al., 1974). The O-B mechanism supplants the Criegee mechanism. The Criegee mechanism has proved to be a satisfactory

explanation of O_3-olefin chemistry in solution (Leighton, 1961), but not in the gas phase, where the formation of a "zwitterion" intermediate is not as appealing.

The O-B mechanism proceeds through the formation of an equilibrium between a molozonide and an oxy-peroxy biradical. This biradical may undergo many transformations, but, based on O'Neal and Blumstein's estimates, the most likely is an α-hydrogen abstraction:

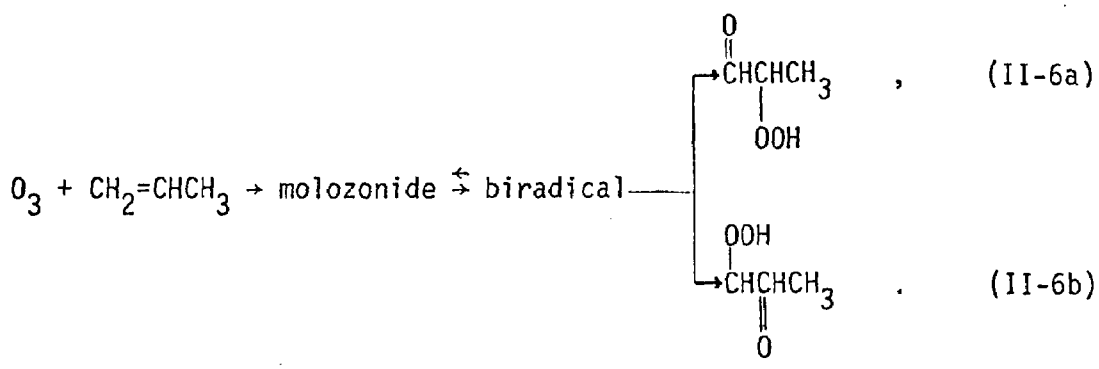

Both Routes a and b could occur, depending on the nature of the biradical intermediate. The α-keto hydroperoxide products of Reaction (II-6) will be formed in an excited state. Their fractionation results in the following overall reactions:

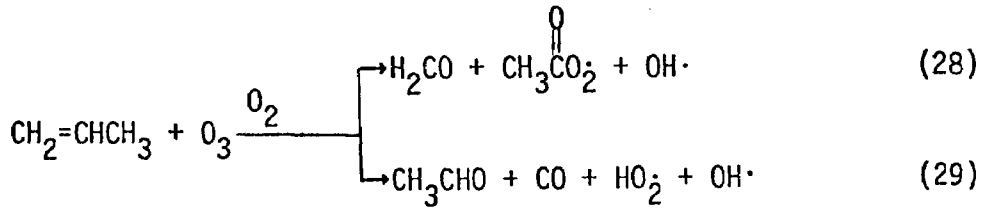

These products are consistent with the mass spectra obtained by Becker et al. (1974). The split between Routes (28) and (29) is determined by which hydroperoxide is formed in Reaction (II-6). In the present work, $k_{29}/k_{28} = 2$ was chosen arbitrarily to improve model predictions. Combining Reactions (28) and (29) with this rate constant ratio gives

$$CH_2{=}CHCH_3 + O_3 \xrightarrow{O_2} 0.33\ H_2CO + 0.33\ CH_3\overset{O}{\overset{\|}{C}}O_2\cdot + 0.67\ CH_3CHO + 0.67\ HO_2\cdot$$

$$+ 0.67\ CO + 1.0\ OH\cdot \quad .$$

This reaction can be compared with Reaction (33) in Table 8 of last year's report:

$$CH_2{=}CHCH_3 + O_3 \xrightarrow{O_2} 0.75\ H_2CO + 0.25\ CH_3\overset{O}{\overset{\|}{C}}O_2\cdot + 0.5\ CH_3CHO + 1.0\ HO_2\cdot$$

$$+ 0.75\ OH\cdot + 0.75\ CO \quad .$$

The new reaction differs from last year's in showing reduced formaldehyde, $HO_2\cdot$, and CO yields in favor of increased $OH\cdot$, acetaldehyde, and $CH_3C(O)O_2\cdot$. Becker et al.'s (1974) yields of CO from propylene + O_3 was 0.6 molecules of CO produced per molecule of propylene consumed. Because secondary reactions of aldehydes could have contributed to this yield, the stoichiometric coefficient of 0.67 is probably an overestimate.

5. Radical-Radical Reactions

The reactions discussed so far have been hydrocarbon-organic chain initiation and propagation reactions. Chain termination occurs through radical-radical reactions, such as $NO + OH\cdot \rightarrow HNO_2$ [Reaction (13)], $NO_2 + OH\cdot \rightarrow HNO_3$ [Reaction (14)], or $HO_2\cdot + HO_2\cdot \rightarrow H_2O_2 + O_2$ [Reaction (46)]. To provide adequate damping, one must include similar reactions for organic radicals. This can be done with reactions analogous to those just cited. In the present formulation, the production of organic hydroperoxides,

$$RO_2\cdot + HO_2\cdot \rightarrow ROOH + O_2 \quad , \qquad (47\text{-}48)$$

has been chosen. On an effective collision probability basis (likelihood of an $RO_2\cdot$-$HO_2\cdot$ collision) these reactions were assigned a rate constant of one-half that of the reaction $HO_2\cdot + HO_2\cdot \rightarrow H_2O_2 + O_2$ [Reaction (46)]. Further thermal or photolytic reactions of organic hydroperoxy species have not been included.

6. PAN Chemistry

The formation of peroxyacetylnitrate (PAN), and its homologs, occurs by another radical-radical reaction. Reaction (44),

$$RC(=O)O_2\cdot + NO_2 \rightarrow RC(=O)O_2NO_2 \quad , \qquad (44)$$

was discussed in last year's final report (Hecht et al., 1974b). It was speculated there that PAN might hydrolyze on the walls of the UCR chamber. Although this undoubtedly could occur, an analogy to N_2O_5 suggests that gas phase collisional destruction could be several orders of magnitude faster than surface reactions under ambient conditions. Thus, we presently propose that PAN may undergo a thermal decomposition reaction, resulting in the rupture of the peroxy and carbon-carbon bonds:

$$(M+)\ PAN \xrightarrow{O_2} NO_3 + CO_2 + CH_3O_2\cdot\ (+M) \qquad (45)$$

Based on data contained in Benson (1968) and Domalski (1971), this reaction is exothermic by about 14 kcal $mole^{-1}$.

The occurrence of Reaction (45) is supported by the experiments of Schuck et al. (1972) and recent PAN decay experiments in the Riverside chamber (UCR monthly report No. 4). In the former study, PAN was found to oxidize NO to NO_2. The reaction was first order in PAN and zeroth order in NO. The ratio of CO_2 produced to PAN consumed was nearly 1. The ratio of NO_2 formation to PAN consumption was approximately 2 in a nitrogen atmosphere, but was much greater than 2 in an oxygen atmosphere. This is further evidence for the occurrence of Reaction (45), followed by $NO_3 + NO \rightarrow 2NO_2$ [Reaction (6)] in an N_2 atmosphere, and Reaction (6) plus $CH_3O_2\cdot + NO \rightarrow CH_3O\cdot + NO_2$ [Reaction (42)], $CH_3O\cdot + O_2 \rightarrow H_2CO + HO_2\cdot$ [Reaction (46)], and $HO_2\cdot + NO \rightarrow OH\cdot + NO_2$ [Reaction (15)] in an O_2 atmosphere. Schuck et al.'s rate constant, $k_{45} = 2.06 \times 10^{-2}\ min^{-1}$, is 10 times that obtained from the half-lives observed in the UCR chamber. This difference

may be due to additional wall decomposition in Schuck et al.'s reactor. The Riverside half-lives of 5.7 ± 0.1 hours in the light and 5.5 ± 0.4 hours in the dark provide further confirmation that PAN does not photodecompose at an appreciable rate (Leighton, 1961).

C. PHOTOCHEMISTRY

A distinctive feature of "Los-Angeles-type" air pollution is the role played by sunlight in its causation. The free radicals that initiate the process of oxidant production in Los Angeles air come from photolytic splitting of molecular bonds. In smog chamber studies of the type considered in Chapter III, sunlight is replaced by artificial illumination. Aside from the overall intensity of the light source, the spectral distribution of photon flux is the major light source characteristic. The spectrum of the Riverside solar simulator and the solar spectrum are reproduced in Figure 4. The solar simulator consists of a light source and a light filter. The dark solid line in Figure 4 represents the filtered spectrum.

1. Photolysis Rate Constants

Given a light source spectrum, such as that in Figure 4, rate constants for the various photolysis reactions included in Table 1 can be computed. For this purpose, quantum yields and absorption coefficients for the absorbing molecules must be known. Photolysis rate constants can then be computed from

$$k = \int I_\nu \phi_\nu \alpha_\nu \, d\nu \qquad \text{(II-7)}$$

and

$$I_\nu = I_\nu^\circ F_\nu \quad , \qquad \text{(II-8)}$$

where

I_ν° = photon flux provided by the light source at wavelength ν,
α_ν = absorption coefficient for the absorbing molecule,
F_ν = filter factor,
ϕ_ν = quantum yield (molecules dissociated per photon absorbed),

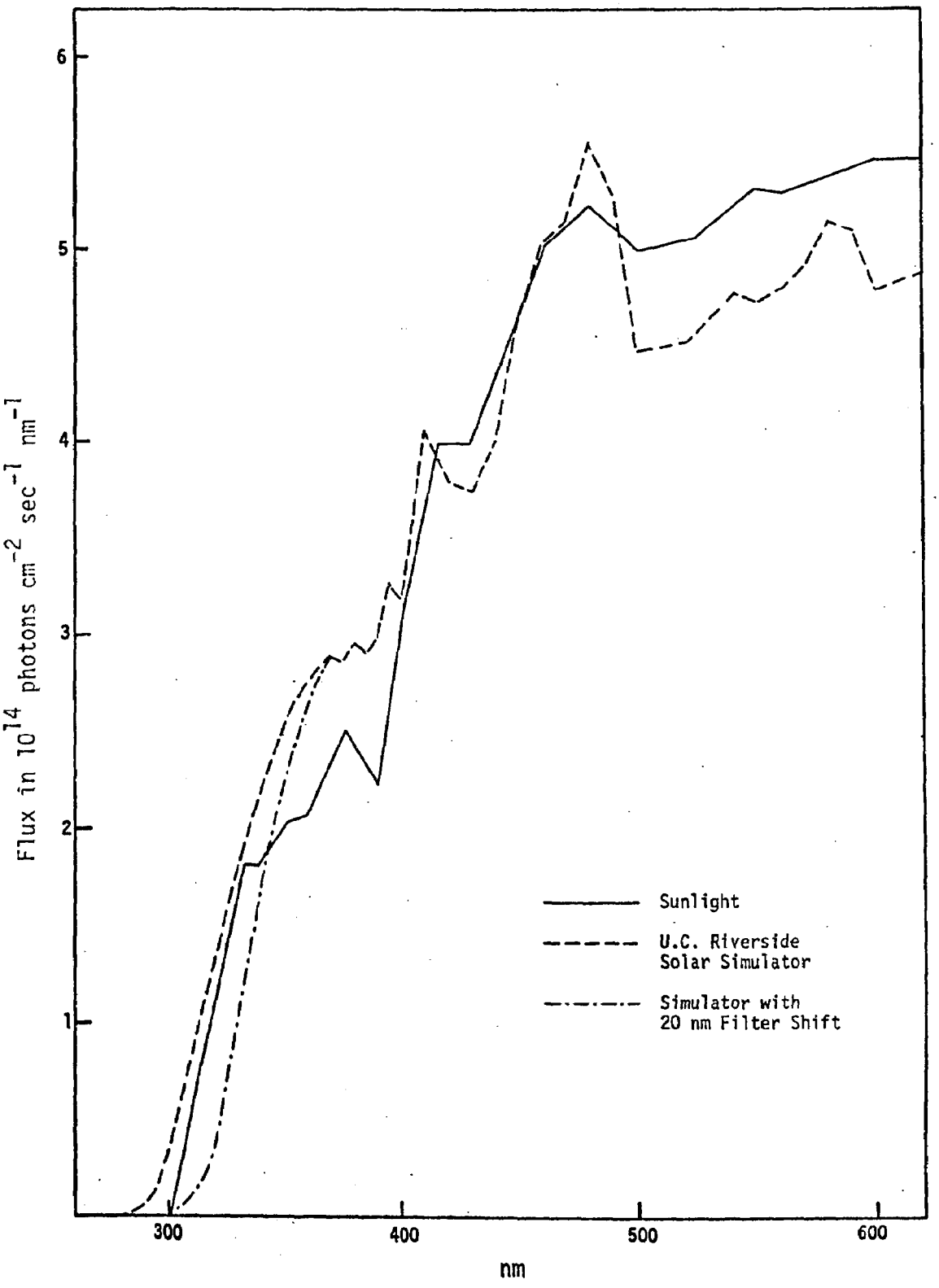

FIGURE 4. SPECTRA OF SUNLIGHT AND U.C. RIVERSIDE SOLAR SIMULATOR

and where integration extends over the entire light spectrum. Rate constants for the present investigation were computed from Eq. (II-7) using I_ν values obtained when UCR first installed their solar simulator in the chamber,* and values of α_ν and ϕ_ν extracted from Calvert and Pitts (1967) and Johnston and Graham (1974). The values of these rate constants, normalized by k_1, for $NO_2 \rightarrow NO + O$ [Reaction (1)] are presented in Table 3.

Measurements of k_1 are made periodically at UCR, and $k_d(\approx 9/4\ k_1)$ is obtained from light meter readings during the Battelle simulations. The procedure used in carrying out the computations presented in Chapter III was to multiply the measured values of k_1 by the ratios in Table 3 to obtain the needed photolysis rate constants. The shortcomings of this procedure are critically assessed below. Obviously, periodic measurements of I_ν would facilitate a more accurate approach.

2. Spectrum Decay

For most of the photoabsorbers participating in smog reactions, molecular dissociation occurs primarily as a result of the absorption of ultraviolet light. As is to be expected, different chemical species have different absorption spectra. For example, the absorption by NO_2, resulting in NO and O, is largest and fairly uniform over the 300 to 400 nm range, whereas the absorption by acetaldehyde, to form either CH_4 and CO or CH_3 and HCO, exhibits a peak in the 250 to 300 nm range and very little absorption elsewhere. Hence, the ratio of k_1 to other photolysis rate constants will be very sensitive to the intensity and distribution of UV light from the irradiation source.

Periodic measurements of k_1 by experimentalists at UCR have shown a consistent light deterioration. Between smog chamber experiments EC-38 and EC-60 k_1 decreased by about 40 percent (UCR monthly report No. 5). The cause of this reduction was not investigated, but there are two obvious possibilities. The first is a reduction in light source emission, perhaps resulting from a buildup of UV-absorbing material on the inside of the light bulb (Burton, 1975). The second is increased UV absorption by mirrors. Absorption by mirrors could slowly impair their reflection properties. Indeed, the

*Data obtained through private communications.

Table 3

PHOTOLYSIS CONSTANT CHANGES FROM UV LOSS

Reaction	Standard Ratio	Reduced Ratios		
		5 nm Shift	10 nm Shift	20 nm Shift
$NO_2 \rightarrow NO + O$	1.0	1*	1*	1*
$HNO_2 \rightarrow OH\cdot + NO$	0.070	0.070	0.070	0.069
$O_3 \rightarrow O_2 + O(^1D)$	0.026	0.013	0.006	0.0009
$O_3 \rightarrow O_2 + O(^3P)$	0.035	0.034	0.033	0.0031
$H_2CO \rightarrow H\cdot + HCO\cdot$	0.0049	0.0040	0.0031	0.0018
$H_2CO \rightarrow H_2 + CO$	0.011	0.010	0.0089	0.0069
$CH_3CHO \rightarrow$ Products†	0.0077	0.0060	0.0045	0.0022
$CH_3CH_2CHO \rightarrow$ Products†	0.0085	0.0065	0.0047	0.0022
$H_2O_2 \rightarrow 2OH\cdot$	0.0036	0.0031	0.0028	0.0021
MEK $\rightarrow CH_3\dot{C}H_2 + CH_3C(O)\cdot$	0.0036	0.0024	0.0015	0.0005

* k_1 itself was reduced 1.9 percent by a 5 nm shift, 4.2 percent by a 10 nm shift, and 10 percent for a 20 nm shift. Reduced ratios listed have been renormalized to new k_1.

† These products include radicals and stable species, as shown in Table 1. Precise quantum yields are not known. We have assumed that the quantum yield for stable products is approximately one-third of that for radicals.

mirrors were observed to be damaged and were sent out to be recoated after Run EC-61.) This reduced reflection and increased absorption would probably be most pronounced in the UV region.

Although spectrum decay must ultimately be determined experimentally, its potential effect can be assessed theoretically. For this purpose, rate constants were recomputed using the following variation of

$$k = \int I'_\nu \alpha_\nu \phi_\nu \, d_\nu \quad , \tag{II-9}$$

where

$$I'_\nu = F_{\nu-\gamma} \cdot I^o_\nu \quad , \tag{II-10}$$

and γ is the magnitude of a shift in the filter factor to lower frequencies. Replacing I_ν in Eq. (II-7) by I'_ν in Eq. (II-9) reduces the UV intensity. The spectrum change due to a 20 nm shift in the filter factor is illustrated in Figure 4. Percentage reductions in rate constant ratios, computed for ν = 5, 10, and 20 nm, appear in Table 3, along with their unshifted values. In Figure 5, the effect of a 20 nm shift on smog profiles is illustrated. The spectrum deterioration clearly delays the NO_2 peak, as observed experimentally at UCR. Although Experiments EC-16 and EC-60 were nominally the same, EC-60 took almost twice as long to reach the NO_2 peak. Using only the reported initial conditions and values of k_1, we could not reproduce this delay by computer simulation (see Figure 6). However, a simulation employing a 20 nm filter shift showed that the observed delay could easily be accounted for by UV spectrum deterioration. We concluded that more complete spectrum characterization in smog chambers is needed.

D. SO_2 OXIDATION

In the previous two years, our smog chemistry modeling efforts have focused on systems containing olefins, paraffins, and NO_x. During this year, we also considered systems containing SO_2 and toluene. The next two sections are devoted to a discussion of chemical processes related to these two species.

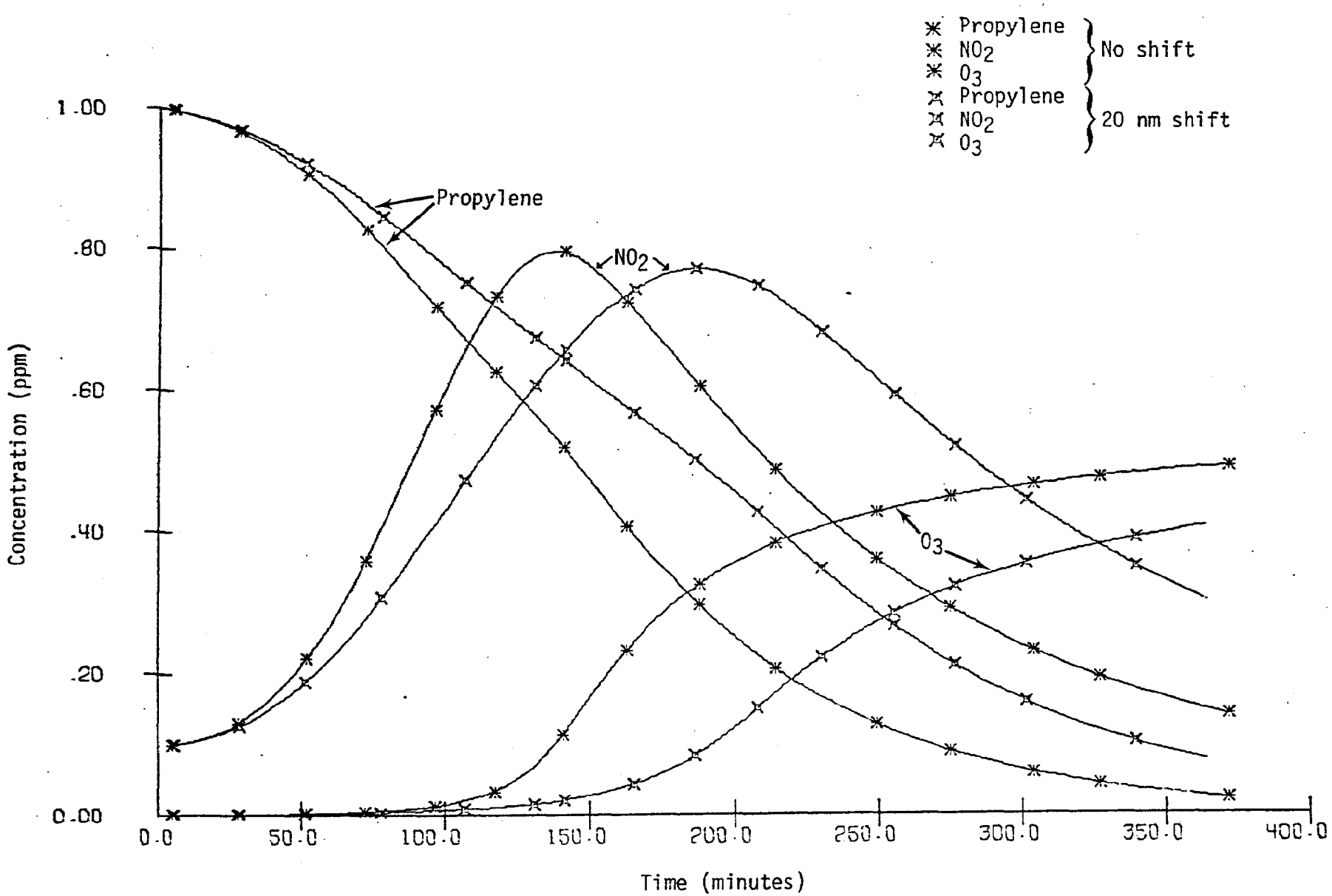

FIGURE 5. EFFECT OF A 20 NM FILTER SHIFT ON SMOG PROFILES

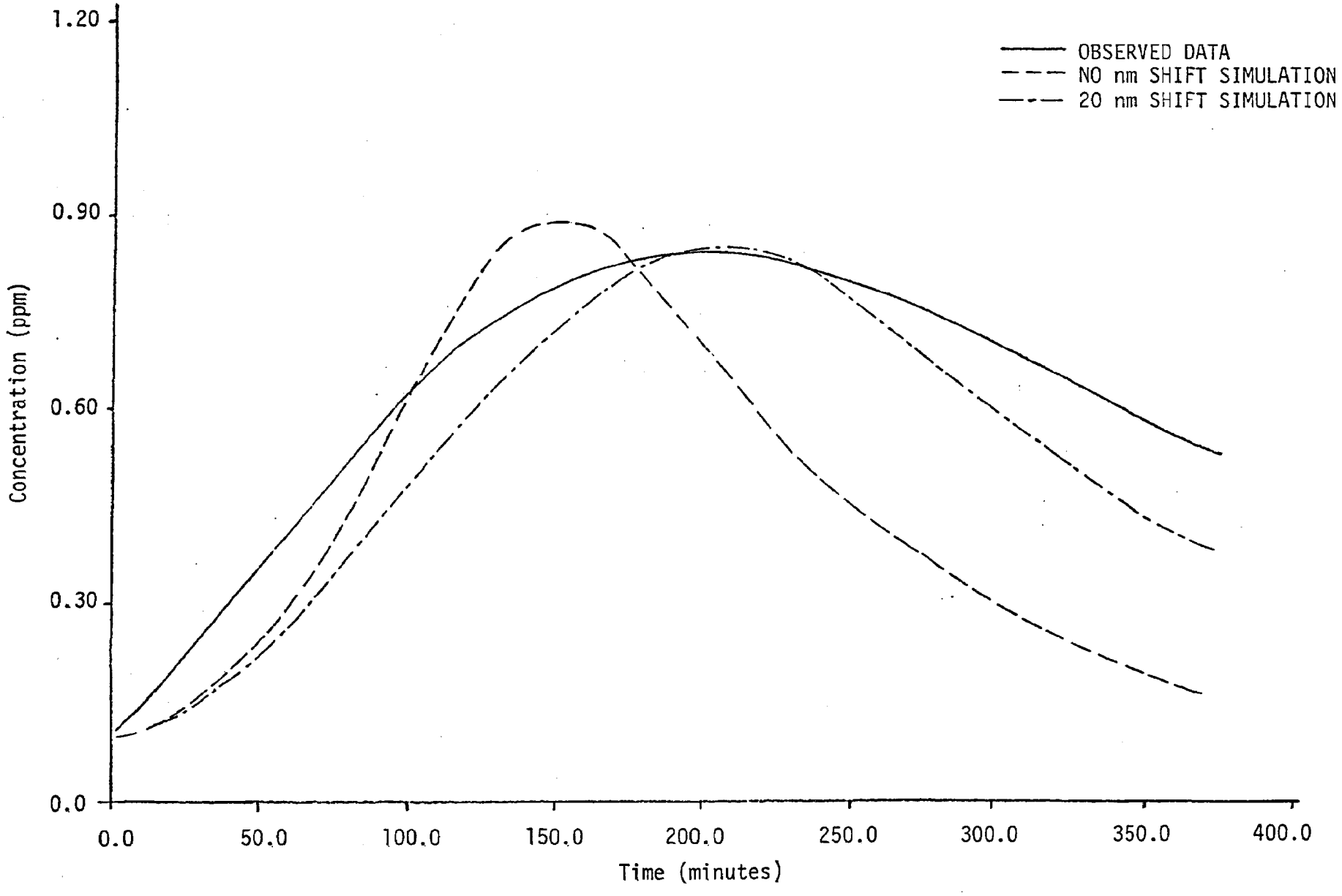

FIGURE 6. EFFECT OF A 20 nm FILTER SHIFT ON NO_2 BEHAVIOR FOR EC-60

1. Some Observations

Past smog chamber studies of irradiated SO_2-NO_x-hydrocarbon and SO_2-O_3-olefin mixtures have resulted in a variety of qualitative and quantitative observations, many of which are inconclusive or even contradictory. Of particular significance is an uncertainty about the effect of SO_2 on the yields of carbonyl products (see reviews by Leighton, 1961; Wilson and Levy, 1970) and ozone (Wilson and Levy, 1970; Altshuller et al., 1968). Wilson and Levy (1970) have shown that the overall reaction is strongly dependent on relative humidity. Undoubtedly, chamber effects also play a role in causing these inconsistencies. There is agreement, however, on the observation that the addition of SO_2 to the hydrocarbon-NO_x-air system results in increased aerosol production and that this aerosol formation occurs after the NO_2 peak. It has also been generally observed that the addition of propylene to an irradiated SO_2-NO_x mixture increases SO_2 consumption and aerosol production. The aerosol is thought to be chiefly sulfuric acid and water, though it may contain small concentrations of organic and nitrite-type material (Filby and Penzhorn, 1974; Bufalini, 1971).

An examination--which appears later--of the Battelle data (S-110 and S-115) permits two further observations. The addition of $\sim$ 0.5 ppm SO_2 to an irradiated NO_x-olefin-air mixture does not substantially alter either the ozone production or the propylene oxidation rate.

A free radical mechanism for SO_2 oxidation is in accord with these observations. Because oxidation occurs mainly after the NO_2 peak and because added hydrocarbon increases aerosol production, the radicals that oxidize SO_2 are probably the same as those oxidizing NO. These radicals must be either organic or of organic origin. The low reactivity of SO_2 accounts for the smallness of its effect on both hydrocarbon oxidation and ozone production. Sulfuric acid is probably the main oxidation product of SO_2.

2. Kinetic Mechanisms for SO_2 Oxidation

Recent investigators of atmospheric SO_2 chemistry (e.g., Davis et al., 1974; Calvert and McQuigg, 1975; Castleman et al., 1974) have suggested that the oxidation of SO_2 by $OH\cdot$ and $HO_2\cdot$ is the primary means of SO_2 removal in the gas phase. Several recent measurements of the SO_2-$OH\cdot$ rate constant are reviewed in Table 4. They cover a wide range, but the value of 900 ppm^{-1} min^{-1} selected for the current mechanism encompasses the full range with a 50 percent uncertainty.

As shown in Table 4, Davis (1974) measured a rate constant of k_{50} = 1.3 ppm^{-1} min^{-1} for

$$HO_2\cdot + SO_2 \rightarrow OH\cdot + SO_3 \quad . \tag{50}$$

Because alkyl and acyl peroxy radicals should be more reactive than $HO_2\cdot$, we have incorporated Reactions (51) and (52) into the kinetic mechanism with rate constants of 1.5 ppm^{-1} min^{-1}, slightly higher than k_{50}:

$$RO_2\cdot + SO_2 \rightarrow RO\cdot + SO_3 \quad , \tag{51}$$

$$SO_2 + RC(=O)O_2\cdot \xrightarrow{O_2} RO_2\cdot + CO_2 + SO_3 \quad . \tag{52}$$

Reactions of NO_3 and N_2O_5 with SO_2 were postulated by Wilson and Levy (1969) to explain a rapid reaction observed between NO_2, O_3, and SO_2. As shown in Table 4, this could not be explained by a direct reaction of SO_2 with O_3. Thus, the following sequence was invoked:

$$NO_2 + O_3 \rightarrow NO_3 + O_2;\ NO_3 + NO_2 \underset{M}{\rightleftarrows} N_2O_5 \quad , \quad (5,\ 7 \text{ and } 8)$$

$$NO_3 + SO_2 \rightarrow SO_3 + NO_2 \quad , \tag{49}$$

$$N_2O_5 + SO_2 \rightarrow SO_3 + 2NO_2$$

Table 4

RATE CONSTANTS FOR SO_2 OXIDATION

(In $ppm^{-1}\ min^{-1}$)

Reaction	Davis (1974)	Calvert and McQuigg (1975)	Castleman et al. (1974)	Others	Present Mechanism
$SO_2 + OH \rightarrow HSO_3$	1350 ± 130		590	860 ± 120 (Cox, 1974)	900
$SO_2 + O \xrightarrow{M} SO_3$	(7.6±0.9)exp(-2240/RT)			3000 (Leighton, 1964)	
				270 ± 50 (Mulcahy et al., 1967)	
$SO_2 + NO_3 \rightarrow SO_3 + NO_2$	< 14.7	$< 10^{-5}$			14
$SO_2 + HO_2 \rightarrow SO_3 + OH\cdot$	1.35 ± 0.2	$10^{-4}k(OH\cdot + SO_2)$, if HSO_2 is a product			1.3
$SO_2 + RC(O)O_2 \rightarrow R + CO + SO_3$ $SO_2 + RO_2 \rightarrow RO\cdot + SO_3$		$\approx HO_2 + SO_2$			1.5
$SO_2 + h\nu \rightarrow SO_2^*$				$\sim 10^{-4}\ min^{-1}$ (Leighton, 1961)†	
$SO_2 + N_2O_5 \rightarrow 2NO_2 + SO_3$	$\leq 1.2\ 10^{-8}$	$< 6.2\ 10^{-8}$			
$SO_2 + O_3 \rightarrow SO_3 + O_2$	3×10^{-7}	$< 1.2\ 10^{-10}$			
$SO_3 + H_2O \xrightarrow{M} H_2SO_4$			740		Immediate
$RO_2 + SO_2 \rightarrow ROSO_3$		$10^{-4}k(OH\cdot + SO_2)$			
$RC^+OO^- + SO_2 \rightarrow SO_3 + RCHO$				~ 6.3 (Cox and Penkett, 1972)	
$HSO_3 + O_2 \rightarrow HSO_5 \rightarrow SO_3 + HO_2$					See text
$HSO_5 + NO \rightarrow HSO_4 + NO_2$					800
$HSO_4 + HO_2 \rightarrow H_2SO_4 + O_2$					9000
$HSO_4 + NO_2 \xrightarrow{H_2O} H_2SO_4 + HNO_3$					1×10^4

† Quantum yields for SO_3 production (ϕ_{SO_3}) measured in an SO_2 atmosphere vary from 3×10^{-4} (Cox, 1972) to 0.1 (Chung et al., 1975). Chung et al. (1975) explained this discrepancy by considering secondary reactions. Extrapolation of these results to atmospheric condition is not possible at present because ϕ_{SO_3} varies with atmospheric pressure and type of diluent.

The upper limits of the $N_2O_5 + SO_2$ reaction rate (Table 4) indicate its insignificance. In contrast, the upper limits recorded for k_{49} (Table 4) are in severe disagreement. We can estimate k_{49} assuming reactions of HO_2 and NO_3 with SO_2 and NO are similar (all are "oxygen abstraction" reactions). Using the ratio, $k_{(SO_2 + HO_2^{\cdot})}/k_{(NO + HO_2^{\cdot})}$, to be approximately 10^{-3} (from Tables 2 and 4) and $k_{(NO_3 + NO)} \simeq 10^4$ ppm^{-1} min^{-1} (from Table 2) we find

$$k_{49} \cong \left[k_{(SO_2 + HO_2)}/k_{(NO + HO_2^{\cdot})}\right] \cdot k_{(NO_3 + NO)} \cong 10 \text{ ppm}^{-1} \text{ min}^{-1} \quad . \tag{II-11}$$

This estimate is in closest agreement with Davis' (1974) reported value. Reaction (49) could therefore be significant, and it has been initially included in the mechanism with k_{49} = 14 ppm^{-1} min^{-1} (Davis' value).

Cox and Penkett (1972) found that SO_2 added to the olefin-O_3 system was oxidized to sulfuric acid aerosol. They also found that, when the ozone-olefin consumption ratio in the absence of SO_2 was greater than 1, the addition of SO_2 reduced this ratio. The addition of SO_2 also enhanced carbonyl product yields. From these and other results, Cox and Penkett inferred that a short-lived intermediate of the ozone-olefin reaction, which they speculated might be a zwitterion, was responsible for SO_2 oxidation. However, in light of the discussion of the mechanism for O_3 + propylene in Subsection 4 and the data in Table 4, it seems more reasonable to account for Cox and Penkett's observations in terms of reactions of SO_2 with hydroxyl, hydroperoxyl, peroxyalkyl, and peroxyacyl radicals rather than zwitterions.

The final modes of SO_2 oxidation included in Table 4 are direct oxidation by O atoms and photooxidation. The former can be ruled out, because the maximum O concentration is only about 10^{-9} ppm. With SO_2 in ppm concentrations, this gives rates $\lesssim 10^{-6}$ min^{-1}. Photooxidation has been widely investigated (Cox, 1972; Sidebottom et al., 1972; Demerjian et al., 1974b; Smith and Urone, 1974); the experimental results show that it is an unimportant oxidation process in polluted atmospheres. The inefficiency of photooxidation is due, in part, to the forbiddenness of direct excitation of SO_2 from the ground state to its reactive triplet state $SO_2(^3B_1)$ (Sidebottom et al., 1972). Sidebottom et al. (1972) estimated an upper limit of 2 percent SO_2 consumption per hour for gas phase photooxidation in the atmosphere. However, as they noted,

this could be an extreme upper limit because the efficiency for singlet-triplet intersystem crossing may have been overestimated, and the assumption that all quenching of $^3SO_2$ by O_2 was chemical rather than physical was probably faulty. Because of the results of the investigations cited above, SO_2 photooxidation does not appear in the present mechanism.

Direct reaction between $^3SO_2$ and hydrocarbons has been reported at high reactant pressures (Badcock et al., 1971; Sidebottom et al., 1971; Filby and Penzhorn, 1974). However, at ppm levels, Demerjian et al. (1974b) found that the primary result of the interaction of $^3SO_2$ with 2-butene was the interconversion of cis and trans isomers. Thus, a direct chemical reaction between $^3SO_2$ and olefins under atmospheric conditions can also be ruled out.

As shown in Tables 1 and 4, SO_3 is produced by the reaction of $RO_2^{\cdot}$, $RC(O)O_2^{\cdot}$, $HO_2^{\cdot}$, and NO_3 with SO_2. Castleman et al. (1974) found that SO_3 rapidly combines with water to form H_2SO_4. Presumably, H_2SO_4 then nucleates and adds more water to form aerosol droplets ($H_2SO_4 \cdot nH_2O$). The studies carried out by Cox and Penkett (1972) and the more recent mass spectrometric measurements made by Schulten and Schurath (1975) indicate that H_2SO_4 is the major sulfur-containing product of the olefin/O_3/SO_2 reactions. In Bufalini's (1971) survey, she reported that the aerosol produced as a result of the irradiation of 3 ppm of lower olefins in the presence of 1 ppm NO_2 and 0.5 SO_2 at 50 percent relative humidity was primarily composed of sulfuric acid. Accordingly, no other products have been accounted for in the present mechanism. Furthermore, we assumed that SO_3 is rapidly converted to H_2SO_4.

Davis et al. (1974) and Calvert and McQuigg (1975) have speculated on the formation of compounds containing S, O, H, and N when NO_x is present. Presumably, the formation of these nitrogen-containing species results from radical-radical reactions with oxidation products of the $OH\cdot$-SO_2 adduct. For example, HSO_4, formed as shown in Table 4, could combine with NO_2 to form HSO_4NO_2. Subsequent hydrolysis at the wall would produce nitric and sulfuric acid:

$$HSO_4^{\cdot} + NO_2 \xrightarrow[\text{surface}]{H_2O} H_2SO_4 + HNO_3 \quad . \qquad (56)$$

This represents one possible fate of the HSO_4 molecule produced in the following series:

$$OH\cdot + SO_2 \rightarrow HSO_3^{\cdot} \xrightarrow{O_2} HSO_5^{\cdot} \quad , \qquad (50)^*$$

$$HSO_5^{\cdot} + NO \rightarrow HSO_4^{\cdot} + NO_2 \quad . \qquad (54)$$

Other possible reactions of HSO_4 (and HSO_5) have been assembled by Calvert and McQuigg (1975), including hydrogen abstractions from alkanes and $HO_2^{\cdot}$ and addition to olefinic double bonds. Davis et al. (1974) proposed that HSO_6 could be produced by the addition of O_2 to HSO_4. It could then oxidize two NO molecules, reforming HSO_4, which would then repeat the process:

$$HSO_4^{\cdot} + O_2 \rightarrow HSO_6^{\cdot} \xrightarrow{2NO} HSO_4^{\cdot} + 2NO_2 \quad .$$

This mechanism was presented to explain an ozone bulge found by Davis et al. (1974) in the plume downwind of the Potomac Electric Power Company's power plant at Morgantown. However, laboratory studies have shown that the addition of SO_2 to the hydrocarbon-NO_x system actually causes either little change or even a reduction in O_3 production (Wilson and Levy, 1970). As stated at the outset of this discussion, we assumed in the present mechanism formulation that SO_2 has only minor effects on O_3 yield; so Davis et al.'s suggestion has not been incorporated. In addition to Reaction (56), a simple termination reaction,

$$HO_2^{\cdot} + HSO_4 \rightarrow H_2SO_4 + O_2 \quad , \qquad (55)$$

---

* An alternative to the last step in Reaction (50), $HSO_3 + O_2 \rightarrow HO_2\cdot + SO_3$, seems implausible thermodynamically. ΔH is approximately 0 to 20 kcal mole^{-1} for this step, compared with $\Delta H \sim -50$ kcal mole^{-1} for the last step in Reaction (50).

has been included. In light of the current lack of experimental studies, this seems a pragmatic and adequate closure to the SO_2 oxidation mechanism.

E. THE TOLUENE-NO_x-AIR SYSTEM

The development of a toluene oxidation mechanism has been greatly hindered by a lack of information on the pertinent reactions of toluene and by a dearth of detailed product analyses of smog chamber experiments. For these reasons, the mechanism proposed in Subsection 3 below is sketchy and possibly premature. The first two following subsections briefly review the currently available literature relating to the smog reactions of toluene.

1. Toluene + $O(^3P)$

Jones and Cvetanovic (1961) and Atkinson and Pitts (1975) have determined rate constants for this reaction. According to the latter, k (toluene + O) $\sim$ 120 ppm^{-1} min^{-1}. At a typical O concentration of $\sim 10^{-9}$ ppm, this reaction is of little importance. In the present mechanism, OH· is taken to be the sole oxidant.

2. Toluene + OH·

Davis et al. (1975) measured a rate constant of $9.0 \pm 0.6 \times 10^3$ ppm^{-1} min^{-1} for the toluene-OH· reaction under a pressure of 100 torr (M = He), where the reaction was still in the pressure fall-off region. However, extrapolation to room pressure via a Lindemann (1/k versus 1/P) plot indicated that this value was very close to the high pressure limit. The pressure effect Davis et al. observed (k at 100 torr was nearly twice its value at 3 torr) is evidence that a significant fraction of the reaction proceeds initially through the formation of a collisionally stabilized adduct. The rate constant measured at 3 torr ($k = 5.3 \pm 0.4 \times 10^{-3}$ ppm^{-1} min^{-1}) implies that addition to the ring accounts for at least one-half of the toluene-OH· reaction.

Doyle et al. (1975) used a 6000-liter glass smog chamber to measure the disappearance rates of several aromatic compounds relative to that of butane. The hydrocarbons, along with ∿0.27 ppm NO and ∿0.04 ppm NO_2, were irradiated and aromatic concentrations were measured after 1 and 2 hours. After presenting evidence that OH· was the primary hydrocarbon oxidant in their system, Doyle et al. obtained $k_{(\text{toluene + OH}\cdot)} = 6.2 \pm 2.3 \times 10^3$ ppm^{-1} min^{-1}, though, of course, this value depends on the value of the rate constant used for butane + OH. Doyle's measurements of relative rates for the three isomers of xylene indicate that the primary mechanism for aromatic hydrocarbon-OH· reactions is electrophilic addition to the ring (see Section 3).

Although neither of these two investigations give direct evidence of the existence of an abstraction route, the resonant stability of the phenalkyl radical, produced by hydrogen abstraction from the methyl group, makes this an appealing pathway. That this process does indeed occur (to some extent) is implied by the observation of benzaldehyde and peroxybenzolnitrate (PB_ZN) in the toluene-NO_X system by Heuss and Glasson (1968). Following Davis et al. (1975), we have set a limit of 50 percent for the relative frequency of H-abstraction to OH-addition.

Another noteworthy observation was made by Altshuller et al. (1970), who identified formaldehyde as a product of the same (toluene-NO_X) system. Simultaneously, they detected only trace amounts of acetaldehyde. Formaldehyde could be formed subsequent to oxidation of the methyl group on toluene or after displacement of the methyl group by OH.*

The investigations just cited are the basis for our current toluene oxidation mechanism. Obviously, more product measurements are sorely needed.

3. The Proposed Mechanism

Reactions (33) and (34) are the initial H abstraction and OH addition reactions:

---

* Another possibility, not included in the current mechanism, is the opening of the aromatic ring with the subsequent formation of fractionation products. As these are likely to include acetylene, testing for this possibility experimentally should be straightforward.

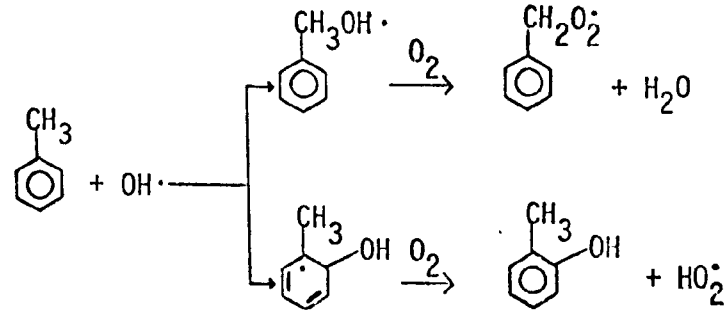

(33)

(34)

In both cases, an immediate reaction with O_2 has been assumed. The o-cresol product of Reaction (34) is taken as a prototype for o, p (i.e., electrophilic addition) cresols.*

The peroxy phenalkyl radical, produced in Reaction (33), could react as follows, to produce benzaldehyde and PB_zN.

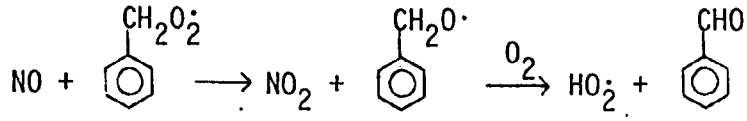

(42, 36)

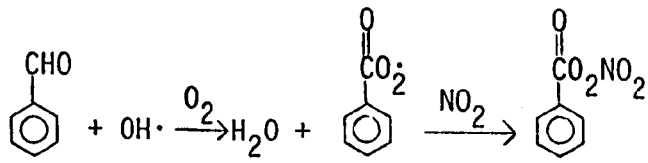

(32, 44)

Other radical reactions, selected in analogy to those included in Table 1, are

* The procedure of using o- as a prototype for o, p- was used throughout.

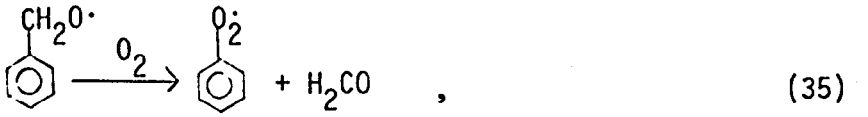

(35)

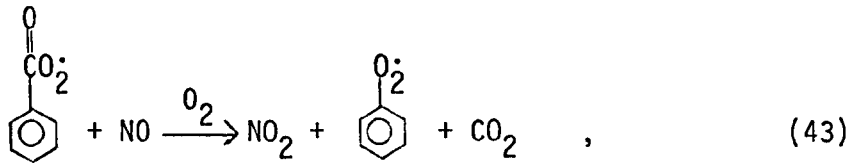

(43)

both of which produce a peroxy-phenyl radical. Subsequent reactions [Nos. (42'), (42")] produce (o,p) quinones:

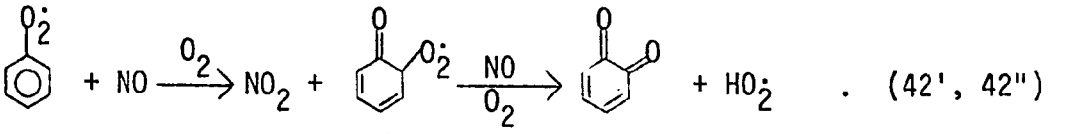

(42', 42")

Because of the diradical character of quinones, they could react further, but such speculation has not been included here.

If in Reaction (34) OH· has combined with toluene at the ring-methyl bond, Reaction (34) would become

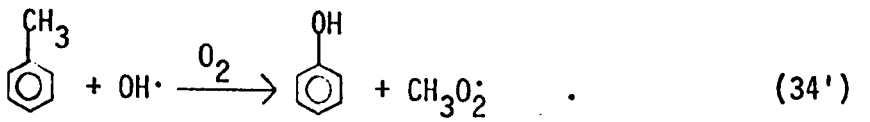

(34')

Phenol and cresols [from Reactions (34) and (34')] should be very reactive. Gitchell et al. (1974) found that addition of phenol had an inhibiting effect on propylene-NO_x systems. Therefore, they suggested that the OH· + phenol reaction proceeds by hydrogen abstraction from the phenolic hydroxyl group. This, and their further speculation that NO and NO_2 add to the phenoxy radicals thus produced, seem reasonable. However, in an attempt to match the predictions of the kinetic mechanism with the NAPCA smog chamber profiles (see Chapter III), -OH hydrogen abstraction from phenol and cresols were assumed to be followed by O_2 addition as in

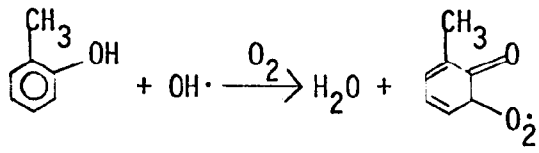

The above reactions, along with appropriate radical + HO_2· reactions, constitute the present kinetic mechanism for toluene oxidation (Table 13, Chapter III). Rate constants have been selected on the basis of reaction analogies.

III SMOG CHAMBER SIMULATIONS

Smog chamber studies done at the University of California, Riverside (UCR), Battelle Memorial Institute, and the National Air Pollution Control Administration (NAPCA) serve as the data base for validating the kinetic mechanisms. Validation involves comparing smog profiles obtained by numerical integration of chemical rate equations with those obtained experimentally. Numerical integration and the derivation of rate expressions from stoichimetric equations and rate constants were done on a CDC-7600 digital computer. The programs used (MODKIN and CHEMK) were developed under previous EPA contracts by SAI and by G. Z. Whitten at Lawrence Berkeley Laboratory specifically for this purpose (see Appendix A of Hecht et al., 1974a).

Unfortunately, rate constants and reaction mechanisms were not accurately known for many of the elementary steps comprising the smog mechanisms. Additionally, chamber characterization was usually incomplete. Thus, an unavoidable aspect of validation was "tuning." Tuning involves adjusting parameters within their range of uncertainty for the sole purpose of improving the fit between experiments and predictions. As in the past, we attempted to minimize the amount of tuning and to maximize the dependence on kinetic data.

Chamber characteristics that were usually available are k_1, dilution rate and heterogeneous O_3 loss. The last two were incorporated as simple first-order reactions. Rate constants for all photolysis reactions were determined from k_1 through the use of Table 3. Other procedural aspects and the simulation results appear in the ensuing subsections.

A. SIMULATIONS OF UCR DATA

The operating characteristics of the UCR chamber and peripheral equipment were described in detail in last year's report (Hecht et al., 1974a). The only addendum to be made here is to note calibration errors in O_3 and

NO_x measurements discovered during the year. The following corrections to the data appearing in last year's report had to be made:

$$O_3' = O_3/1.2 \quad ,$$
$$NO' = 1.2\ NO \quad ,$$
$$NO_2' = 1.2\ NO_2 + 0.2\ PAN \quad .$$

Primes represent the new values, and the absence of primes indicates old values.

1. Results for the Propylene-NO_x-Air Block

The initial concentrations for the propylene-NO_x block appear in Table 5 and Figure 7. The mechanism used to simulate these experiments is presented in Table 6. Photolysis rate constants used in the simulations were computed from a 10 nm filter-shifted spectrum. Chapter II presents these rate constants, normalized by k_1. The choice of a 10 nm shift was somewhat arbitrary, but more complete spectrum decay characterization was not available.

Figures 8 through 23 present the results of UCR experiments and computer simulations thereof. Throughout this chapter, experimental data are represented by plotted symbols, and computer curves by unbroken lines. With the exception of Run EC-12, the predictions of propylene, NO_2, NO, and ozone behavior are fairly good. The exceptions are the lack of correspondence between the asymptotic NO_2 levels in EC-18, and, consequently, low O_3 predictions and a small delay in the NO_2 peak of EC-11, which is also mirrored in the O_3 profile.

The predictions of carbonyl products (except PAN) are consistently low. At least part of this discrepancy might be attributed to spuriously high measurements (Darnell, 1974), especially at low concentrations.

Table 5

PROPYLENE-NO_x EXPERIMENTS

(In ppm)

EC Run	Initial Concentrations Of Primary Reactants				NO_2/NO_x Ratio	k_1
	Propylene	NO	NO_2	NO_x		
11	0.447	0.115	0.020	0.135	0.15	0.223
12	0.082	0.106	0.012	0.118	0.10	0.223
16	1.036	1.12	0.156	1.27	0.12	0.223
18	0.972	0.106	0.0142	0.148	0.12	0.223
21	0.104	0.558	0.066	0.624	0.11	0.223

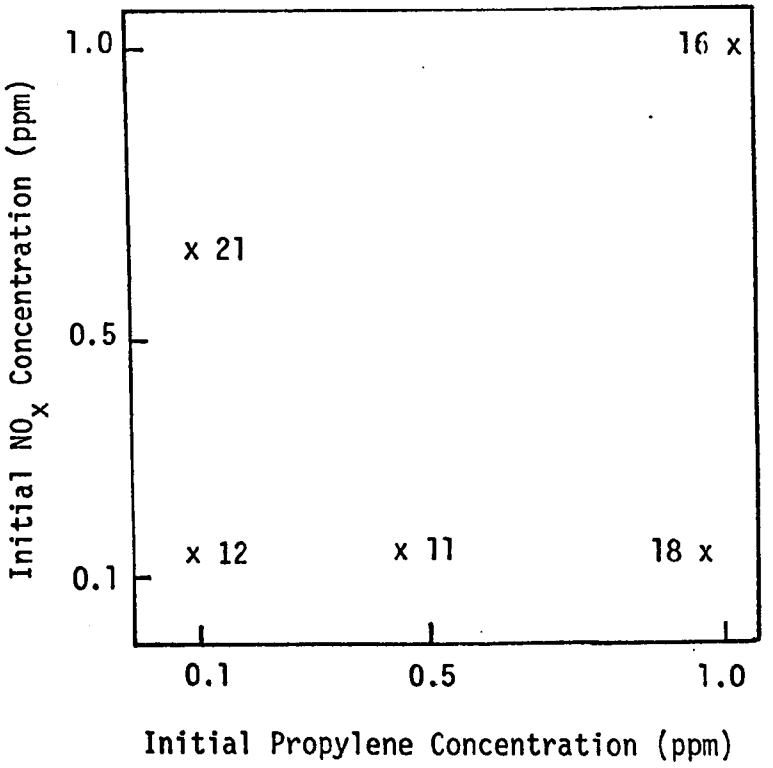

Note: The EC run number is given next to each point

FIGURE 7. PROPYLENE/ NO_x FACTORIAL BLOCK

Table 6

THE PROPYLENE OXIDATION MECHANISM

Reaction	Rate Constant ($ppm^{-1}\ min^{-1}$)
$NO_2 + h\nu \rightarrow NO + O$	0.223[†]
$O + O_2 + M \rightarrow O_3 + M$	2.08×10^{-5}[*]
$O_3 + NO \rightarrow NO_2 + O_2$	25.2
$NO_2 + O \rightarrow NO + O_2$	1.34×10^{4}
$NO_2 + O_3 \rightarrow NO_3 + O_2$	0.05
$NO_3 + NO \rightarrow 2NO_2$	1.3×10^{4}
$NO_3 + NO_2 \rightarrow N_2O_5$	5.6×10^{3}
$N_2O_5 \xrightarrow{M} NO_3 + NO_2$	24[†]
$H_2O + N_2O_5 \rightarrow 2HNO_3$	5×10^{-6}
$NO + NO_2 + 2H_2O \rightarrow 2HNO_2 + H_2O$	1.3×10^{-11}[§]
$2HNO_2 \rightarrow NO + NO_2 + H_2O$	0.24
$HNO_2 + h\nu \rightarrow NO + OH\cdot$	1.5×10^{-2}[†]
$OH\cdot + NO \rightarrow HNO_2$	3×10^{3}
$OH\cdot + NO_2 \rightarrow HNO_3$	1×10^{4}
$HO_2\cdot + NO \rightarrow NO_2 + OH\cdot$	8×10^{2}

Reaction	Rate Constant ($ppm^{-1}\ min^{-1}$)
$O_3 + h\nu \rightarrow O_2 + O(^3P)$	7.3×10^{-3}†
$O_3 + h\nu \rightarrow O_2 + O(^1D)$	1.3×10^{-3}†
$O(^1D) + M \rightarrow O(^3P)$	8.6×10^{4}
$O(^1D) + H_2O \rightarrow 2OH\cdot$	5.1×10^{5}
$O_3 + OH\cdot \rightarrow HO_2\dot{} + O_2$	87
$O_3 + HO_2\dot{} \rightarrow OH\cdot + 2O_2$	2.4
$O_3 \rightarrow$ wall	1×10^{-3}†
$C_3H_6 + OH\cdot \rightarrow CH_3CH(O\cdot)CH_3$	5.0×10^{3}
$C_3H_6 + OH\cdot \rightarrow CH_3CH_2CH_2O\cdot$	2.0×10^{4}
$C_3H_6 + O_3 \rightarrow H_2CO + CH_3C(O)O_2\dot{} + OH\cdot$	0.013
$C_3H_6 + O_3 \rightarrow CH_3CHO + HO_2\dot{} + OH\cdot$	0.007
$C_3H_6 + O \rightarrow CH_3CH_2O\cdot + HO_2\dot{} + CO$	2.66×10^{3}
$C_3H_6 + O \rightarrow CH_3O_2\dot{} + CH_3C(O)O_2\dot{}$	2.66×10^{3}
$H_2CO + OH\cdot \rightarrow H_2O + HO_2\dot{} + CO$	2.1×10^{4}
$CH_3CHO + OH\cdot \rightarrow H_2O + CH_3CO(O)O_2\dot{}$	2.1×10^{4}
$CH_3CH_2CHO + OH\cdot \rightarrow H_2O + CH_3CH_2C(O)O_2\dot{}$	4.5×10^{4}
$CH_3CH(O\cdot)CH_3 \rightarrow CH_3O_2\dot{} + CH_3CHO$	8.35×10^{3}†

Reaction	Rate Constant (ppm^{-1} min^{-1})
$CH_3CH_2CH_2O\cdot \rightarrow CH_3CH_2O_2\cdot + H_2CO$	$8.5 \times 10^{3\dagger}$
$CH_3CH_2O\cdot \rightarrow CH_3O_2\cdot + H_2CO$	$6.0 \times 10^{3\dagger}$
$CH_3CH(O\cdot)CH_3 + O_2 \rightarrow CH_3C(O)CH_3 + HO_2\cdot$	0.04
$CH_3CH_2CH_2O\cdot + O_2 \rightarrow CH_3CH_2CHO + HO_2\cdot$	0.06
$CH_3CH_2O\cdot + O_2 \rightarrow CH_3CHO + HO_2\cdot$	0.04
$CH_3O\cdot + O_2 \rightarrow H_2CO + HO_2\cdot$	0.04
$H_2O_2 + h\nu \rightarrow 2OH\cdot$	$1.06 \times 10^{-3\dagger}$
$H_2CO + h\nu \rightarrow H_2 + CO$	$2.1 \times 10^{-3\dagger}$
$H_2CO + h\nu \rightarrow 2HO_2\cdot + CO$	$6.9 \times 10^{-4\dagger}$
$CH_3CHO + h\nu \rightarrow CH_4 + CO$	$3 \times 10^{-4\dagger}$
$CH_3CHO + h\nu \rightarrow CH_3O_2\cdot + HO_2\cdot + CO$	$7 \times 10^{-4\dagger}$
$CH_3CH_2CHO + h\nu \rightarrow CH_3CH_3 + CO$	$3 \times 10^{-4\dagger}$
$CH_3CH_2CHO + h\nu \rightarrow CH_3CH_2O_2\cdot + HO_2\cdot + CO$	$7 \times 10^{-4\dagger}$
$CH_3O_2\cdot + NO \rightarrow NO_2 + CH_3O\cdot$	1×10^3
$CH_3CH_2O_2\cdot + NO \rightarrow NO_2 + CH_3CH_2O\cdot$	1×10^3
$CH_3CH_2CH_2O_2\cdot + NO \rightarrow NO_2 + CH_3CH_2CH_2O\cdot$	1×10^3
$CH_3C(O)O_2\cdot + NO \rightarrow NO_2 + CH_3O_2\cdot + CO_2$	1×10^3

Reaction	Rate Constant ($ppm^{-1}\ min^{-1}$)
$CH_3CH_2C(O)O_2^{\cdot} + NO \rightarrow NO_2 + CH_3CH_2O_2^{\cdot} + CO_2$	1×10^3
$CH_3C(O)O_2^{\cdot} + NO_2 \rightarrow CH_3C(O)O_2NO_2$	3×10^2
$CH_3CH_2C(O)O_2^{\cdot} + NO_2 \rightarrow CH_3CH_2C(O)O_2NO_2$	3×10^2
$CH_3C(O)O_2NO_2 \rightarrow CH_3O_2^{\cdot} + NO_3 + CO_2$	3×10^{-3}†
$CH_3CH_2C(O)O_2NO_2 \rightarrow CH_3CH_2O_2^{\cdot} + NO_3 + CO_2$	3×10^{-3}†
$HO_2^{\cdot} + HO_2^{\cdot} \rightarrow H_2O_2 + O_2$	6×10^3
$HO_2^{\cdot} + CH_3O_2^{\cdot} \rightarrow CH_3OOH + O_2$	3×10^3
$HO_2^{\cdot} + CH_3CH_2O_2^{\cdot} \rightarrow CH_3CH_2OOH + O_2$	3×10^3
$HO_2^{\cdot} + CH_3C(O)O_2^{\cdot} \rightarrow CH_3C(O)OOH + O_2$	3×10^3
$HO_2^{\cdot} + CH_3CH_2C(O)O_2^{\cdot} \rightarrow CH_3CH_2C(O)OOH + O_2$	3×10^3

† min^{-1}

* $ppm^{-2}\ min^{-1}$

§ $ppm^{-3}\ min^{-3}$

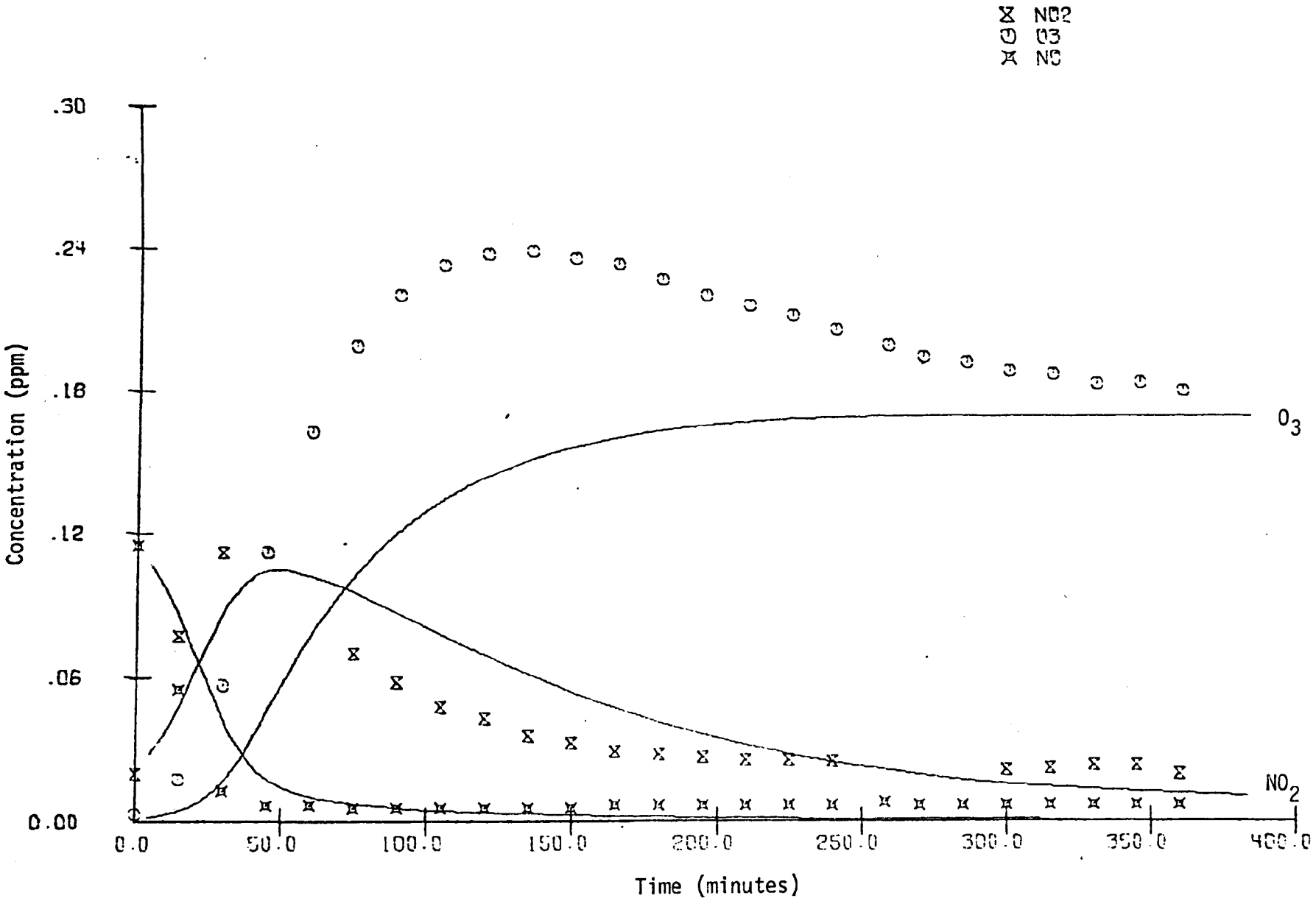

FIGURE 8. EC-11 SIMULATION RESULTS AND UCR DATA FOR NO_2, O_3, AND NO

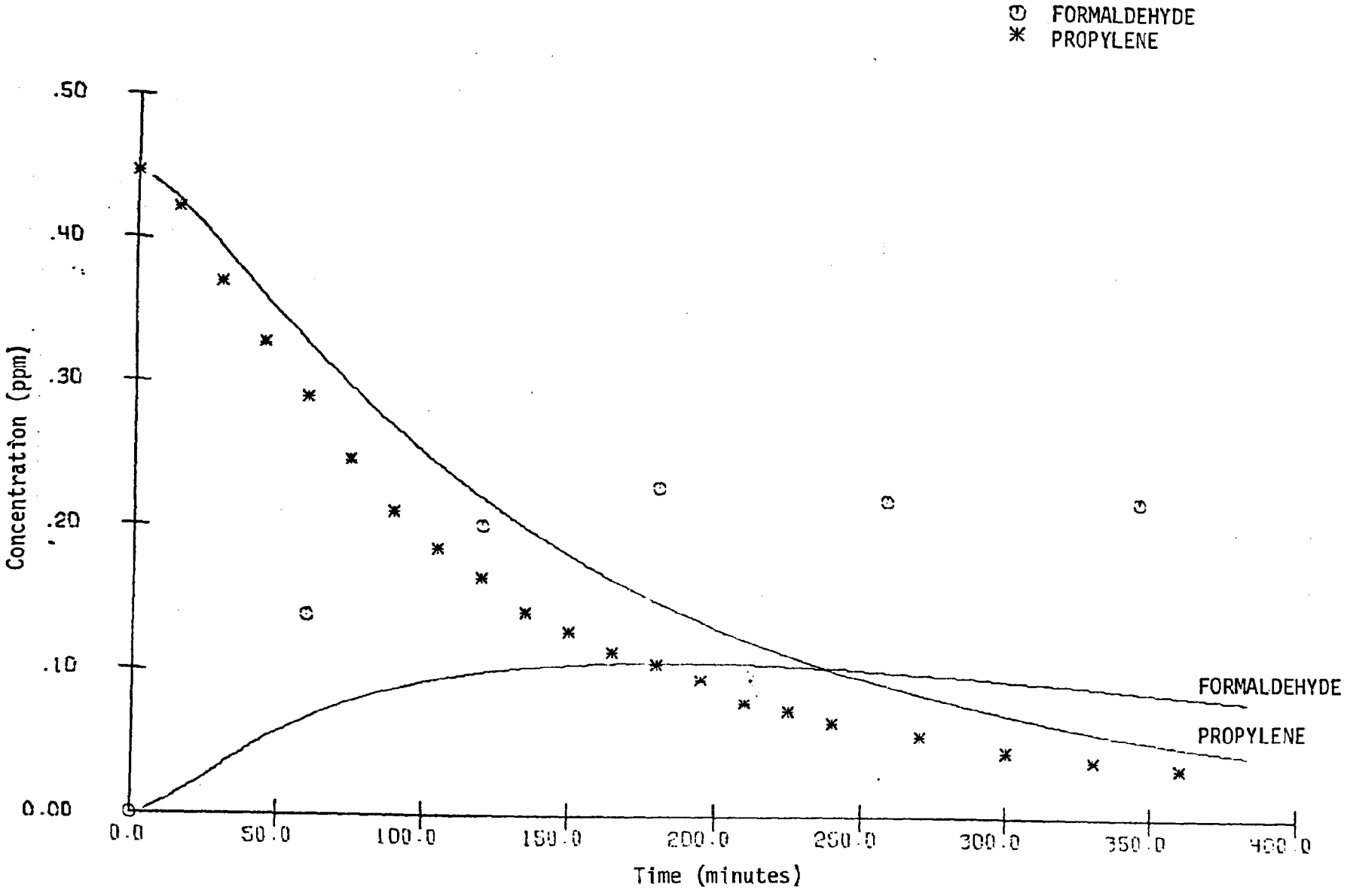

FIGURE 9. EC-11 SIMULATION RESULTS AND UCR DATA FOR PROPYLENE AND FORMALDEHYDE

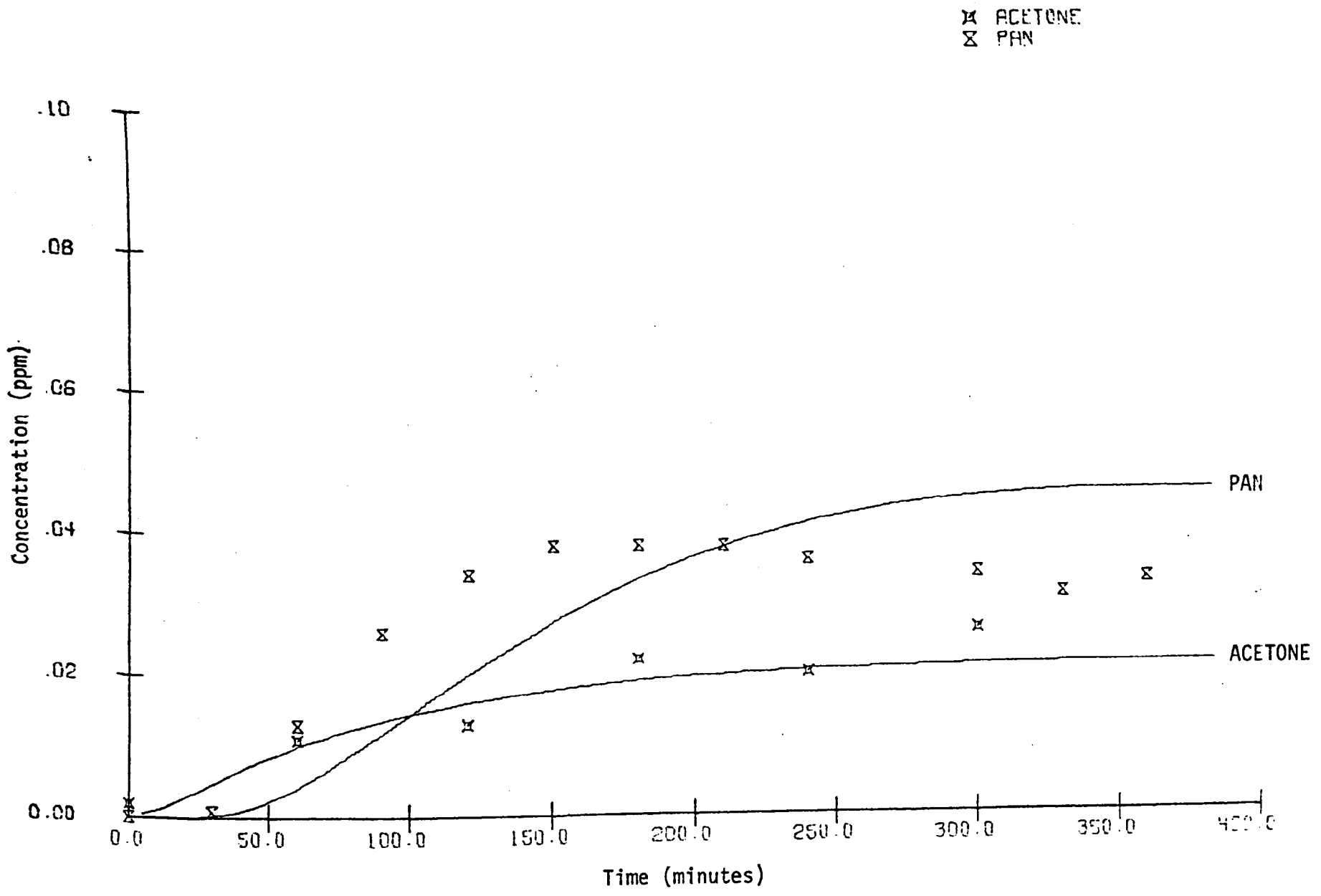

FIGURE 10. EC-11 SIMULATION RESULTS AND UCR DATA FOR ACETONE AND PAN

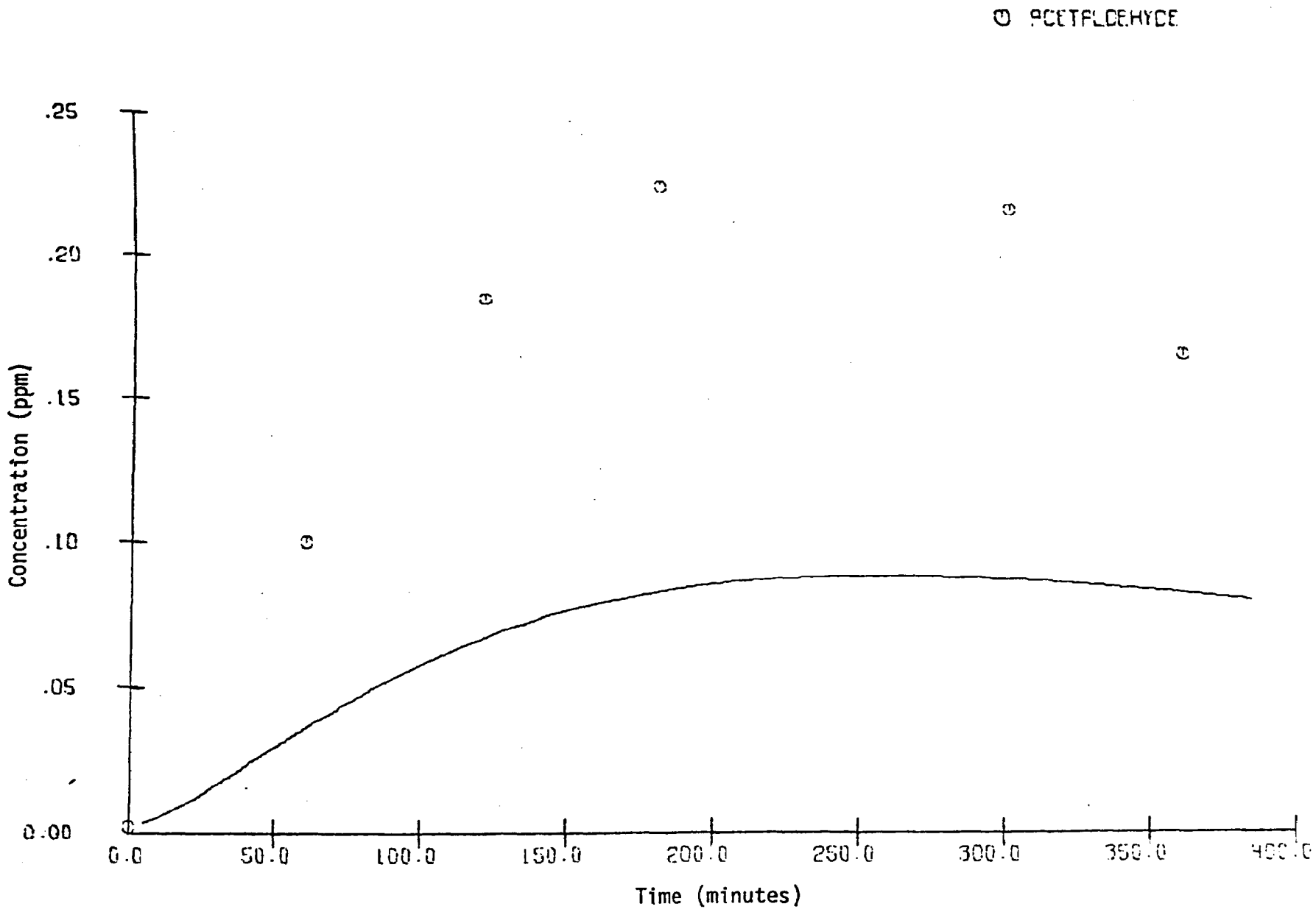

FIGURE 11. EC-11 SIMULATION RESULTS AND UCR DATA FOR ACETALDEHYDE

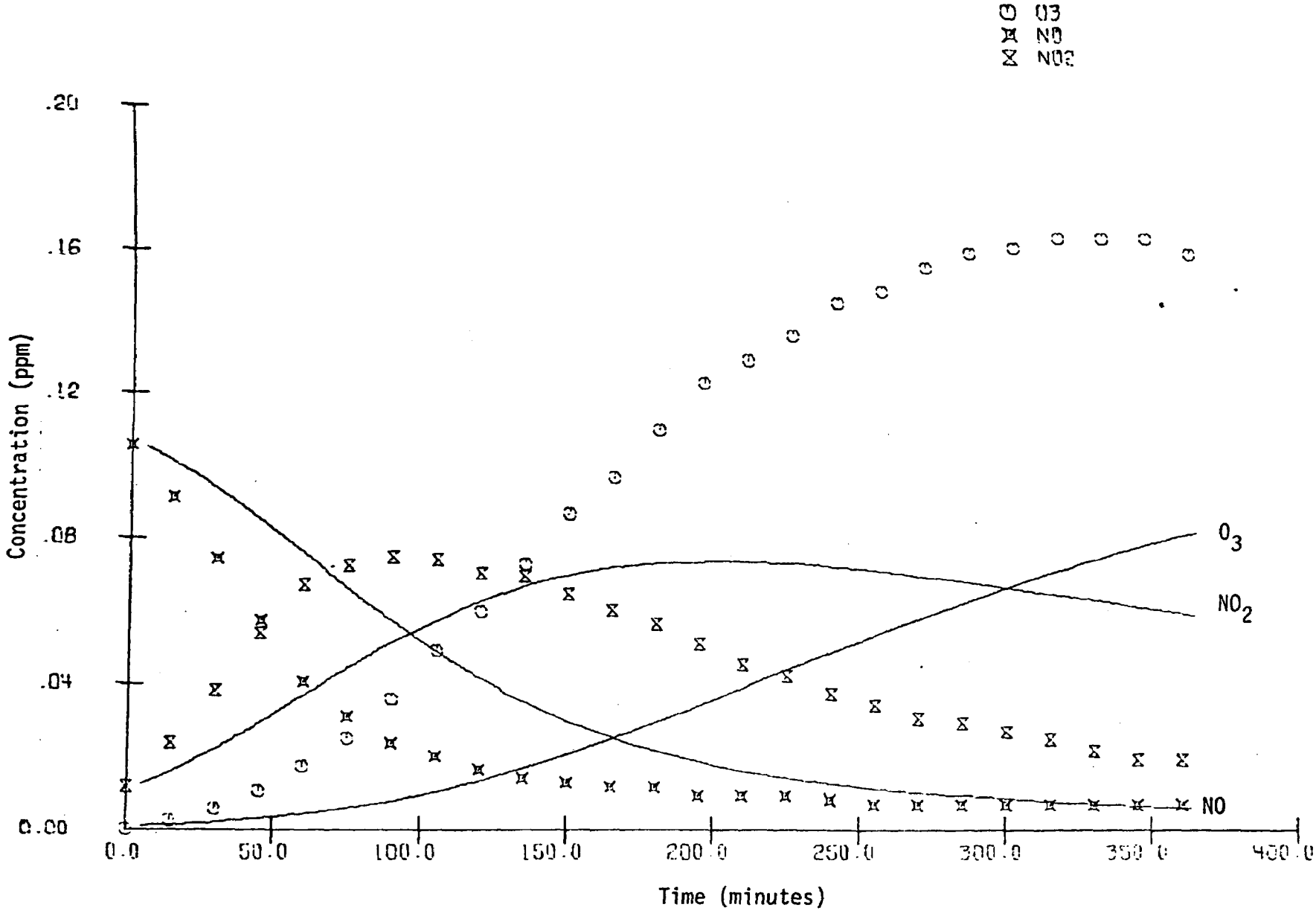

FIGURE 12. EC-12 SIMULATION RESULTS AND UCR DATA FOR O_3, NO, and NO_2

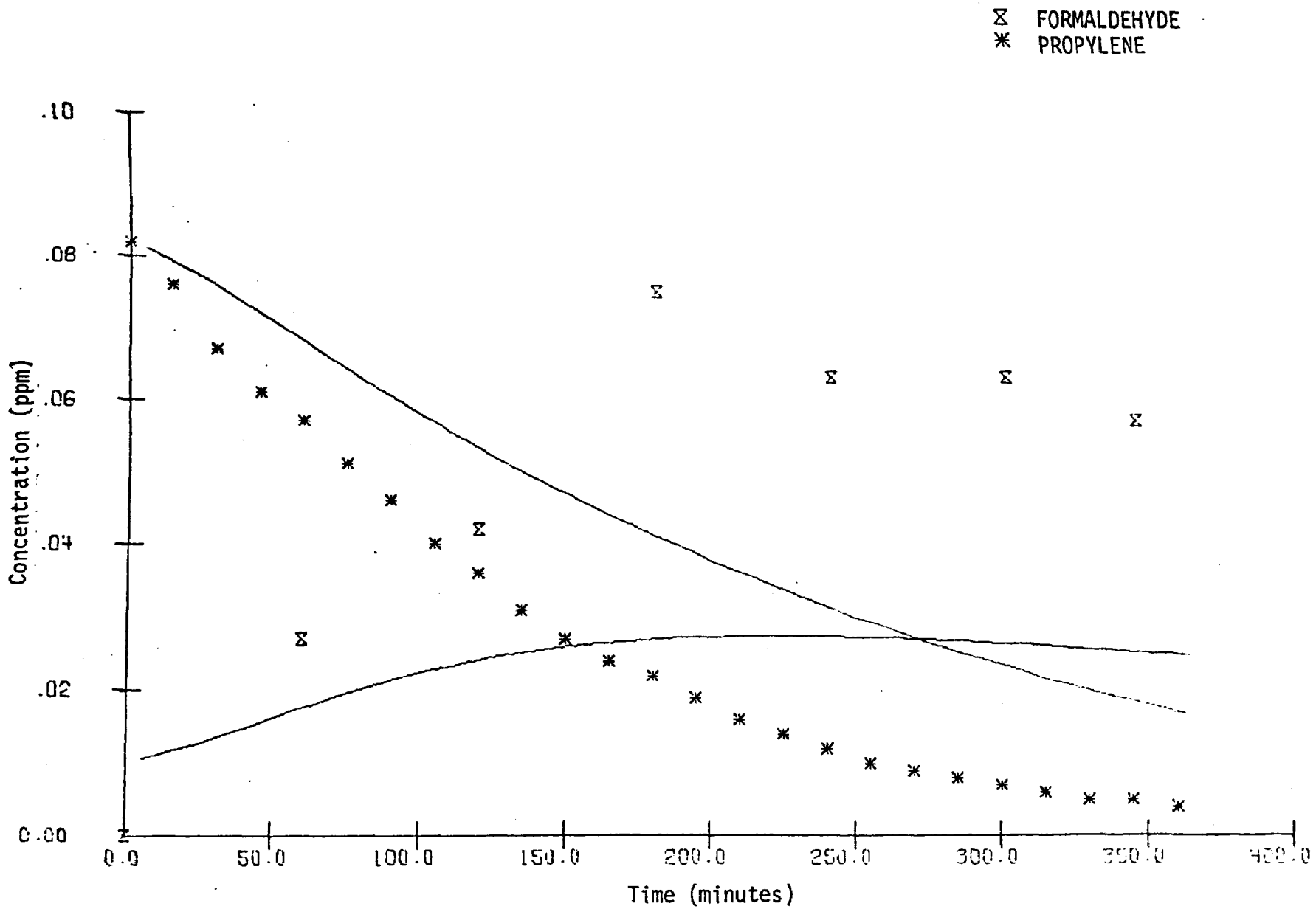

FIGURE 13. EC-12 SIMULATION RESULTS AND UCR DATA FOR PROPYLENE AND FORMALDEHYDE

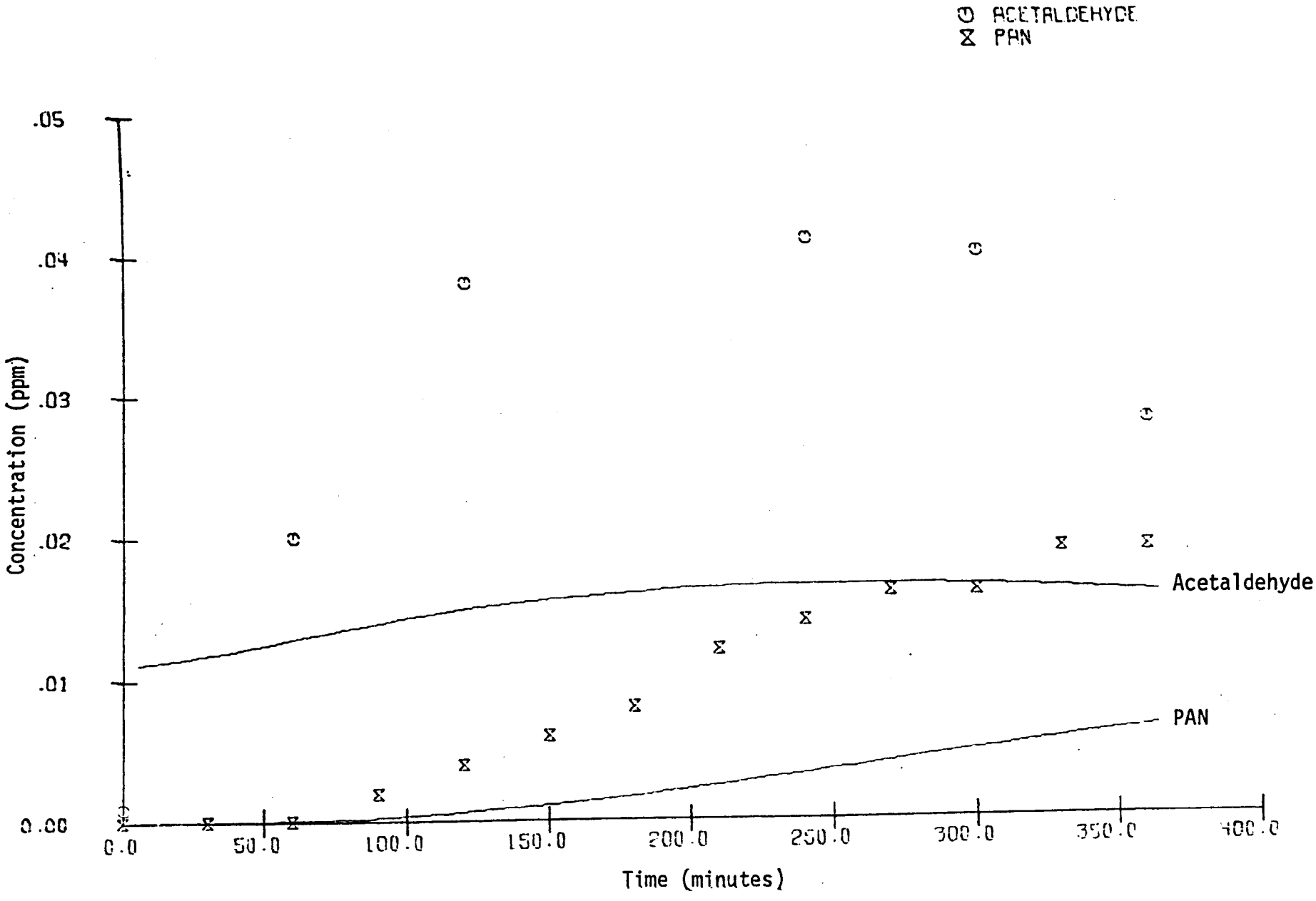

FIGURE 14. SIMULATION RESULTS AND UCR DATA FOR PAN AND ACETALDEHYDE

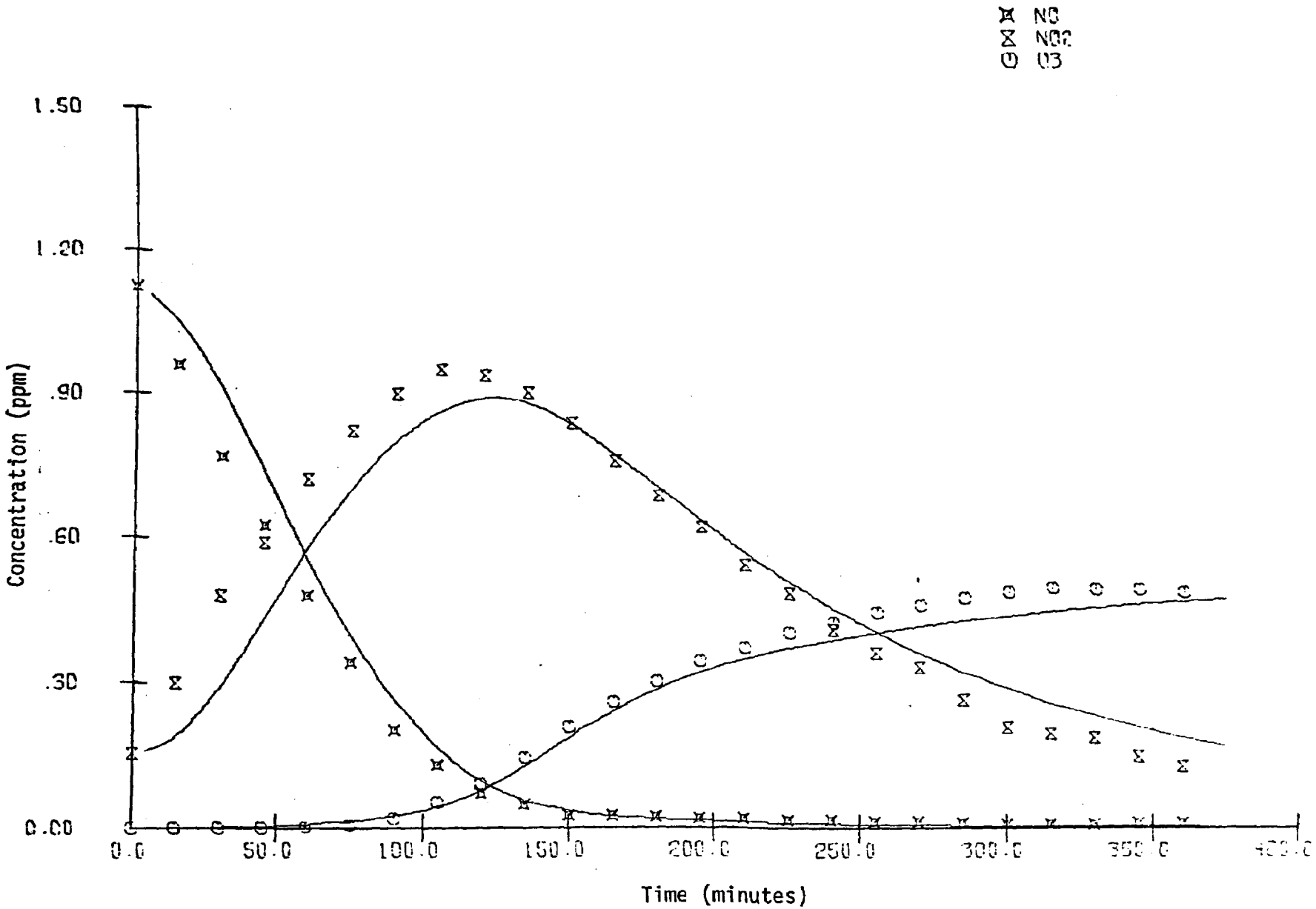

FIGURE 15. EC-16 SIMULATION RESULTS AND UCR DATA FOR O_3, NO, AND NO_2

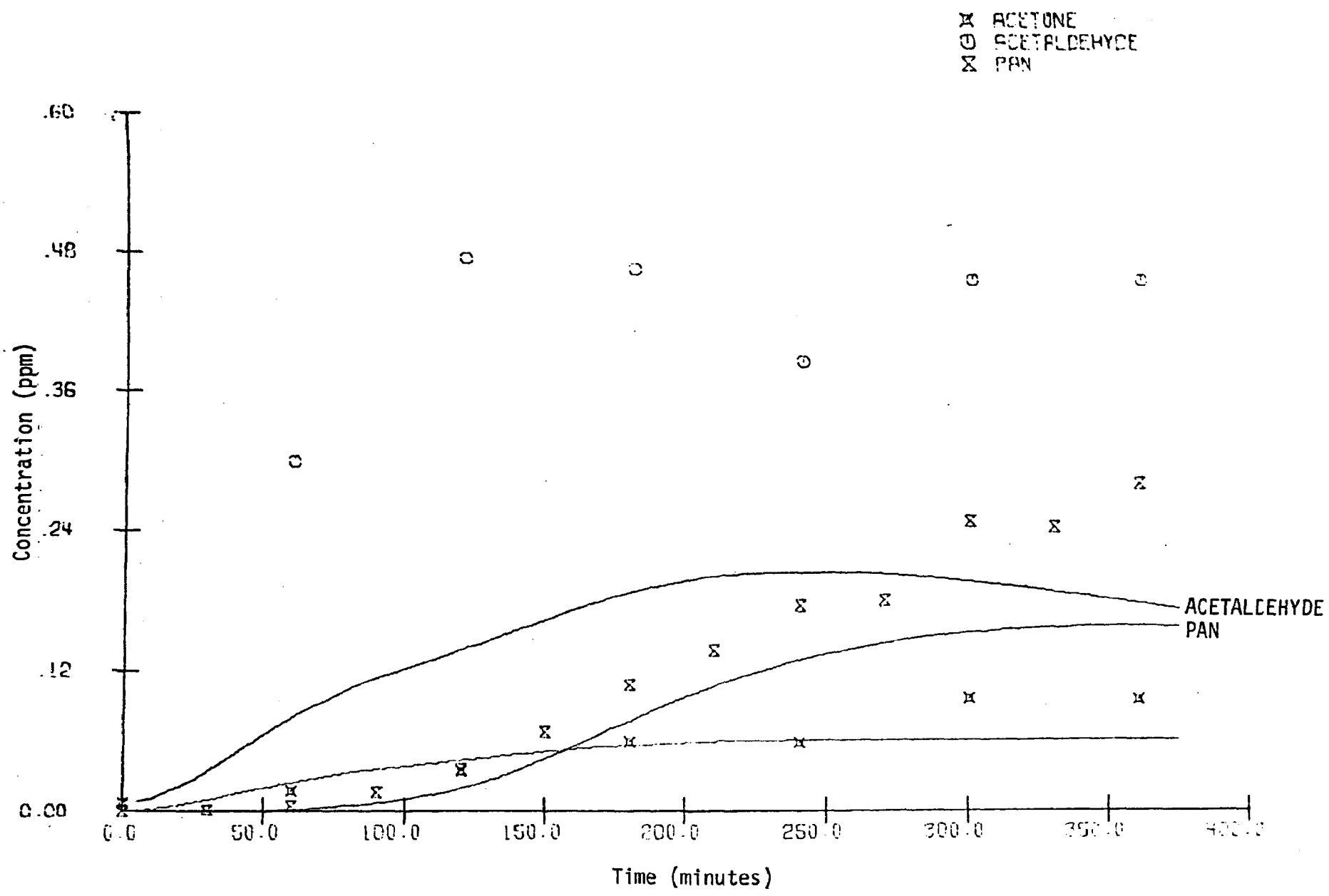

FIGURE 16. EC-16 SIMULATION RESULTS AND UCR DATA FOR ACETONE, ACETALDEHYDE, AND PAN

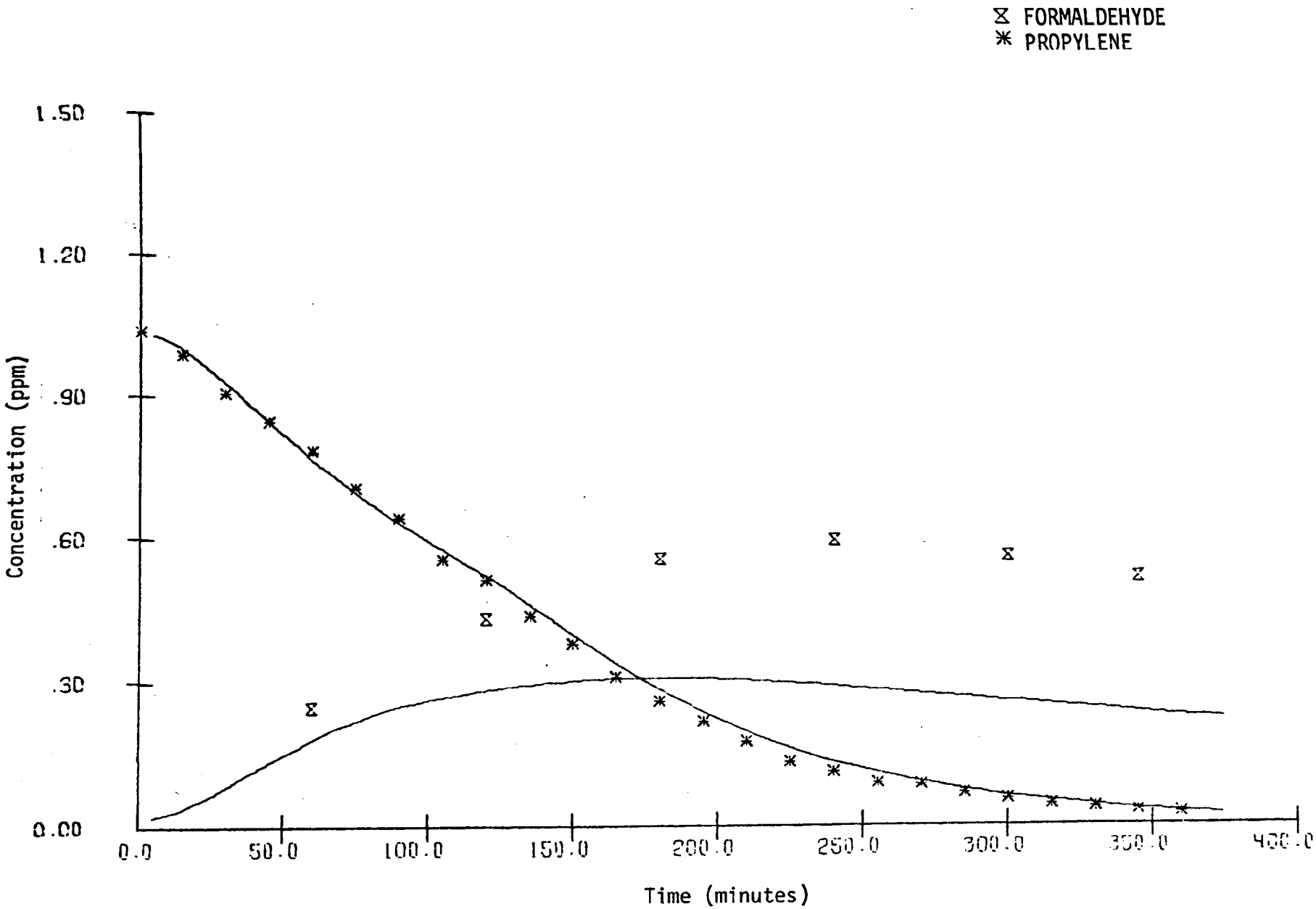

FIGURE 17. EC-16 SIMULATION RESULTS AND UCR DATA FOR PROPYLENE AND FORMALDEHYDE

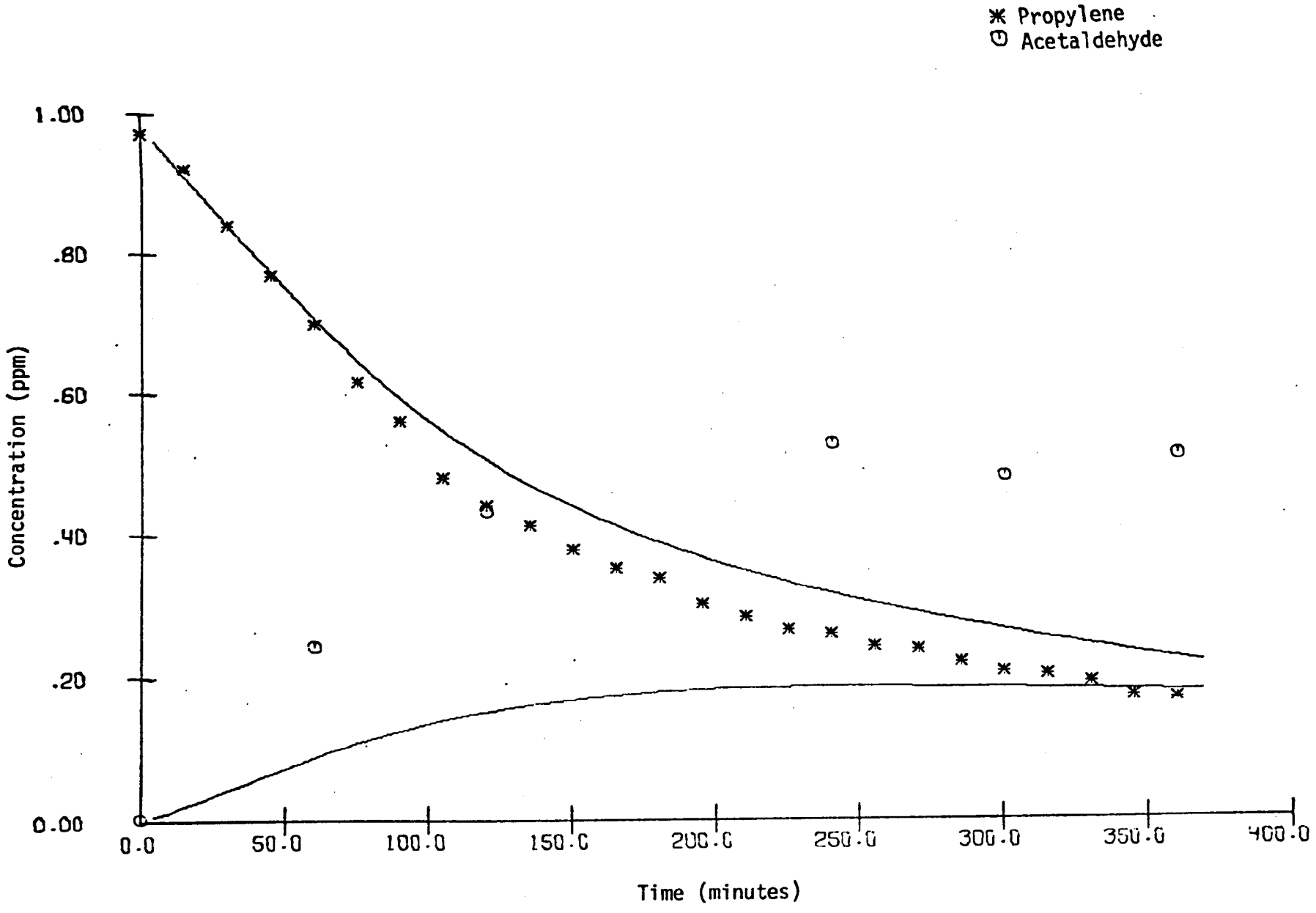

FIGURE 18. EC-18 SIMULATION RESULTS AND UCR DATA FOR PROPYLENE AND ACETALDEHYDE

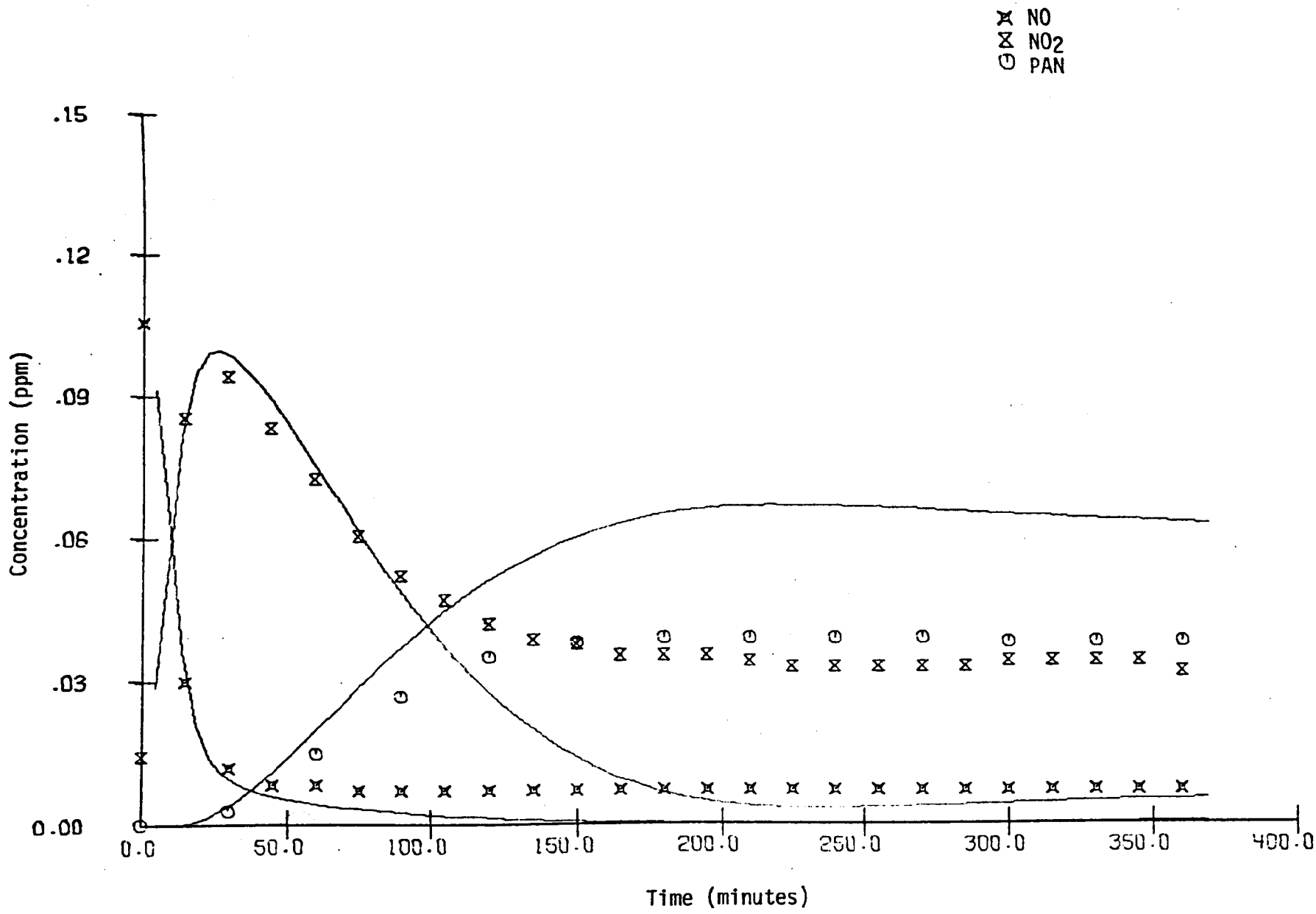

FIGURE 19. EC-18 SIMULATION RESULTS AND UCR DATA FOR NO, NO_2, AND PAN

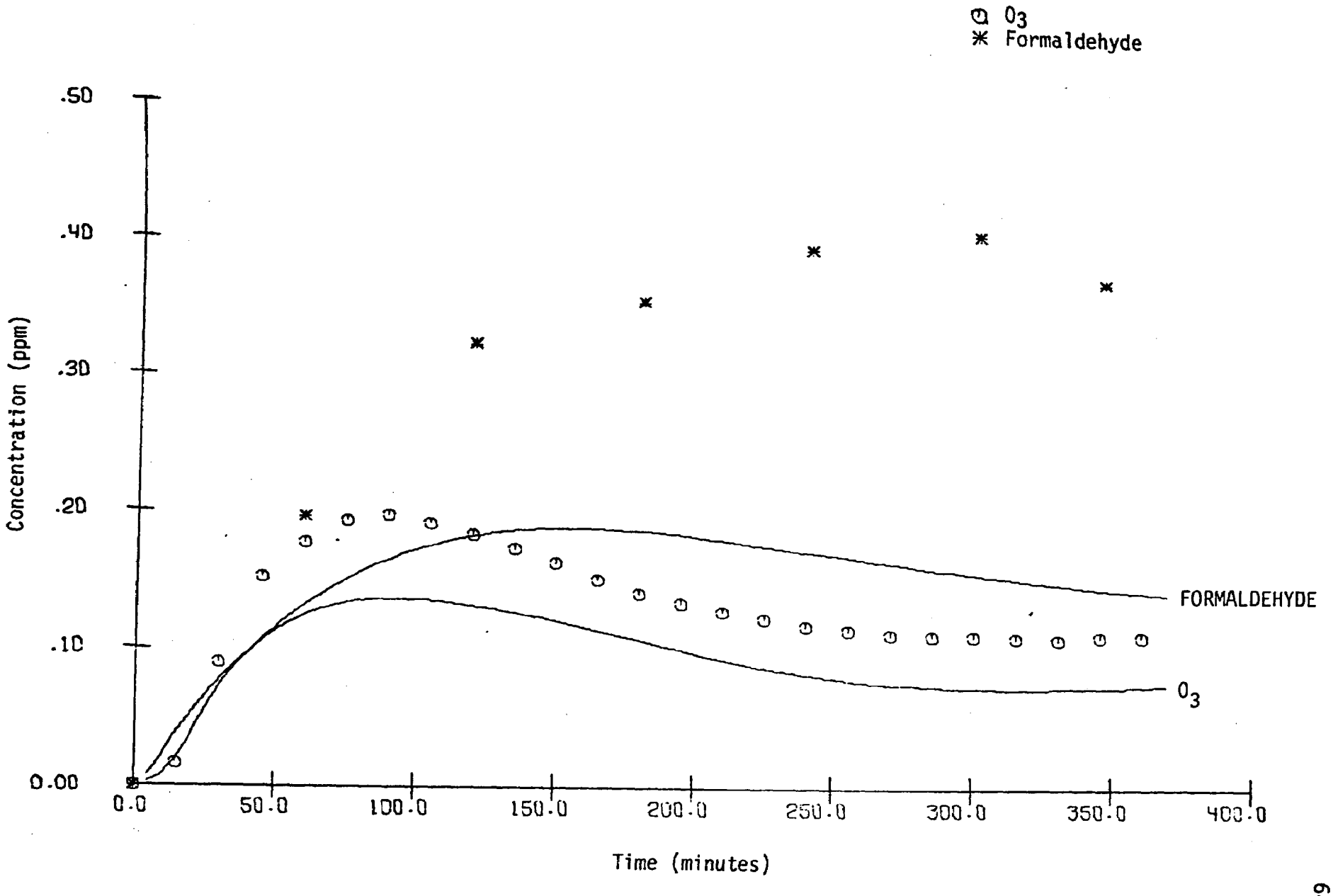

FIGURE 20. EC-18 SIMULATION RESULTS AND UCR DATA FOR O_3 AND FORMALDEHYDE

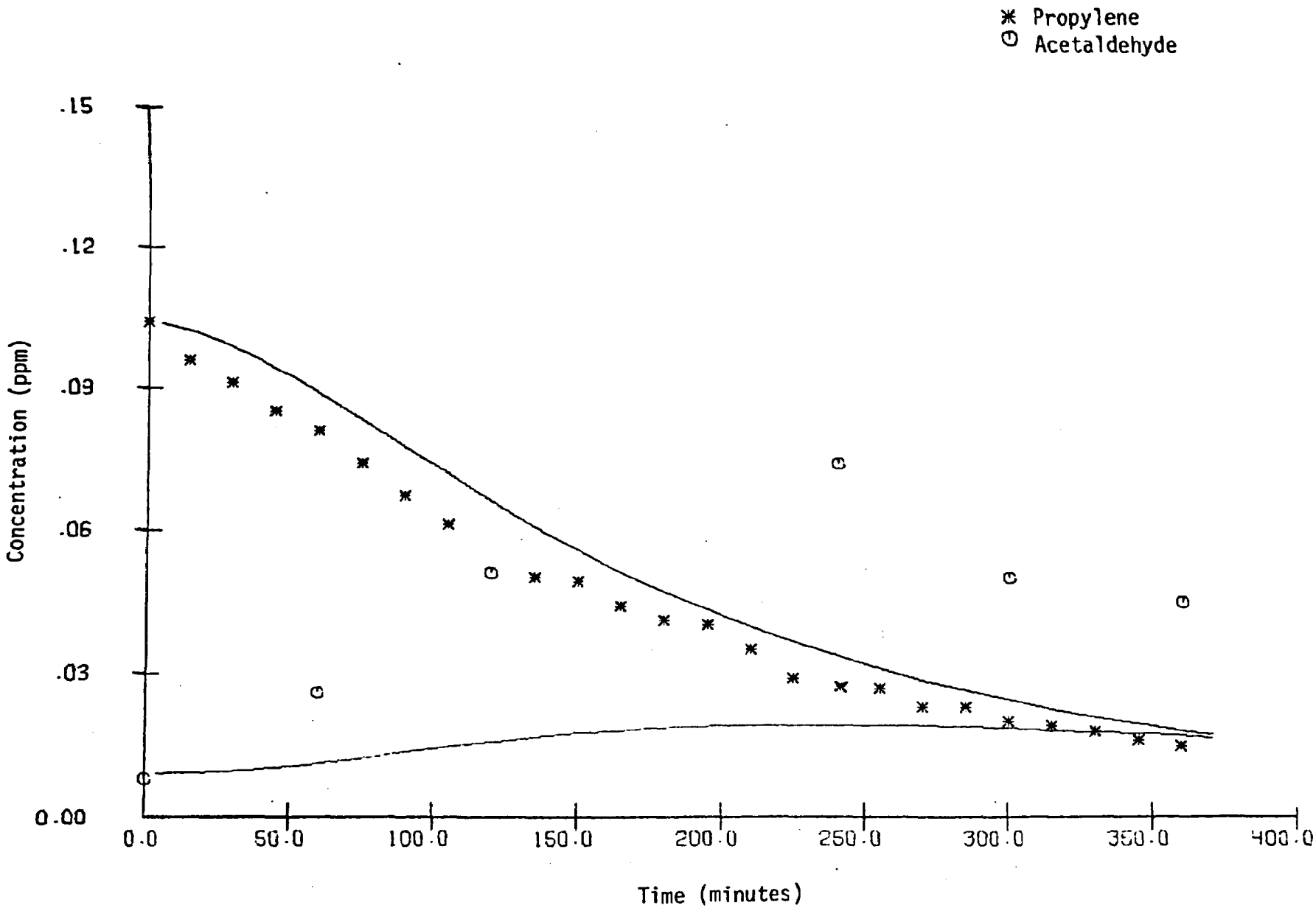

FIGURE 21. EC-21 SIMULATION RESULTS AND UCR DATA FOR PROPYLENE AND ACETALDEHYDE

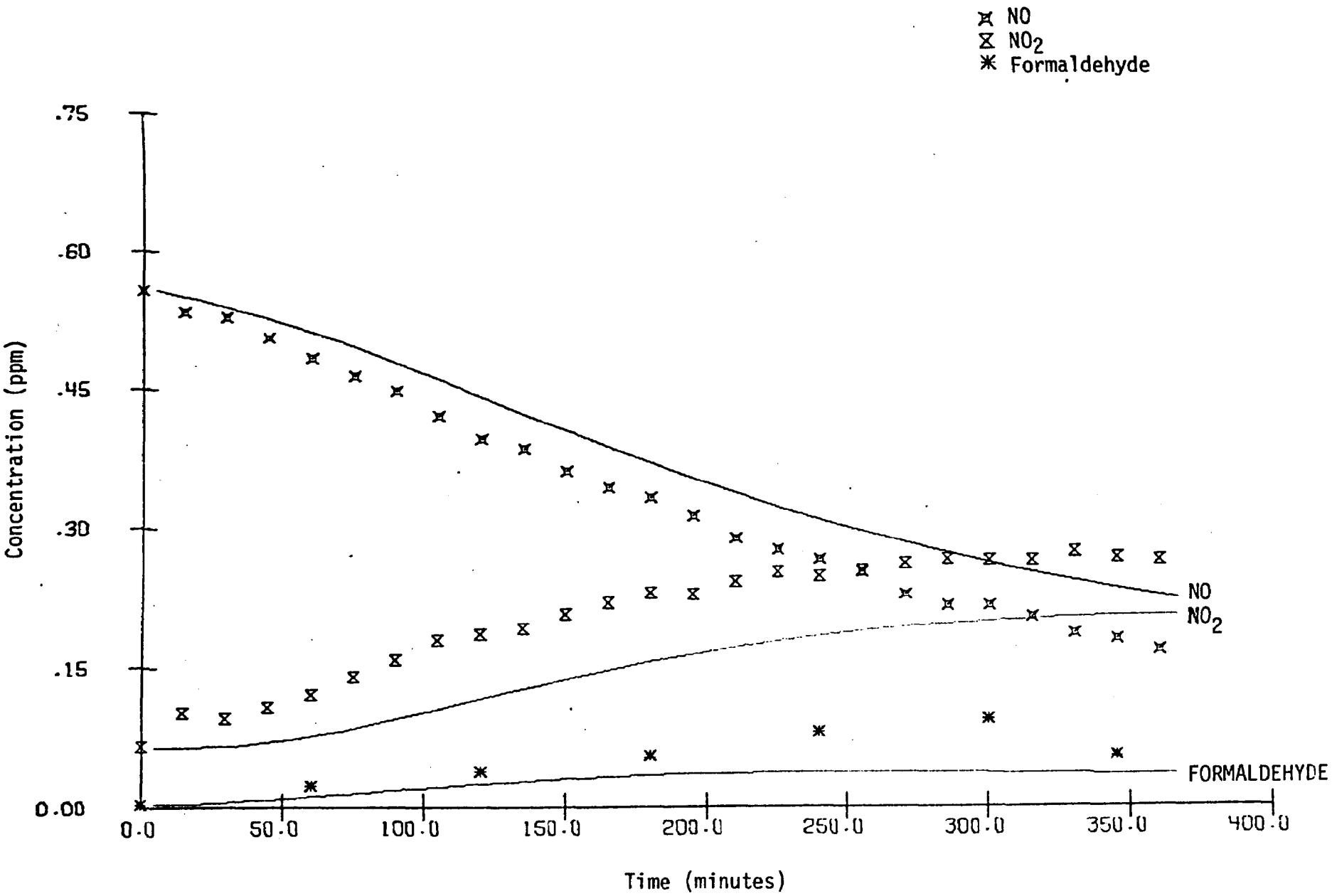

FIGURE 22. EC-21 SIMULATION RESULTS AND UCR DATA FOR NO, NO_2, AND FORMALDEHYDE

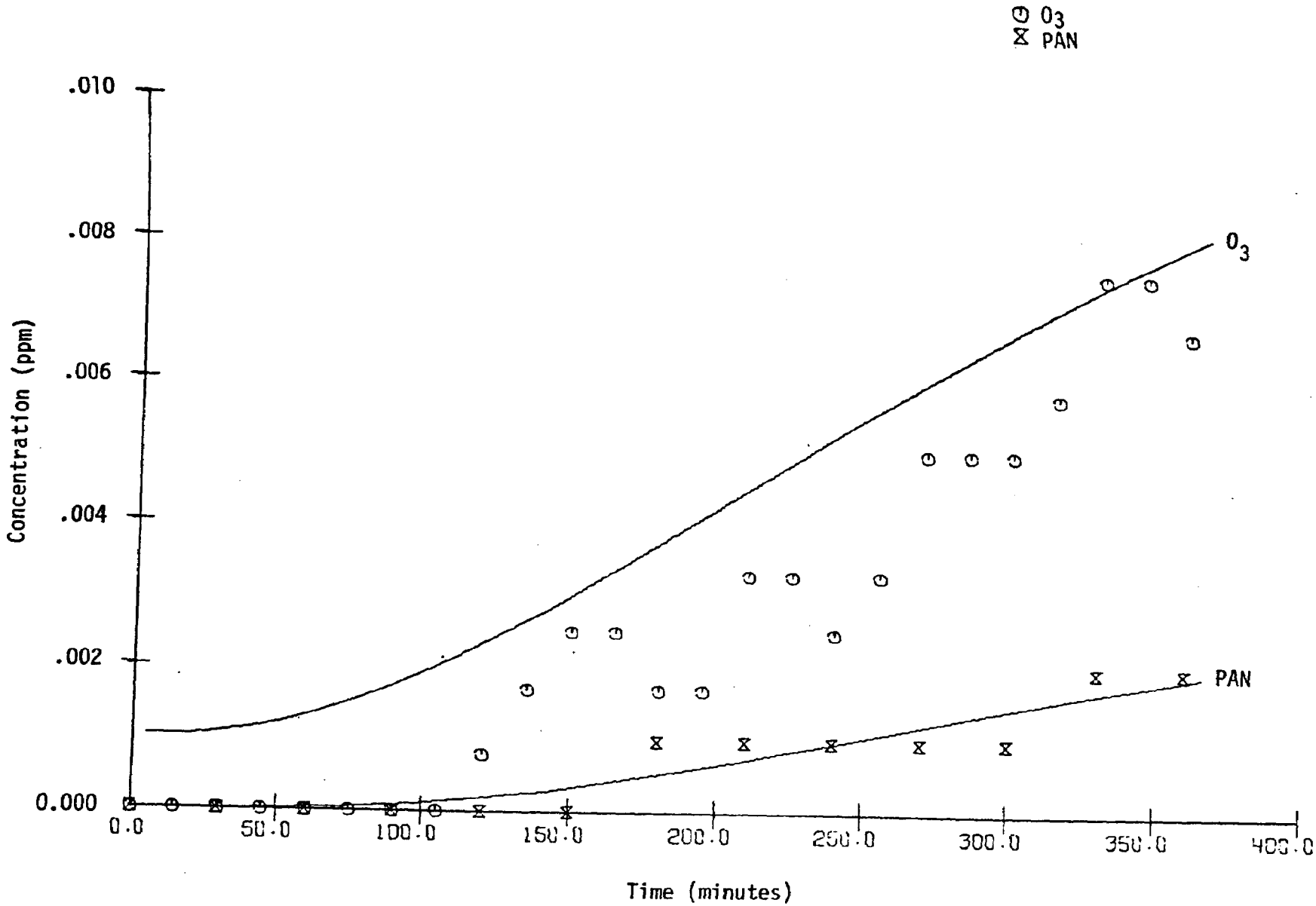

FIGURE 23. EC-21 SIMULATION RESULTS AND UCR DATA FOR O_3 AND PAN

PAN predictions are sometimes high (EC-18 and EC-11) and sometimes low (EC-16 and EC-12). Calibration of the panalyzer has been an enigma; thus, data values may be suspect. But the chemistry of PAN is still largely unexplored, and this is very likely a large part of the problem.

The results for EC-12 are inexplicable. The data indicate a total absence of an induction period, but mechanistic predictions completely disagree with this observation. If the current mechanism's validity is accepted, this completely disparate behavior can be resolved only by blaming wall effects. The reactant concentrations in EC-12 are extremely low, and the wall effects are hence, relatively, at their maximum. A small source of radicals, such as photolysis of off-gassed aldehyde or HNO_2, could provide the initial impetus to this system.* A recent experiment done at UCR provides further evidence in favor of this explanation. CO oxidation to CO_2 was observed upon irradiation of a supposedly clean chamber filled with dry synthetic air. The oxidation rate of $\sim$0.1 ppm per hour with CO present at 100 ppm indicates that the OH· concentration in this system could have reached $\sim 10^{-7}$ ppm. Presumably, this was due to a wall source of radicals.

2. The Butane-NO_x-Air System

a. The Mechanism Used

The butane mechanism was considerably less successful than the propylene mechanism, even though they are similar. The modifications to the propylene mechanisms to adopt it to butane included adding reactions pertiment to butane and reflecting changes in k_1. Photolysis rate constants used in the butane simulations were computed from a 10 nm filter-shifted spectrum (as with propene). The reaction changes are listed in Table 7. Most of the changes included in Table 7 represent merely the addition of four-carbon species. Most notable is the ratio of 2.4 to 1 for internal to terminal hydrogen abstraction by OH· from

* In these simulations, initial concentrations of 0.01 for formaldehyde and acetaldehyde were used. The carbon balance obtained from product measurements (excluding CO) at UCR is usually 60 to 80 percent. However, in EC-12, this balance was about 110 percent--hence, the suspicion that unaccounted-for sources (or initial concentrations) were present.

Table 7

REACTION CHANGES MADE FOR THE BUTANE SIMULATIONS

(With the propylene chemistry eliminated and all photolysis rates scaled to k_1)

Reaction	Rate Constant
$C_4H_{10} + OH\cdot \xrightarrow{O_2} H_2O + C_4H_9O_2\cdot$	1.0×10^3 ppm^{-1} min^{-1}
$C_4H_{10} + OH\cdot \xrightarrow{O_2} H_2O + CH_3CH_2CH(O_2\cdot)CH_3$	2.4×10^3 ppm^{-1} min^{-1}
$C_4H_{10} + O \xrightarrow{O_2} CH_3CH_2CH(O_2\cdot)CH_3 + OH\cdot$	64 ppm^{-1} min^{-1}
$CH_3CH_2CH_2CHO + OH\cdot \xrightarrow{O_2} H_2O + CH_3CH_2CH_2C(O)O_2\cdot$	4.5×10^4 ppm^{-1} min^{-1}
$CH_3CH_2C(O)CH_3 + OH\cdot \xrightarrow{O_2} CH_3C(O)OH + CH_3CH_2O_2\cdot$	1×10^4 ppm^{-1} min^{-1}
$CH_3CH_2CH_2CH_2O\cdot \longrightarrow CH_3CH_2CH_2O_2\cdot + H_2CO$	8.5×10^3 min^{-1}
$CH_3CH_2CH_2CH_2O\cdot + O_2 \longrightarrow CH_3CH_2CH_2CHO + HO_2\cdot$	0.2 ppm^{-1} min^{-1}
$CH_3CH_2CH(O\cdot)CH_3 + O_2 \longrightarrow CH_3CH_2C(O)CH_3 + HO_2\cdot$	0.2 ppm^{-1} min^{-1}
$CH_3CH_2CH(O\cdot)CH_3 \longrightarrow CH_3CH_2O_2\cdot + CH_3CHO$	1.3×10^4 min^{-1}
$CH_3CH_2C(O)CH_3 + h\nu \xrightarrow{2O_2} CH_3CH_2O_2\cdot + CH_3C(O)O_2\cdot$	7.8×10^{-4} min^{-1}
$CH_3CH_2CH_2CHO + h\nu \longrightarrow CH_3CH_2CH_3 + CO$	3.1×10^{-4} min^{-1}
$CH_3CH_2CH_2CHO + h\nu \xrightarrow{2O_2} CH_3CH_2CH_2O_2\cdot + HO_2\cdot + CO$	7.2×10^{-4} min^{-1}
$CH_3CH_2CH_2CH_2O_2\cdot + NO \longrightarrow NO_2 + CH_3CH_2CH_2CH_2O\cdot$	1.0×10^3 ppm^{-1} min^{-1}
$CH_3CH_2CH(O_2\cdot)CH_3 + NO \longrightarrow NO_2 + CH_3CH_2CH(O\cdot)CH_3$	1.0×10^3 ppm^{-1} min^{-1}
$CH_3CH_2CH_2C(O)O_2\cdot + NO \xrightarrow{O_2} NO_2 + CH_3CH_2CH_2O_2\cdot + CO_2$	1.0×10^3 ppm^{-1} min^{-1}
$CH_3CH_2CH_2C(O)O_2\cdot + NO_2 \longrightarrow CH_3CH_2CH_2C(O)O_2NO_2$	3.0×10^2 ppm^{-1} min^{-1}
$CH_3CH_2CH_2C(O)O_2NO_2 \xrightarrow{O_2} CH_3CH_2CH_2O_2\cdot + NO_3 + CO_2$	3.0×10^3 min^{-1}
$CH_3CH_2CH_2C(O)O_2\cdot + NO_2 \longrightarrow CH_3CH_2CH_2C(O)O_2H + O_2$	3.0×10^3 ppm^{-1} min^{-1}

C_4H_{10}. This is lower than the ratio for abstraction by Cl atoms (Morrison and Boyd, 1971), although one might expect it to be higher because OH· has less electron affinity than Cl (Hefter et al., 1972) and should therefore be more selective in its attack. A ratio measurement is desirable.

Another element of Table 7 worth commenting on is the reaction of OH· with $CH_3CH_2C(O)CH_3$ (methlyethylketone, or MEK). The rate of hydrogen abstraction from MEK can be computed from Greiner's formula for paraffins (Johnson et al., 1970), with a modification to take into account the lowering of the secondary C-H bond dissociation energy. Scaled to the current value of 3.7×10^3 ppm^{-1} min^{-1} for C_4H_{10} + OH·, the rate constant for $CH_3CH_2C(O)CH_3$ + OH· → abstraction products is about 2×10^3 ppm^{-1} min^{-1}. However, an analogy with propylene suggests that addition to the C-O double bond may be a faster reaction. Although repeated experiments were performed by UCR (i.e., experiments with the same initial NO_x/butane ratio), we chose only one experiment for each of the different NO_x/butane ratios.

$$CH_3CH_2C(O)CH_3 \rightarrow CH_3CH_2\overset{O\cdot}{\overset{|}{C}}(OH)CH_3 \qquad (32')$$

followed by

$$CH_3CH_2\overset{O\cdot}{\overset{|}{C}}(OH)CH_3 \xrightarrow{O_2} CH_3C(O)OH + CH_3CH_2O_2^{\cdot} \quad .$$

The net products are acetic acid and an ethylperoxy radical. The lower limit to $k_{32'}$ was taken to be 2×10^3 ppm^{-1} min^{-1}, and 1×10^4 ppm^{-1} min^{-1} was used in the simulations.

The carbon balance (excluding CO and CO_2) of the butane data was usually about 20 to 40 percent, which indicates undetected carbon-containing species. Acetic acid may have been one of them.

b. Results

The initial concentrations and values of k_1 for the butane-NO_x block (Figure 24) are recorded in Table 8. Model predictions, along with UCR data, appear in Figures 25 through 39. Generally speaking, the mechanism predicts

an overall rate greatly in excess of that observed, the only exception being the low butane run, EC-42. Excluding EC-42, the universal over-prediction of

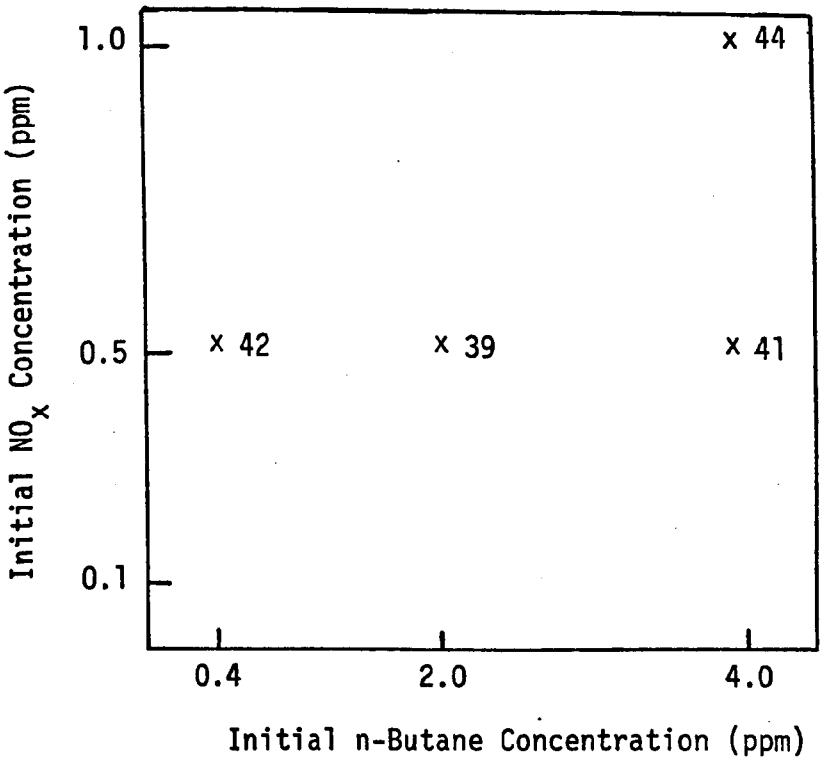

Note: The EC run number is given next to each point.

FIGURE 24. n-BUTANE/NO_x FACTORIAL BLOCK

Table 8

INITIAL CONCENTRATIONS OF PRIMARY REACTANTS AND VALUES OF k_1 FOR THE UCR BUTANE-NO_x EXPERIMENTS

(In ppm)

Run No.	Butane	NO	NO_2	NO_x	NO_2/NO_x	k_1
EC-39	2.2	0.547	0.060	0.607	0.10	0.240
EC-41	4.03	0.524	0.068	0.592	0.12	0.238
EC-42	0.385	0.542	0.059	0.601	0.10	0.235
EC-44	3.92	1.14	0.132	1.27	0.10	0.230

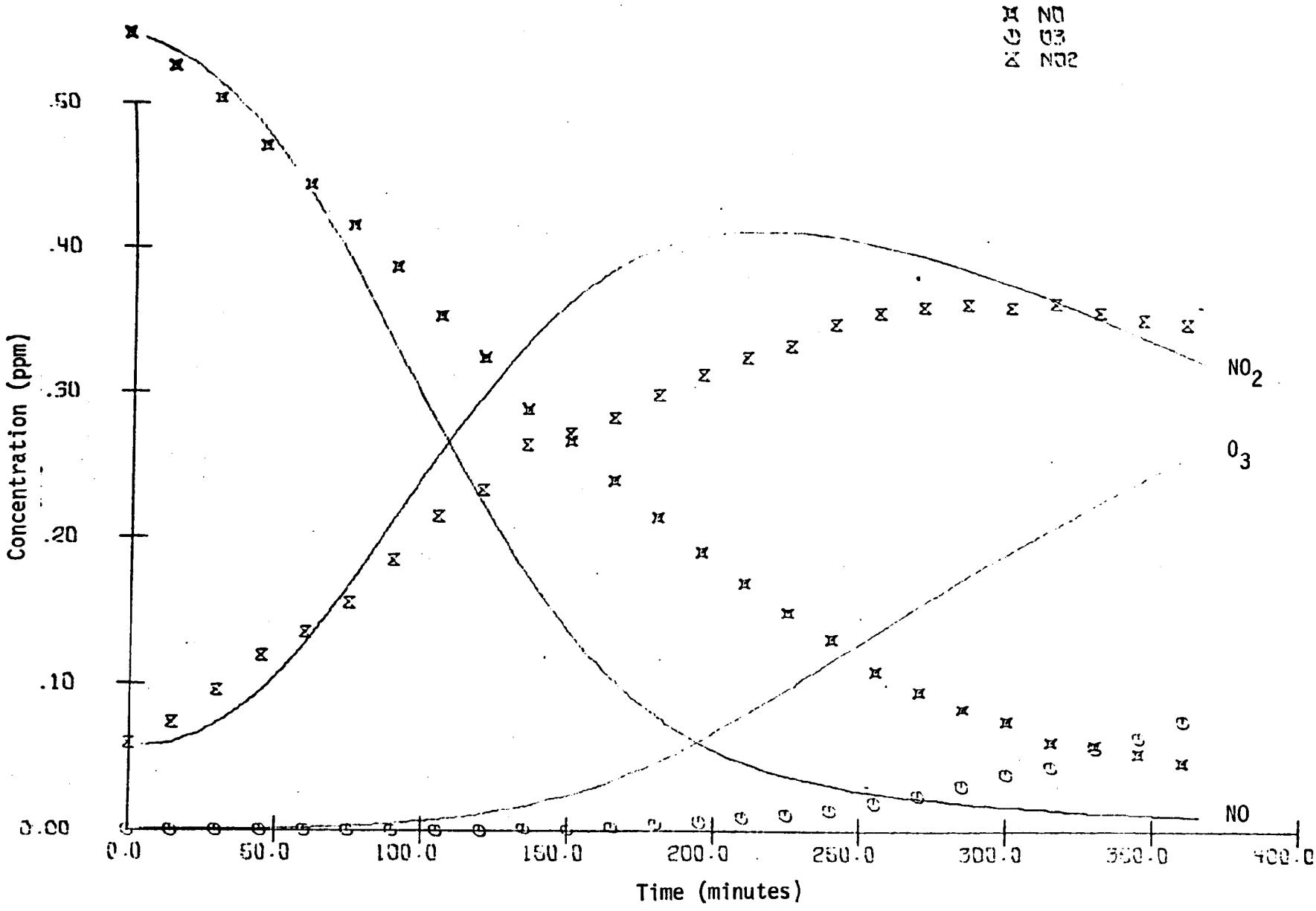

FIGURE 25. EC-39 SIMULATION RESULTS AND UCR DATA FOR O_3, NO, AND NO_2

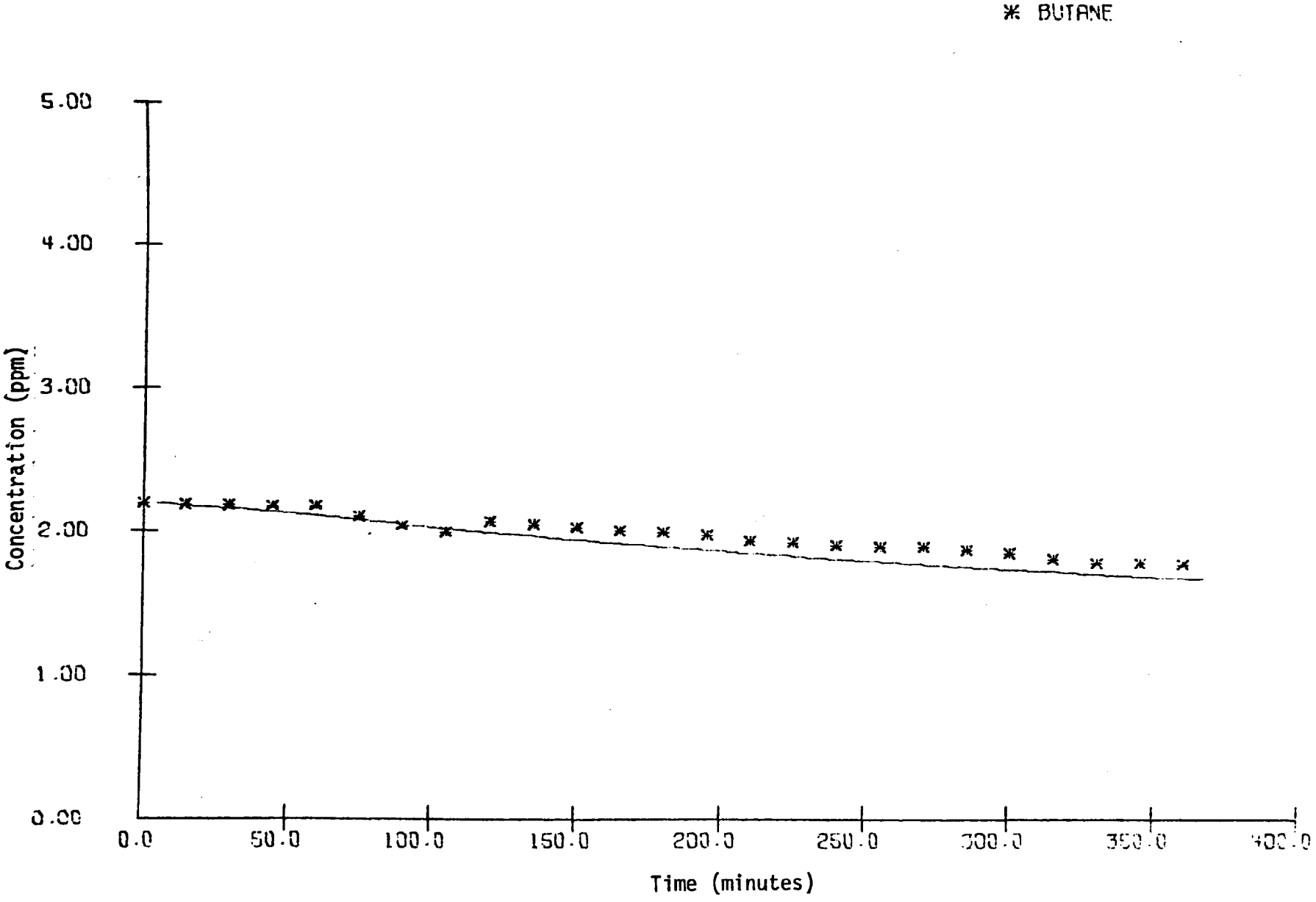

FIGURE 26. EC-39 SIMULATION RESULTS AND UCR DATA FOR BUTANE

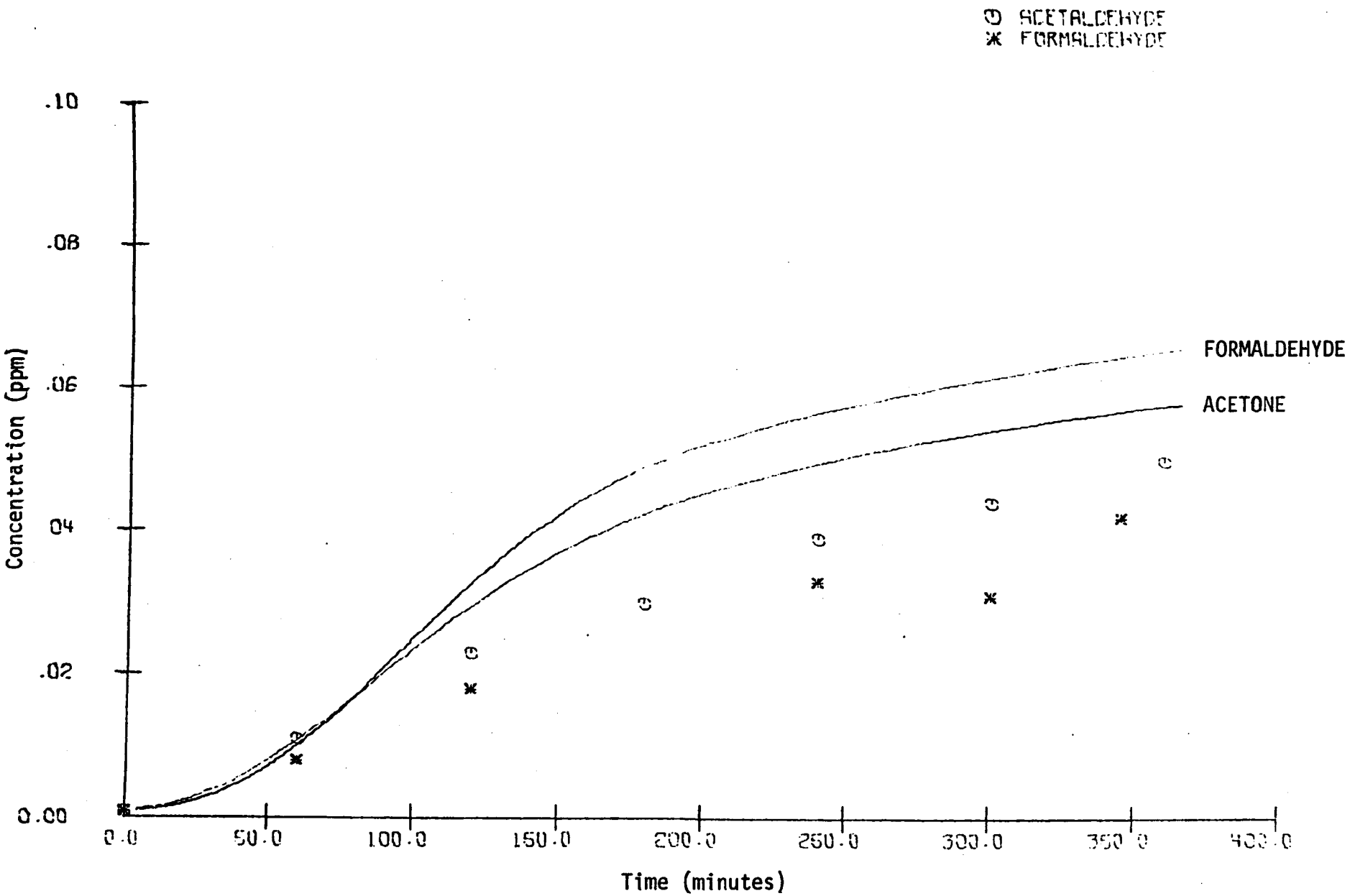

FIGURE 27. EC-39 SIMULATION RESULTS AND UCR DATA FOR ACETALDEHYDE AND FORMALDEHYDE

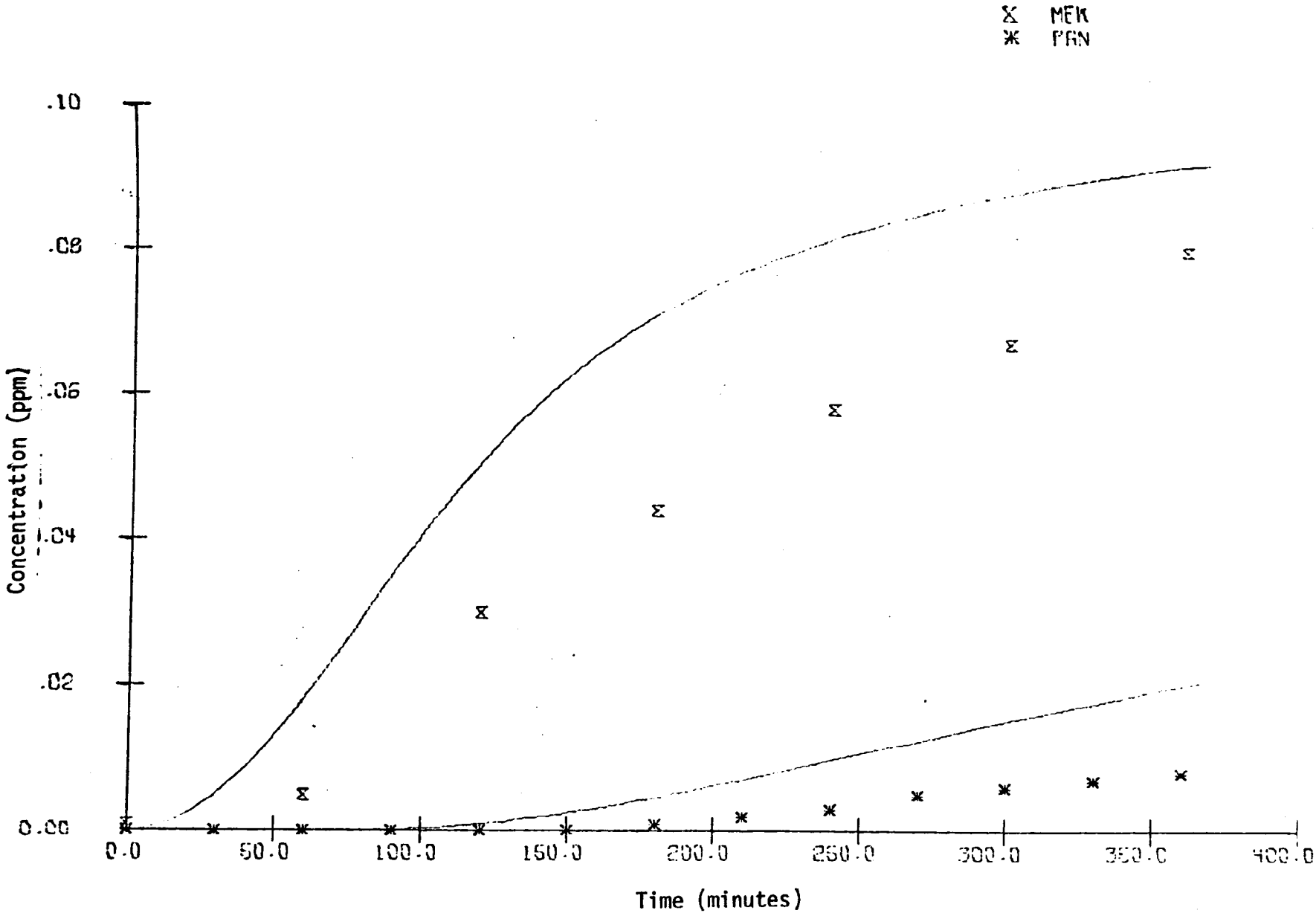

FIGURE 28. EC-39 SIMULATION RESULTS AND UCR DATA FOR MEK AND PAN

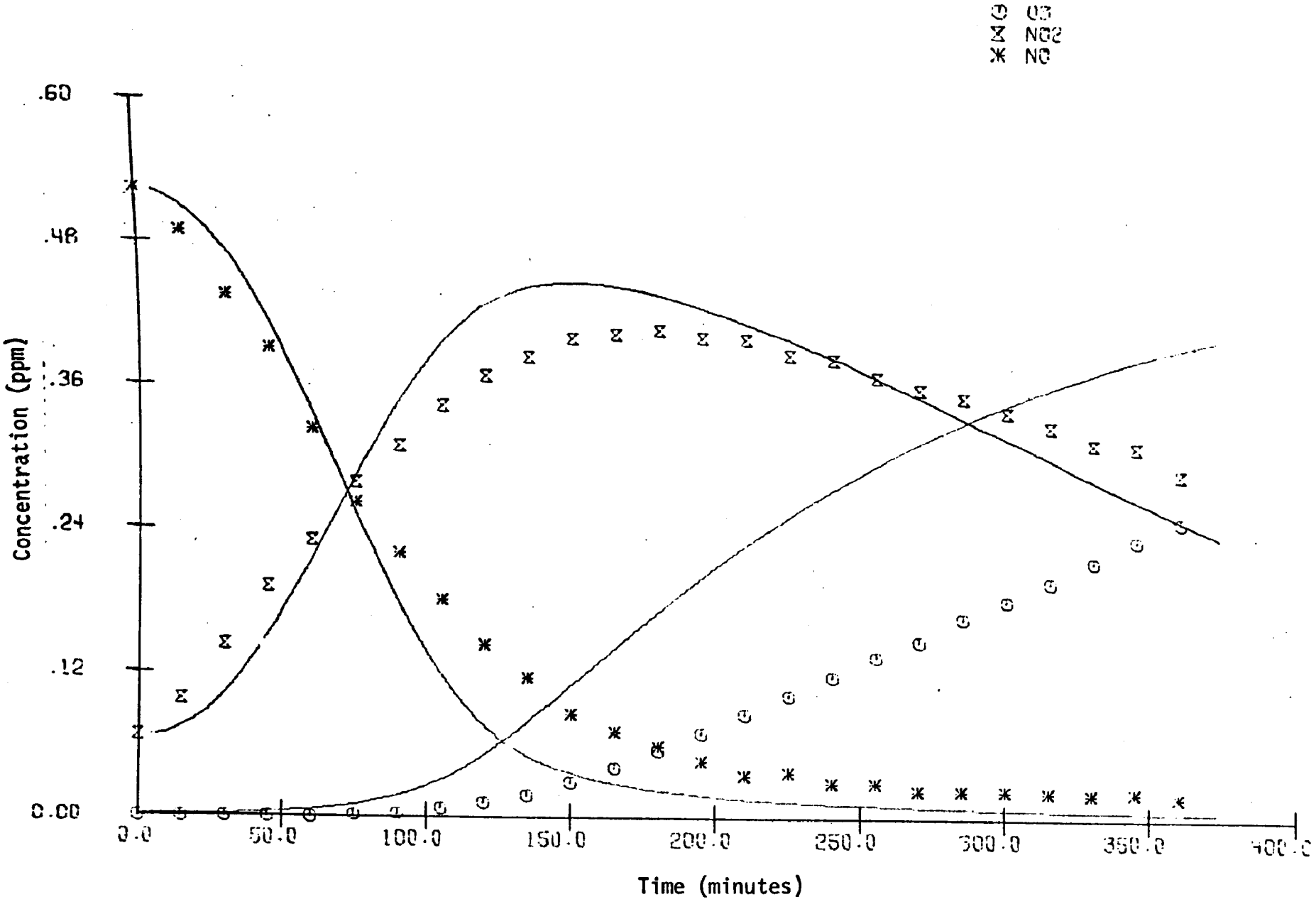

FIGURE 29. EC-41 SIMULATION RESULTS AND UCR DATA FOR O_3, NO, AND NO_2

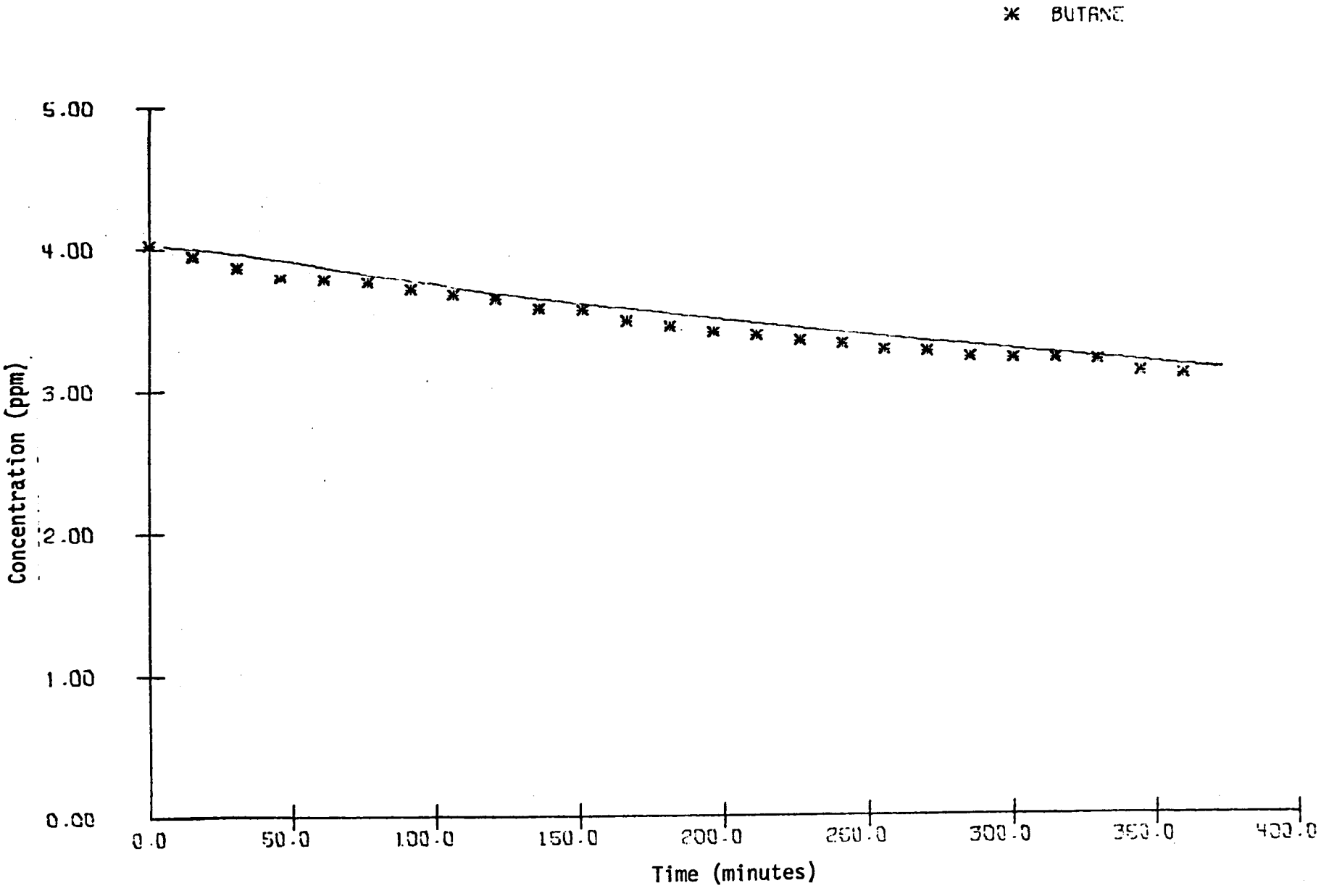

FIGURE 30. EC-41 SIMULATION RESULTS AND UCR DATA FOR BUTANE

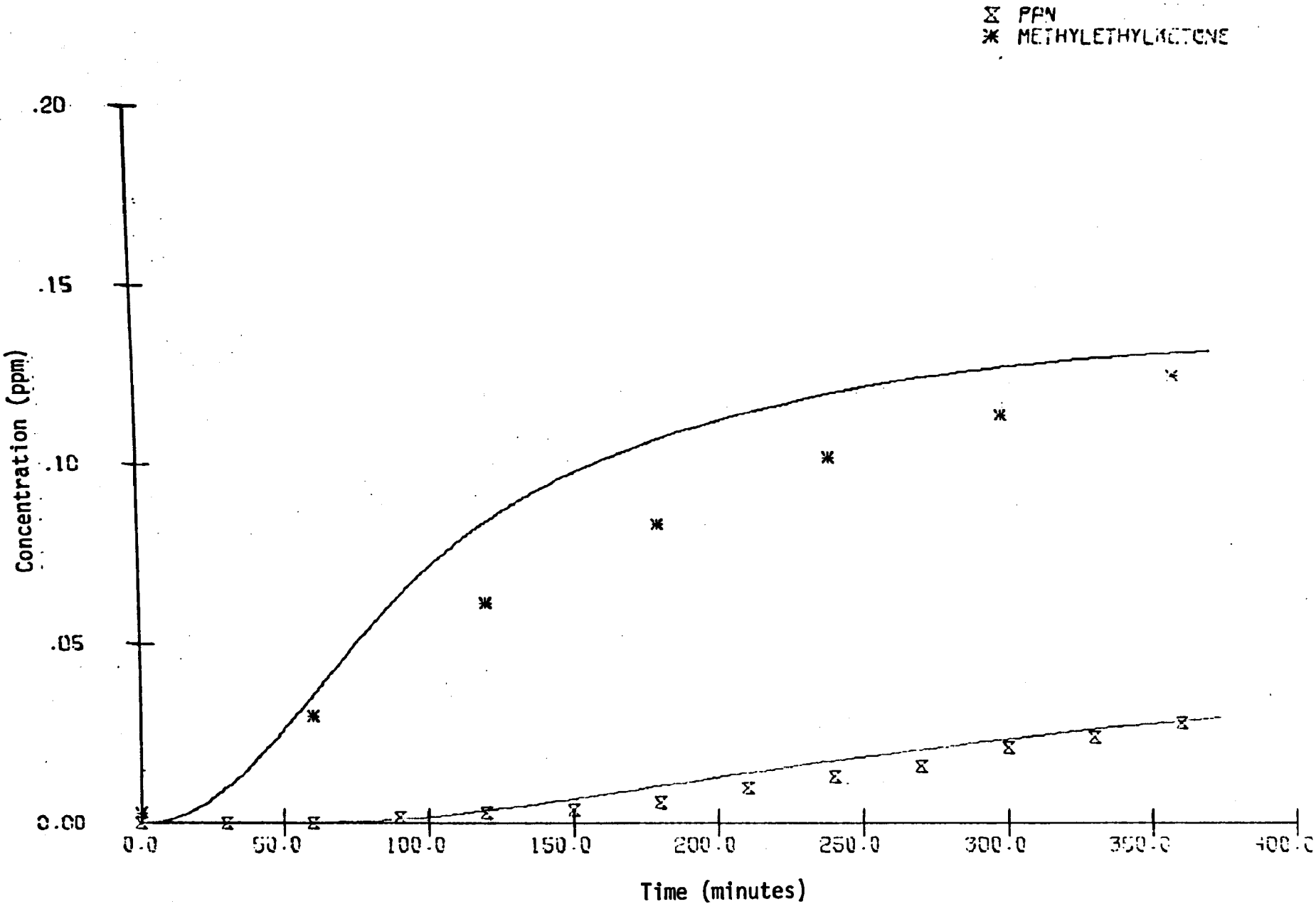

FIGURE 31. EC-41 SIMULATION RESULTS AND UCR DATA FOR MEK AND PAN

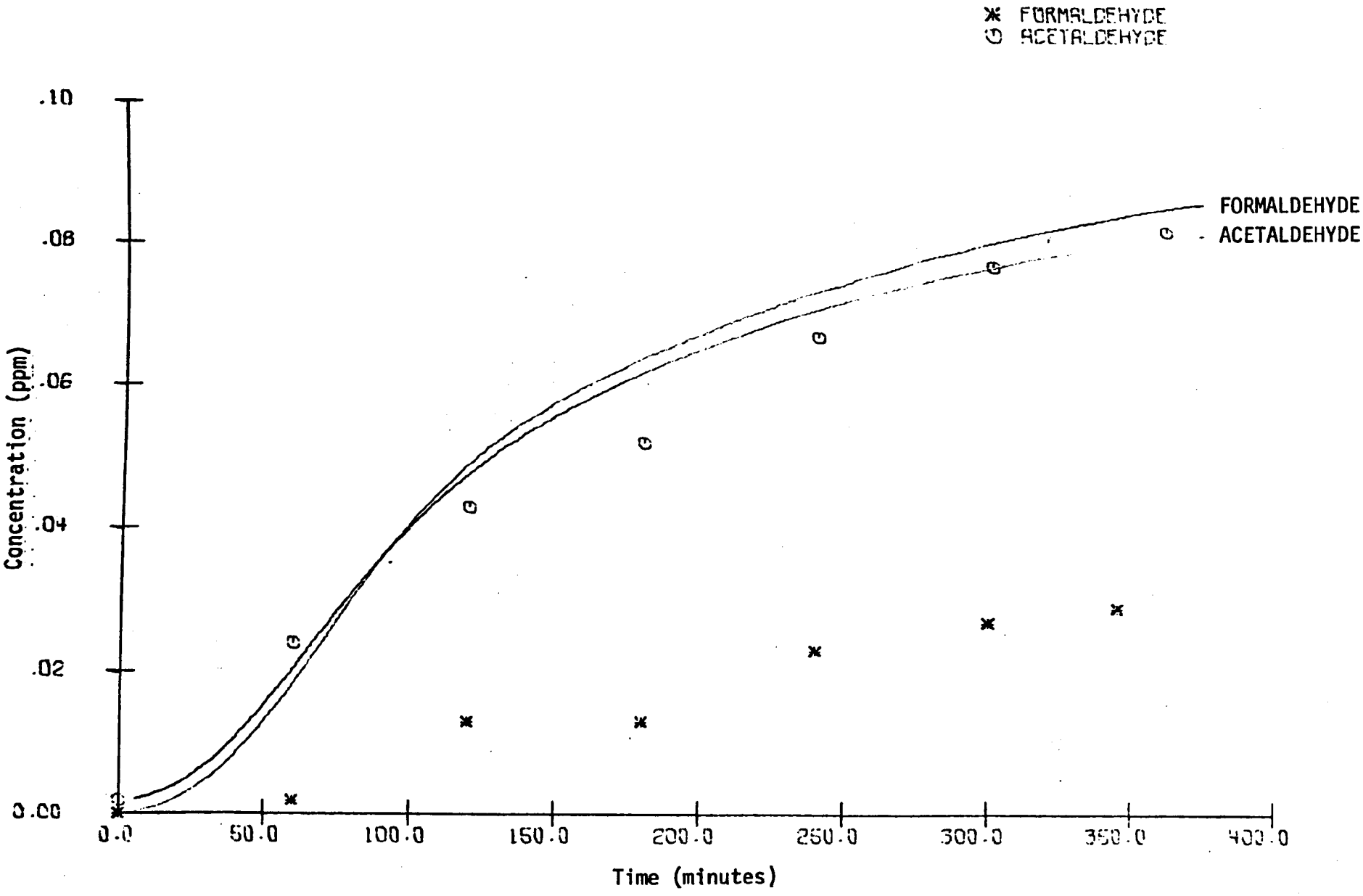

FIGURE 32. EC-41 SIMULATION RESULTS AND UCR DATA FOR ACETALDEHYDE AND FORMALDEHYDE

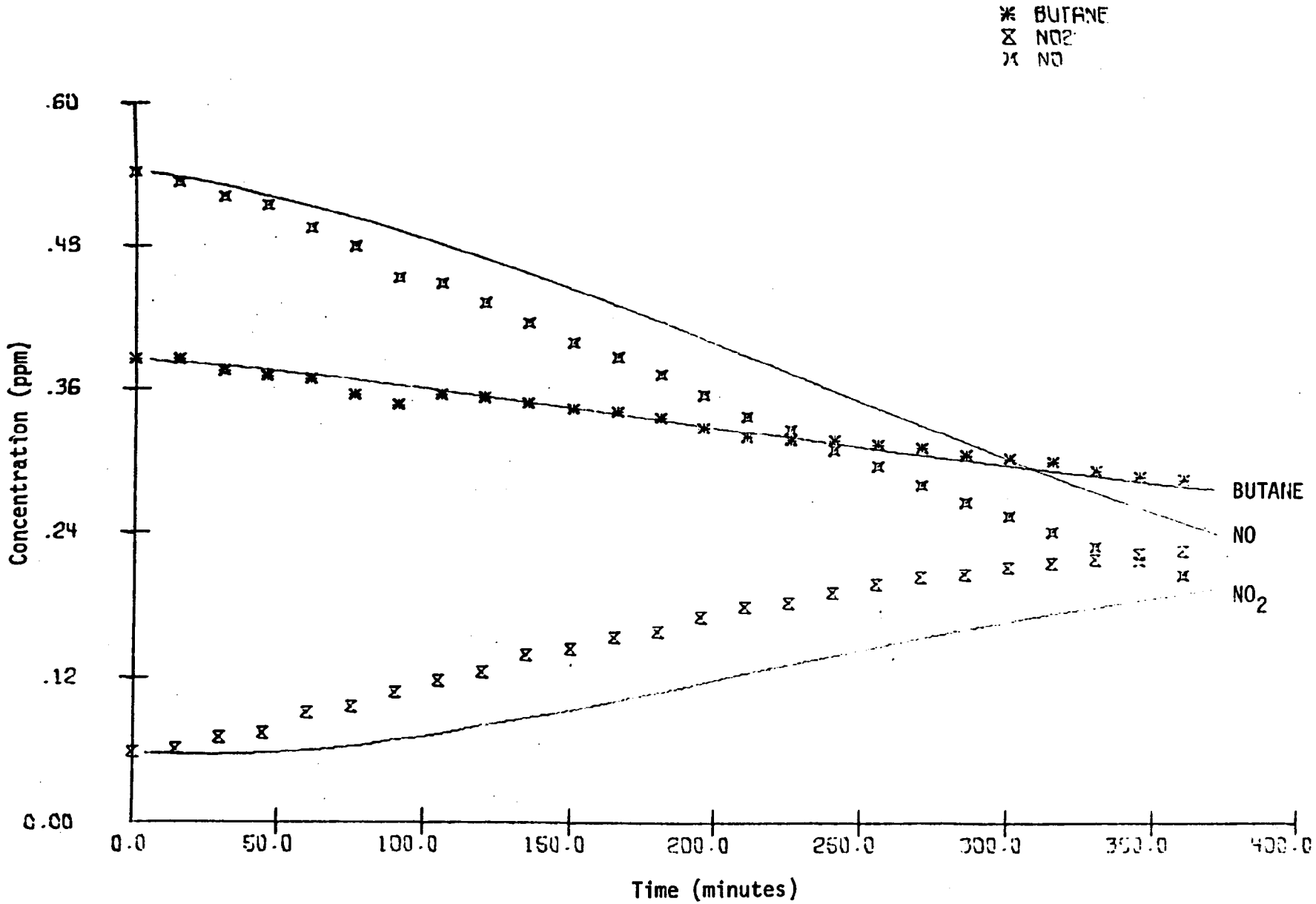

FIGURE 33. EC-42 SIMULATION RESULTS AND UCR DATA FOR BUTANE, NO, AND NO_2

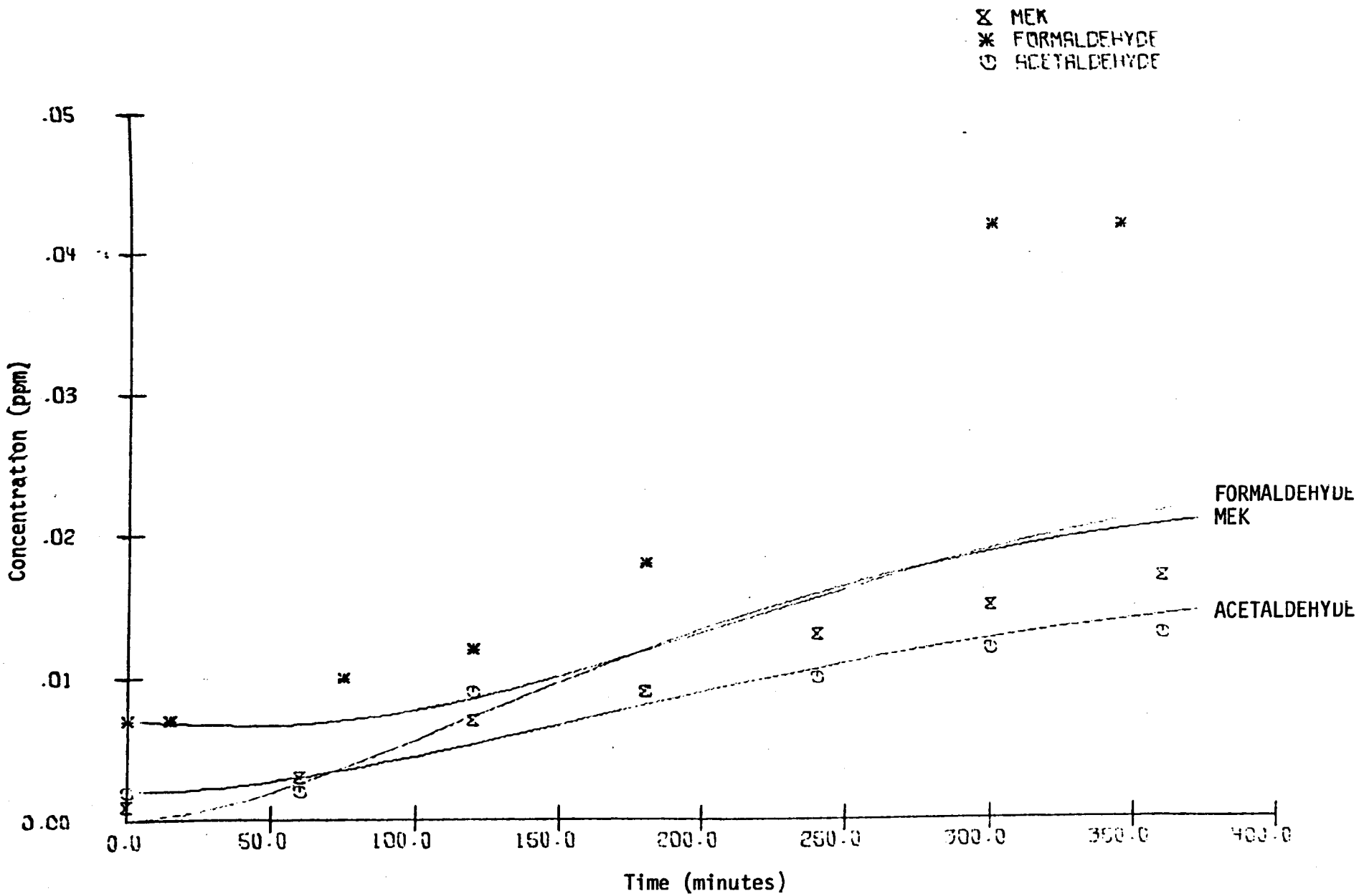

FIGURE 34. EC-42 SIMULATION RESULTS AND UCR DATA FOR MEK, FORMALDEHYDE, AND ACETALDEHYDE

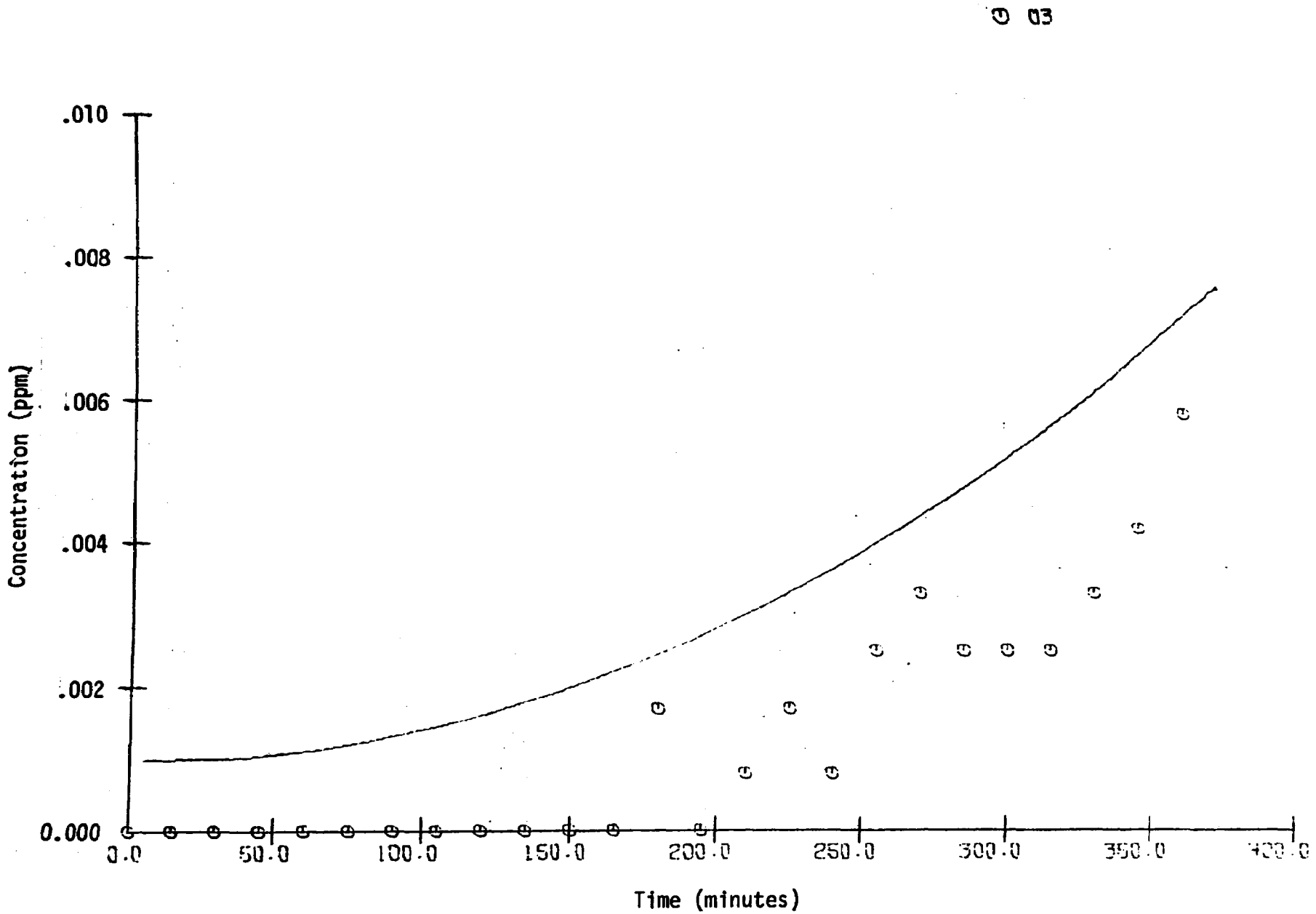

FIGURE 35. EC-42 SIMULATION RESULTS AND UCR DATA FOR OZONE

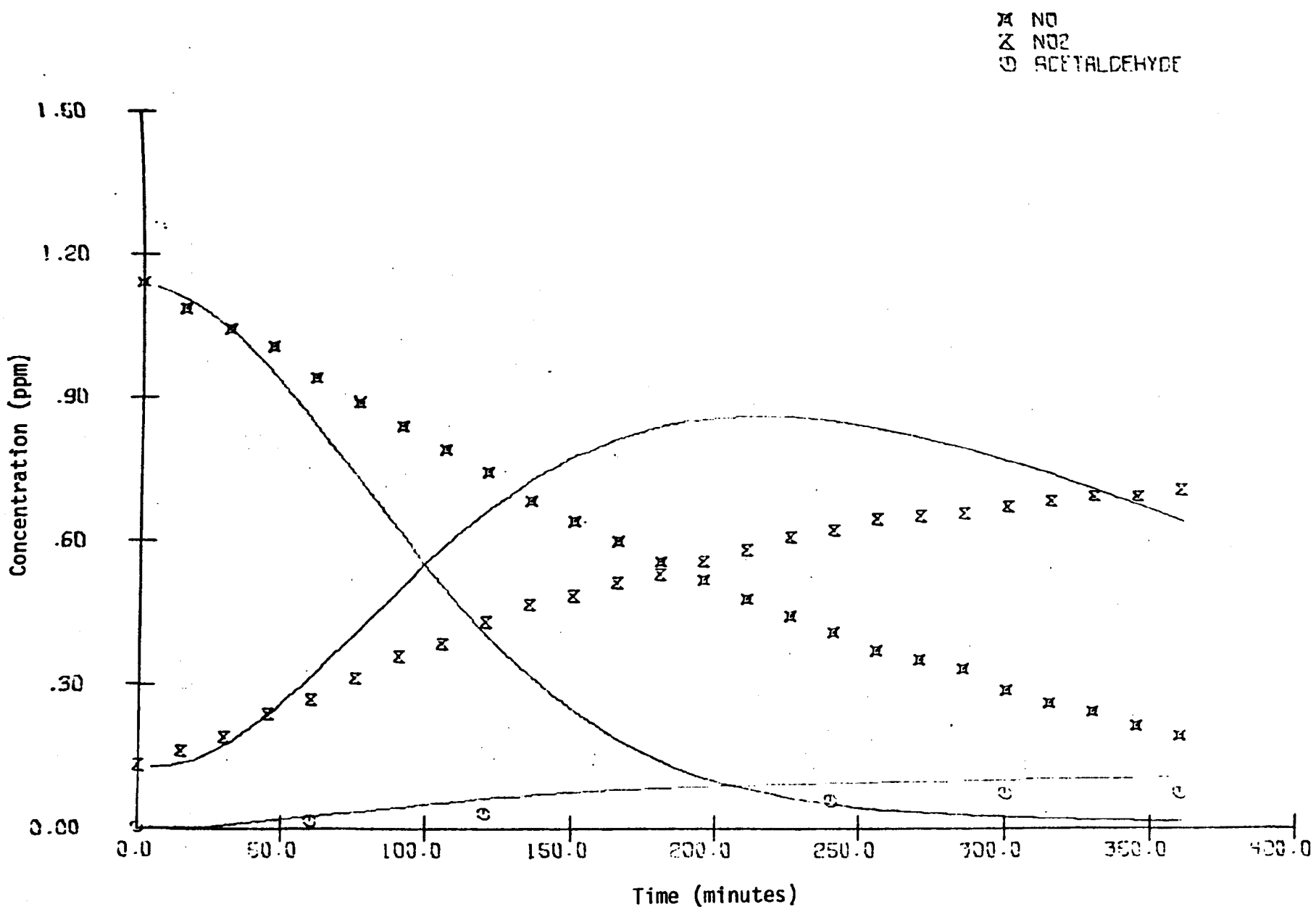

FIGURE 36. EC-44 SIMULATION RESULTS AND UCR DATA FOR NO, NO_2, AND ACETALDEHYDE

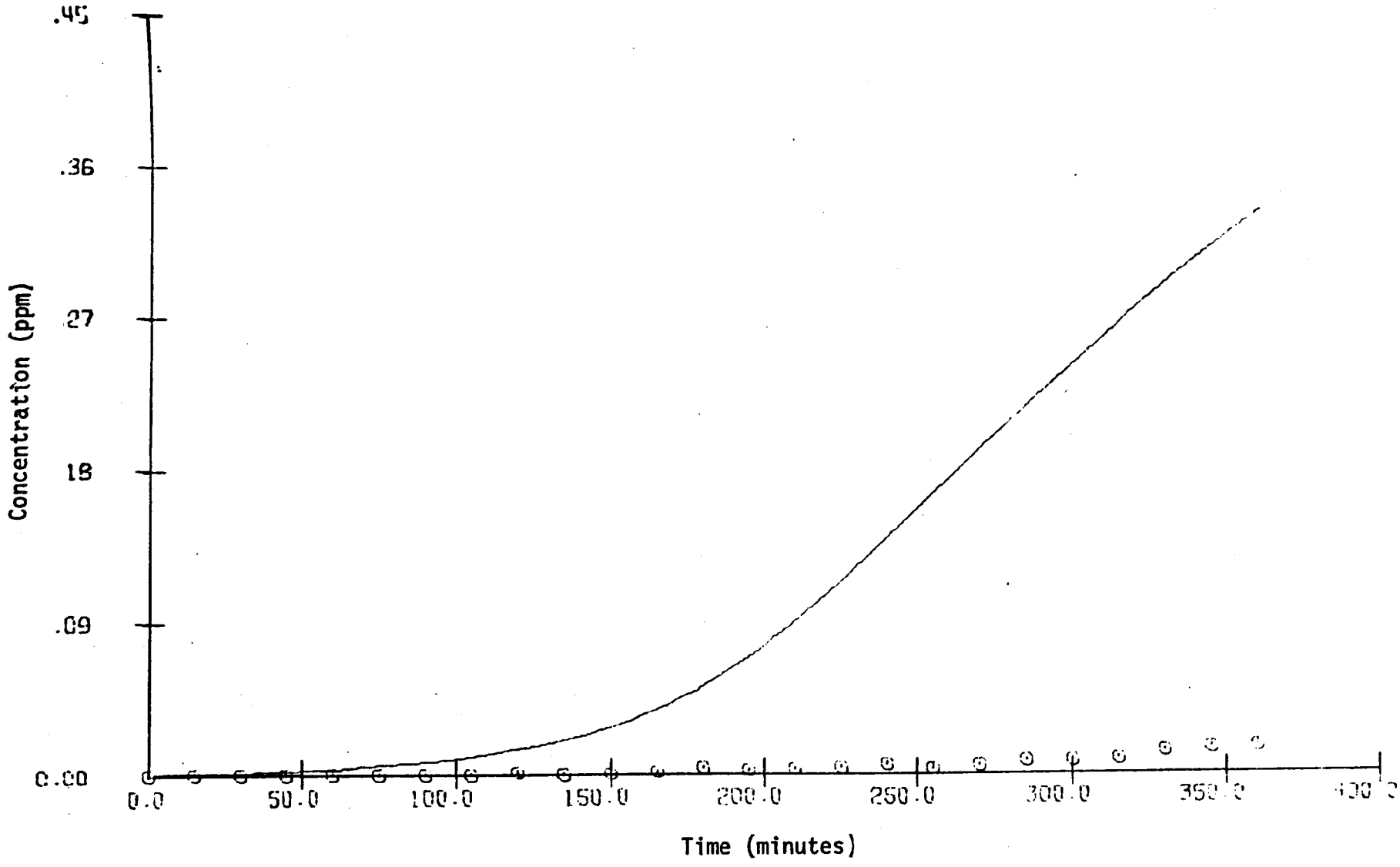

FIGURE 37. EC-44 SIMULATION RESULTS AND UCR DATA FOR OZONE

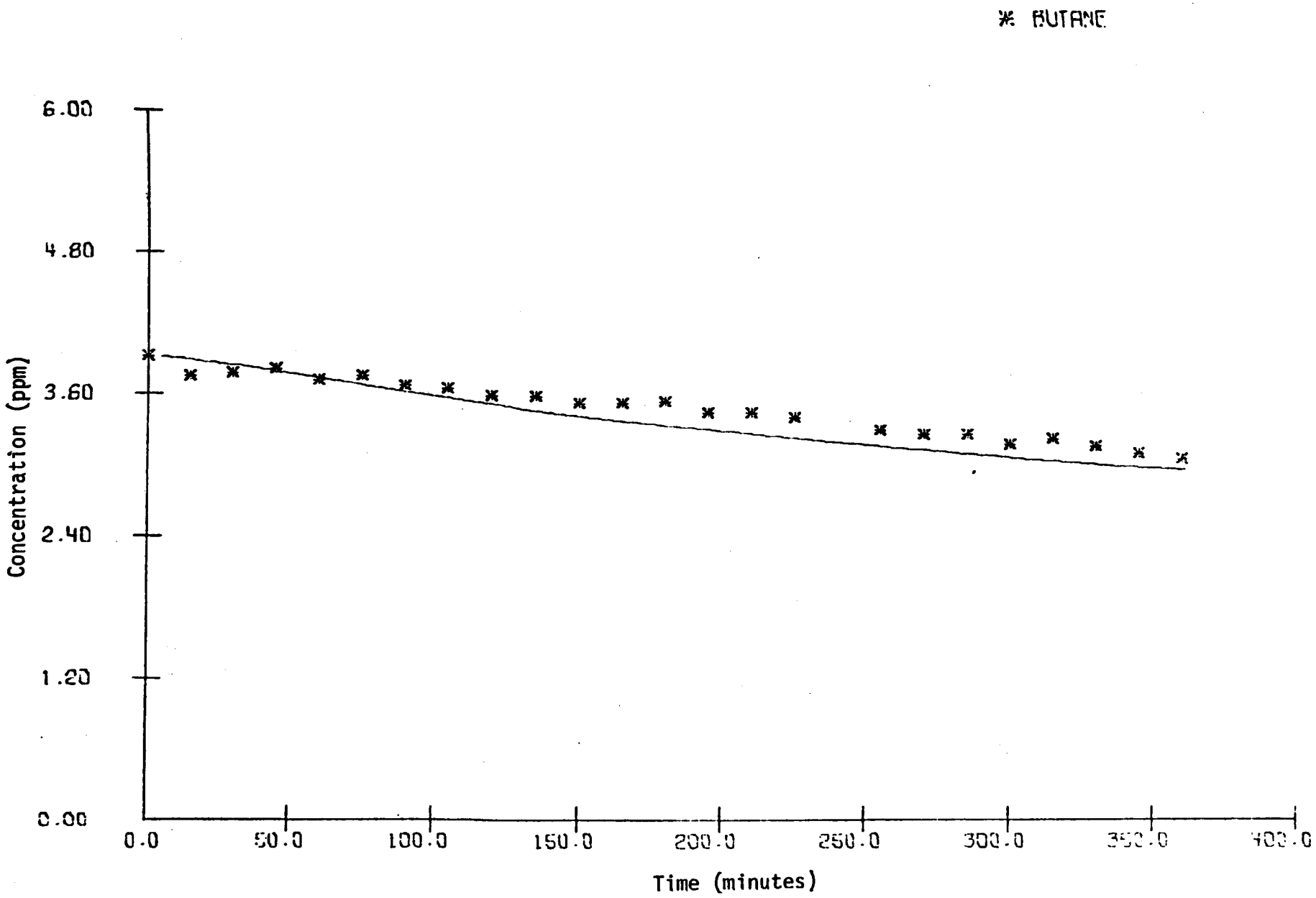

FIGURE 38. EC-44 SIMULATION RESULTS AND UCR DATA FOR BUTANE

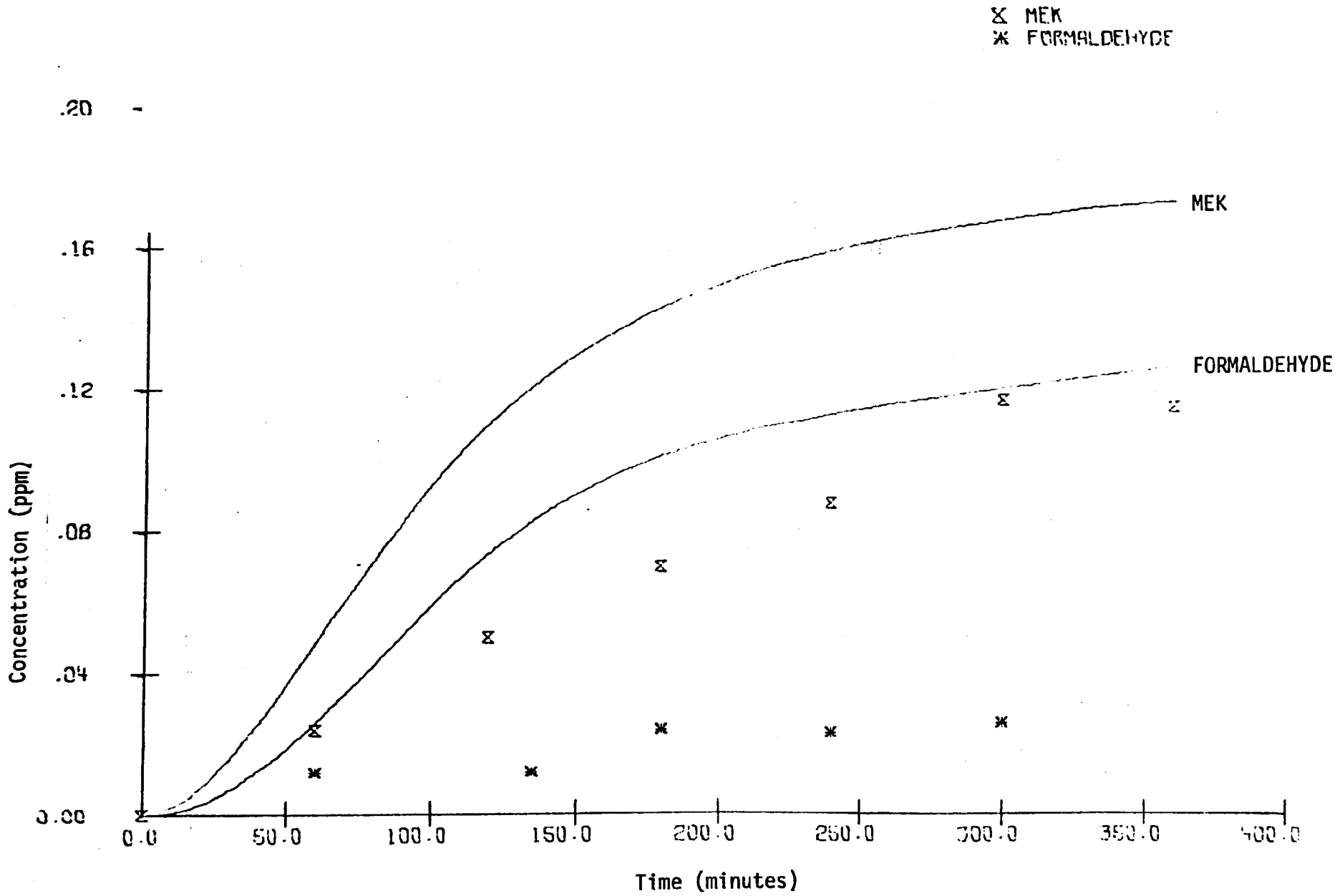

FIGURE 39. EC-44 SIMULATION RESULTS AND UCR DATA FOR FORMALDEHYDE AND MEK

formaldehyde shows that the chain processes whereby butane is broken down into oxygenated products are improperly represented. Correction of this fault must await more complete product measurements and improved kinetic data. Because rate constants for reactions of most of the less-than-four-carbon radicals were determined from propylene simulations, it is possible that C_4 radical reactions are inadequately represented, but this conclusion cannot be drawn on the basis of the results alone.

Of course, the traditional scapegoats, uncertainties of surface and photolysis reactions, can also be blamed for the disparity between model predictions and experimental results. Although they probably exacerbate the problem, they are not the sole culprits. The results of EC-44 are reproduced in Figures 40 through 43, with k_{10} and k_{11} ($NO + NO_2 + H_2O \rightarrow 2HNO_2$) reduced by a factor of 10. The reaction is greatly delayed, and the agreement with the data is improved. However, once the reaction begins, the net rate of NO oxidation is obviously still too fast.

B. SIMULATIONS OF BATTELLE DATA

To clarify the interaction of SO_2 with hydrocarbon-NO_x-air pollutants, EPA has sponsored a series of smog chamber experiments performed at Battelle Memorial Laboratories in Columbus, Ohio. We have received the results of five of these experiments and report here on the kinetic simulation of those data.

1. Instrumentation

The Battelle simulations were carried out in a 17.8 cubic meter environmental chamber. The surface-to-volume ratio of this chamber is 2.6 meters^{-1}. Ozone concentrations were measured using a chemiluminescent method; ethylene, NO, and NO_2 were measured using an automated Saltzman method; SO_2 using a Beckman 906 analyzer; and propylene using gas chromotography with a flame ionization detector. SO_3 concentrations were inferred from aerosol size distributions measured with a Thermo Systems electrical aerosol analyzer, by assuming that equilibrium existed between sulfuric acid aerosol in the condensed and vapor phases. This method was tested by independent chemical

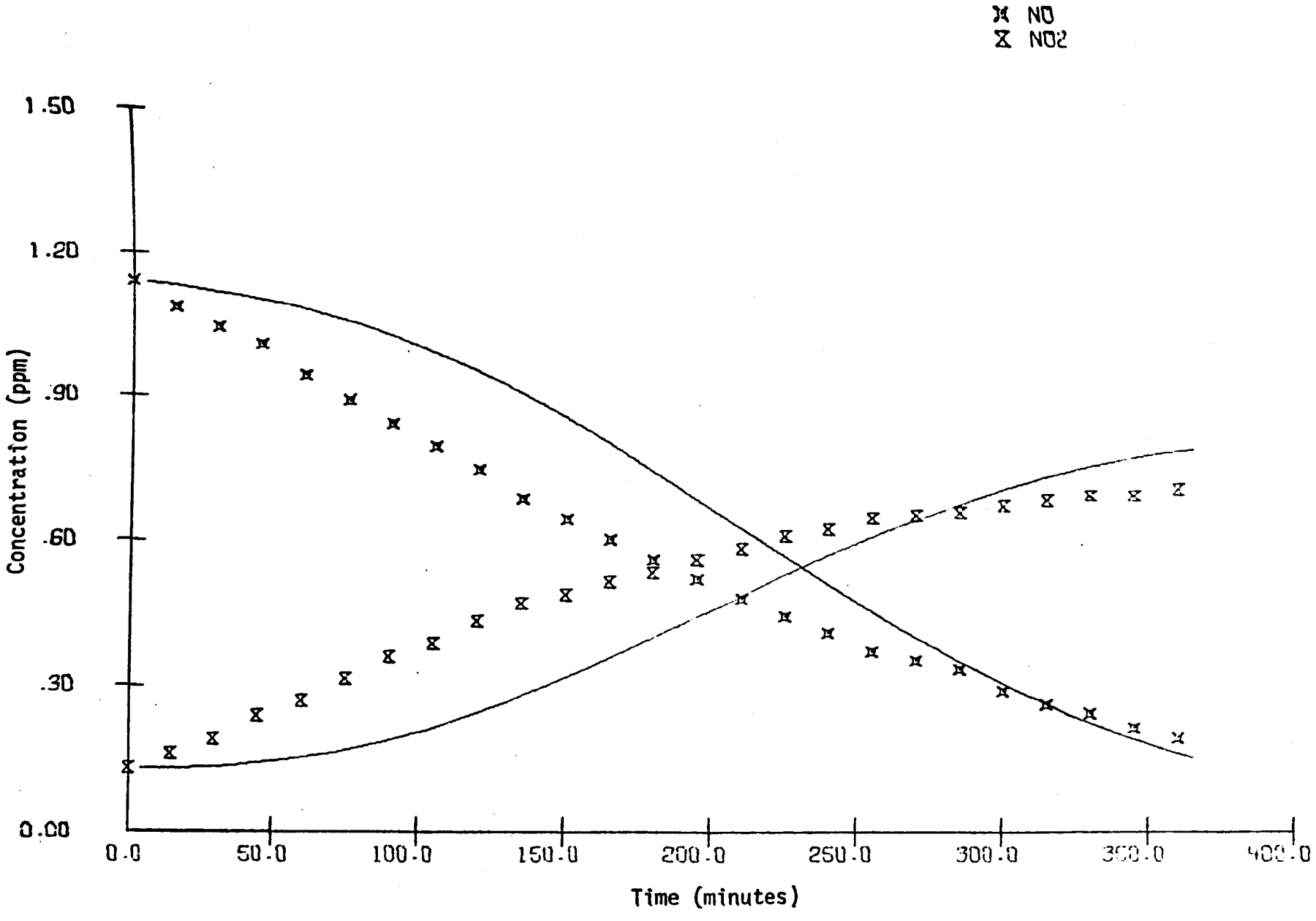

FIGURE 40. EC-44 SIMULATION RESULTS, USING $k_{10} = 1.3 \times 10^{-12}$ ppm^{-3} and $k_{11} = 0.024$ ppm^{-1} min^{-1}, FOR NO AND NO_2

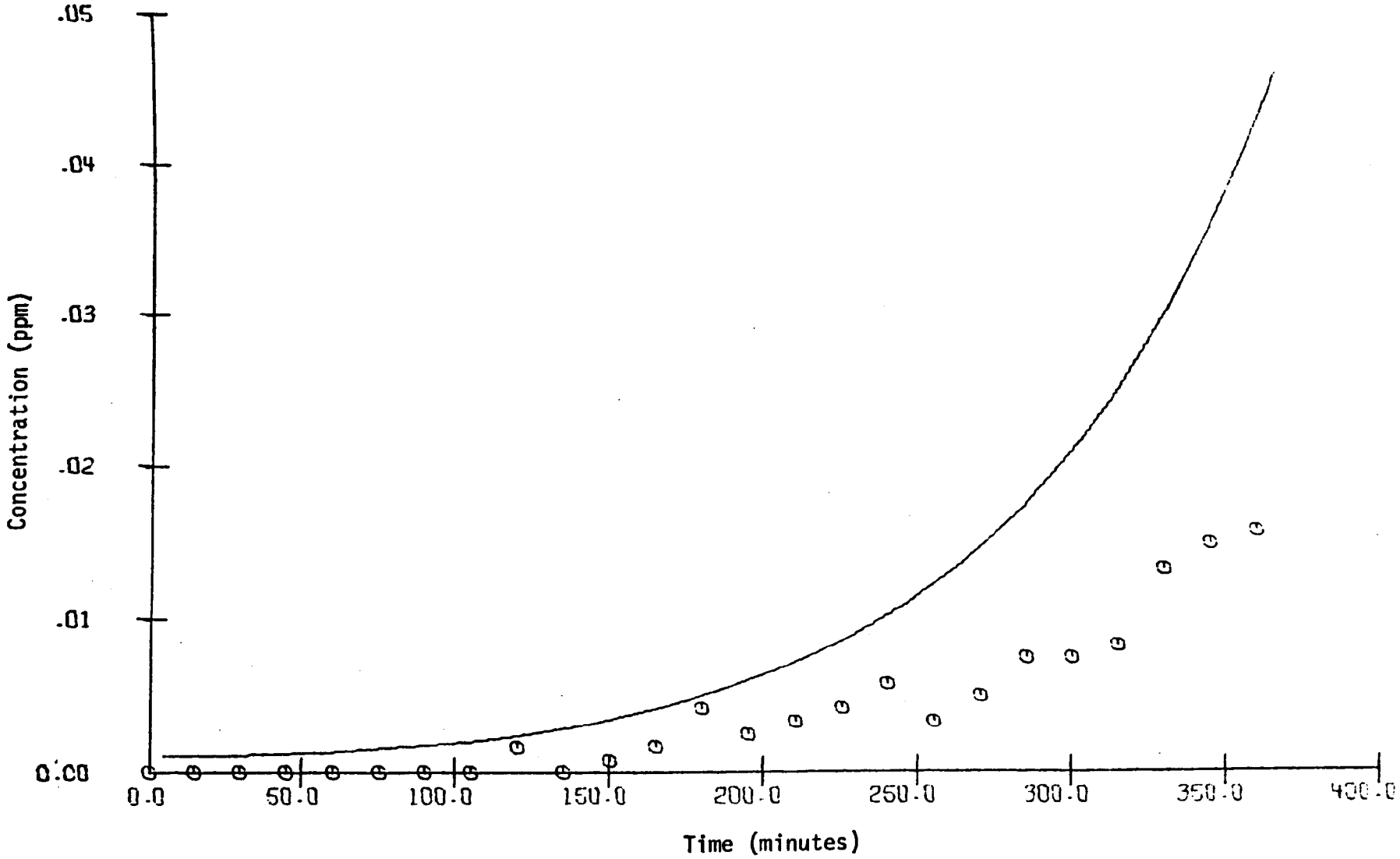

FIGURE 41. EC-44 SIMULATION RESULTS, USING $k_{10} = 1.3 \times 10^{-12}$ ppm^{-3} min^{-1} AND $k_{11} = 0.024$ ppm^{-1} min^{-1}, FOR OZONE

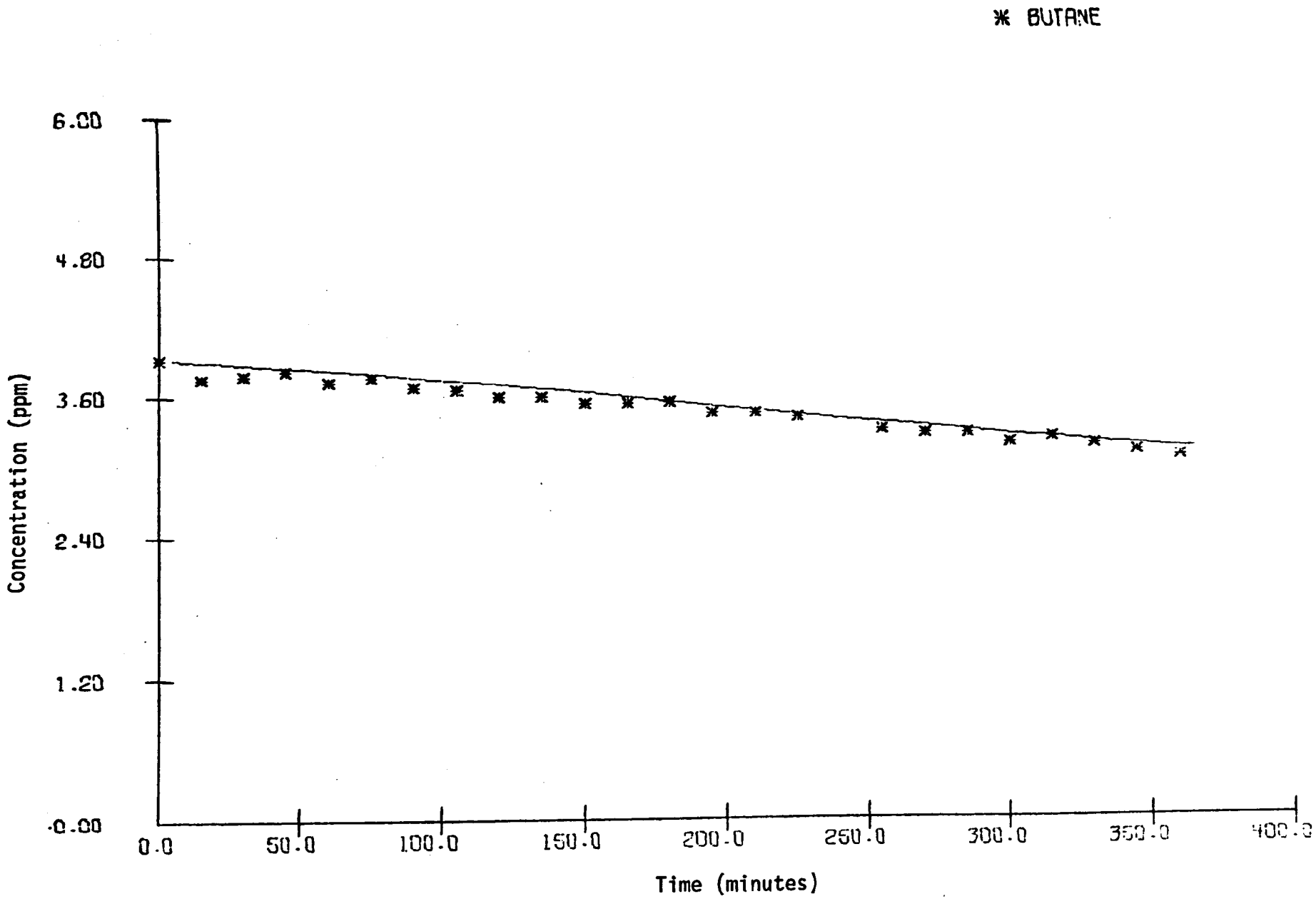

FIGURE 42. EC-44 SIMULATION RESULTS, USING $k_{10} = 1.3 \times 10^{-12}$ ppm^{-3} min^{-1} AND $k_{11} = 0.024$ ppm^{-1} min^{-1}, FOR BUTANE

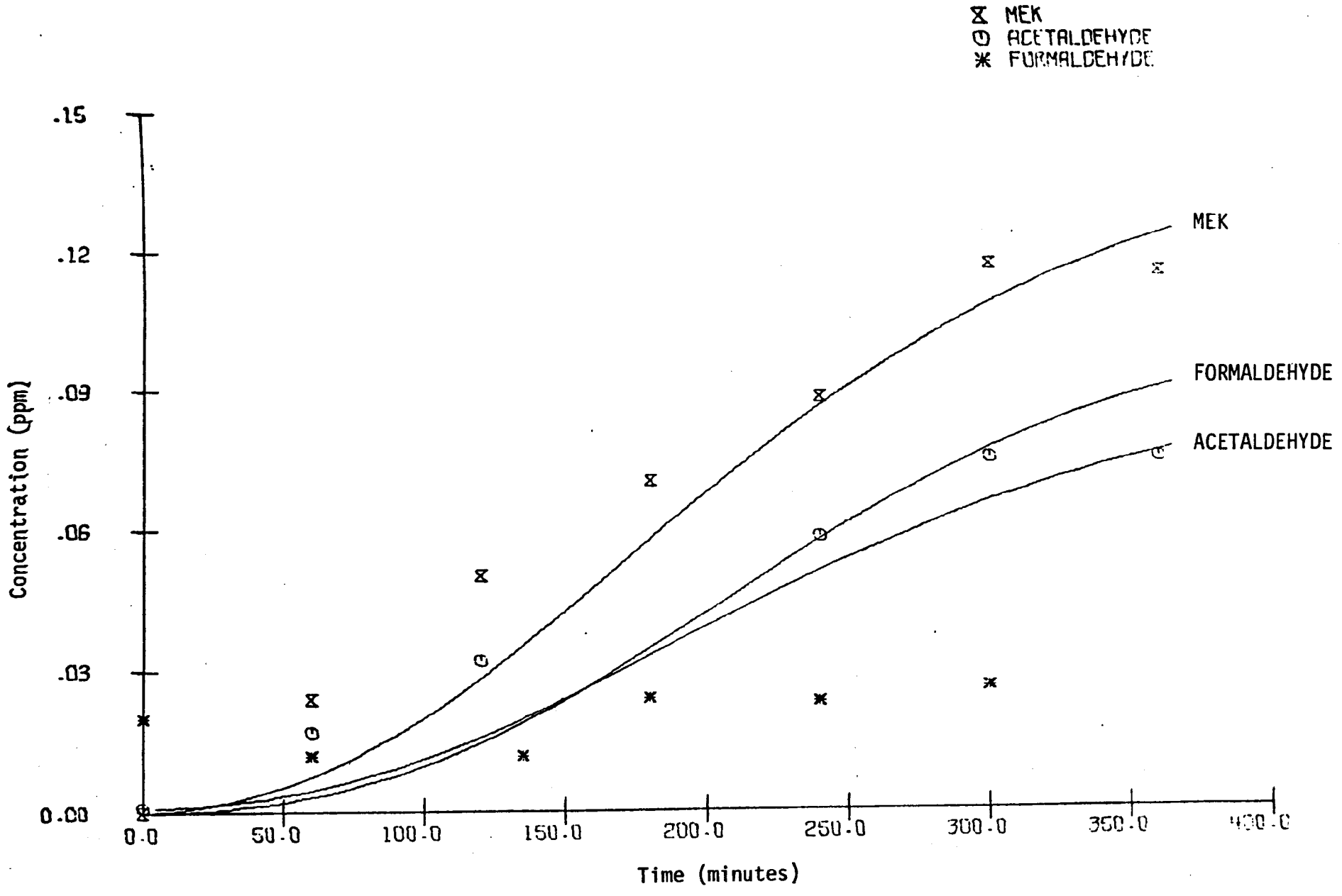

FIGURE 43. EC-44 SIMULATION RESULTS, USING $k_{10} = 1.3 \times 10^{-12}$ ppm^{-3} min^{-1} AND $k_{11} = 0.024$ ppm^{-1} min^{-1}, FOR MEK, ACETALDEHYDE, AND FORMALDEHYDE

measurements of SO_3 and found to be fairly accurate. The NO_2 photodissociation constant, k_d, was determined from photocell readings, the photocell having been previously calibrated. The relation $k_1 = 4/9\ k_d$ (Wu and Niki, 1975) has been used in our model. Other instrument and chamber characteristics are summarized by Table 9 (Miller 1975).

2. The Mechanism Used

The propylene mechanism used in the UCR simulations forms the core of the mechanism used to simulate the Battelle data. The reactions listed in Table 10 were added to this core. In the absence of adequate light spectrum information, photolysis rates were computed from the unshifted ratios included in Table 3. Additionally, a rate constant of 2×10^{-11} ppm^{-3} min^{-1} was assigned to the heterogeneous reaction of NO, NO_2, and H_2O (Reaction 10, Table 1), 0.4 ppm^{-1} min^{-1} was assigned to the reverse Reaction (11), and 1×10^{-5} ppm^{-1} min^{-1} was assigned to the heterogeneous reaction of N_2O_5 and H_2O (Reaction 9). This procedure is in accord with the discussion of heterogenous HNO_x chemistry in Chapter II and was used solely to improve NO_2 profile predictions.

A recent rate constant measurement of 9.0×10^3 ppm^{-1} min^{-1} (Cox, 1974; Atkinson, 1975) for the reaction $OH\cdot + NO \rightarrow HNO_2$ was used in these simulations (but in none of the others).*

3. Results and Discussion

The initial concentrations and value of k_1 for the propylene-NO_x-SO_2 block are contained in Table 11. Two experiments contained no SO_2 (S-114 and S-115); three did contain SO_2 (S-107, S-110, and S-113). Of the three containing SO_2, S-113 was performed with reduced light intensity. All photolysis rates for model predictions were scaled down accordingly.

* These new rate constant determinations were called to our attention late in the contract year. Although their incorporation in the Battelle simulation gave good results, their effect in the UCR simulations was an undesirable delay in the NO_2 peak. This result was expected because rate constant adjustments, made to give the best fit to UCR data, correspond to the lower value of 3×10^3 ppm^{-1} min-1. The $OH\cdot + NO$ reaction is simply the reverse of $HNO_2 + h\nu$. This suggests that a modification of heterogeneous HNO_2 chemistry (within its wide uncertainty bounds) would compensate the delayed NO_2 peak (see Chapter II).

Table 9

ANALYTICAL AND CHAMBER CHARACTERISTICS OF THE BATTELLE EXPERIMENTAL SETUP

(a) Analytical Characteristics

Analysis	Lag time (sec)	Dark time (sec)	Uncertainty Factor
O_3	< 4	< 4	0.1
NO_2	∿ 500	∿ 20	0.2
NO	∿ 500	∿ 20	0.2
SO_2	∿ 300	--	0.15
C_3H_6	--	--	0.15
SO_3	--	--	0.5
Dew point	< 5	--	0.1
Temperature	< 1	--	0.05

(b) Chamber Characteristics

Criteria	Uncertainty Factor
NO_2 photodissociation	
k_d, 0.38 min^{-1}	0.15
k_1, 0.16 min^{-1}	0.15
O_3 half-life (may vary with conditions)	
Dark, 6-8 hrs	0.25
Light, 3-4 hrs	0.25
Dilution (variable with sampling)	0.1-0.25
S/V ratio, meters = 2.6	--
Background conditions (slightly variable)	
CH_4 < 2 ppm	--
Nonmethane hydrocarbons < 0.2 ppm C	--
CO < 3 ppm	--

Table 10

ADDITIONAL REACTIONS USED IN SIMULATING THE SO_2-OXIDATION DATA FROM BATTELLE

Reaction	Rate Constant (ppm^{-1} min^{-1})
$SO_2 + HO_2^{\cdot} \longrightarrow SO_3 + OH\cdot$	1.3
$SO_2 + CH_3O_2^{\cdot} \longrightarrow SO_3 + CH_3O\cdot$	1.5
$SO_2 + CH_3CH_2O_2^{\cdot} \longrightarrow SO_3 + CH_3CH_2O_2^{\cdot}$	1.5
$SO_2 + CH_3CH_2C(O)O_2^{\cdot} \xrightarrow{O_2} SO_3 + CH_3CH_2O_2^{\cdot} + CO_2$	1.5
$SO_2 + CH_3C(O)O_2^{\cdot} \xrightarrow{O_2} SO_3 + CH_3O_2^{\cdot} + CO_2$	1.5
$SO_2 + NO_3 \longrightarrow SO_3 + NO_2$	14
$SO_2 + OH\cdot \xrightarrow{O_2} HSO_5^{\cdot}$	9×10^2
$HSO_5^{\cdot} + NO \longrightarrow NO_2 + HSO_4^{\cdot}$	8×10^2
$HSO_4^{\cdot} + HO_2^{\cdot} \longrightarrow H_2SO_4$	9×10^3
$HSO_4^{\cdot} + NO_2 \xrightarrow{H_2O} H_2SO_4 + HNO_3$	1×10^4
$SO_3 + H_2O \longrightarrow H_2SO_4$	Immediate

Predictions and experimental data are illustrated in Figures 34 through 51. As shown in these figures, the inability of the mechanism to follow the propylene data--in sharp contrast to the UCR propylene simulations--is somewhat disconcerting. In the early stages, the data are followed quite closely, but the mechanism shows gradually tapering decay asymptotically, whereas the measured propylene concentration drops off rapidly to zero. The NO and SO_2 predictions are fairly accurate. Since the latter is relatively unreactive, a sizeable fraction of its disappearance is due solely to dilution. The dilution rate was approximately 10 percent per hour. Thus, 65 percent of the SO_2 disappearance in S-107 and S-110 and 87 percent in S-113 was due to dilution.

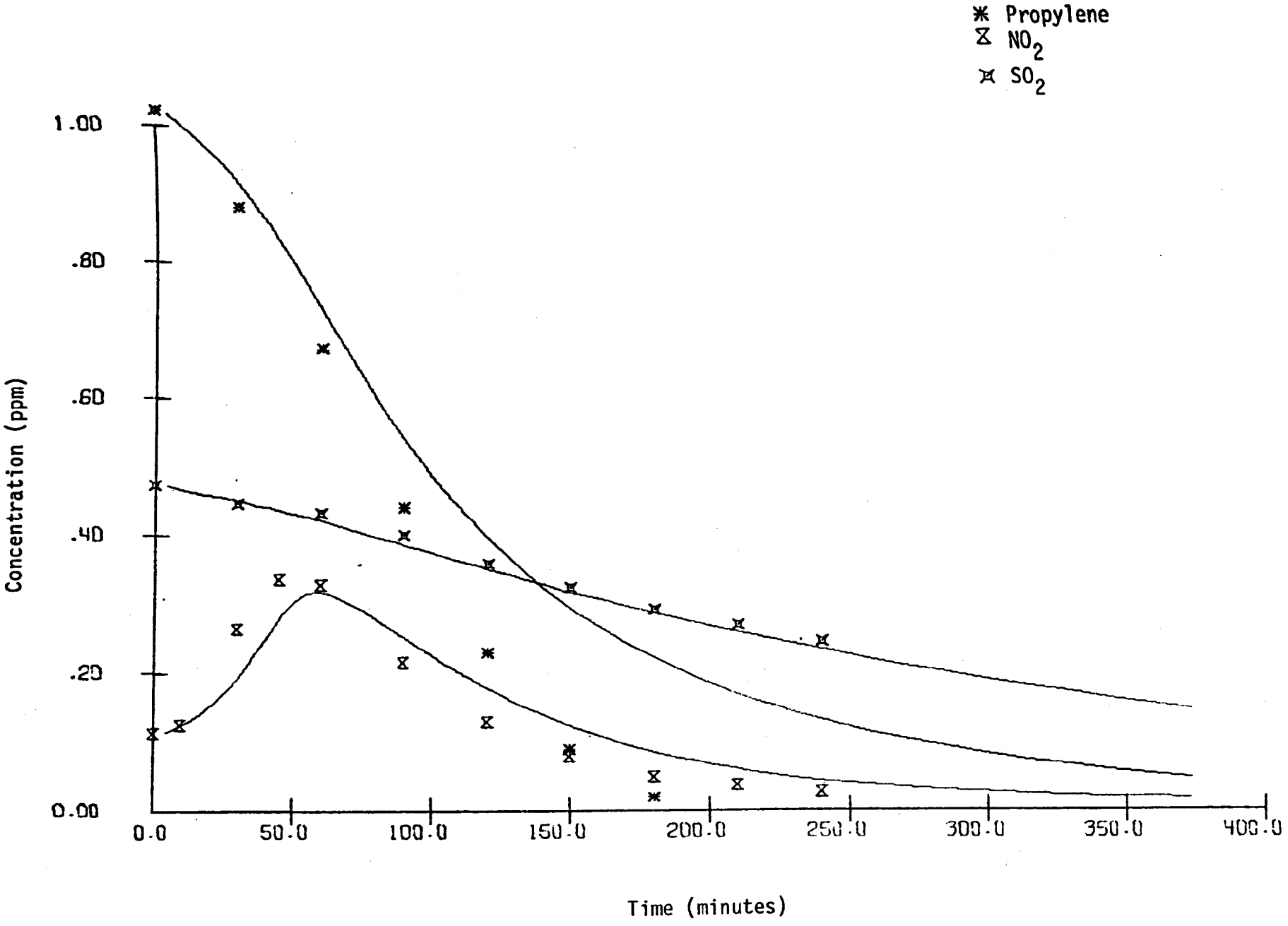

FIGURE 44. S-107 SIMULATION RESULTS AND BATTELLE LABS DATA FOR PROPYLENE, NO_2, AND SO_2

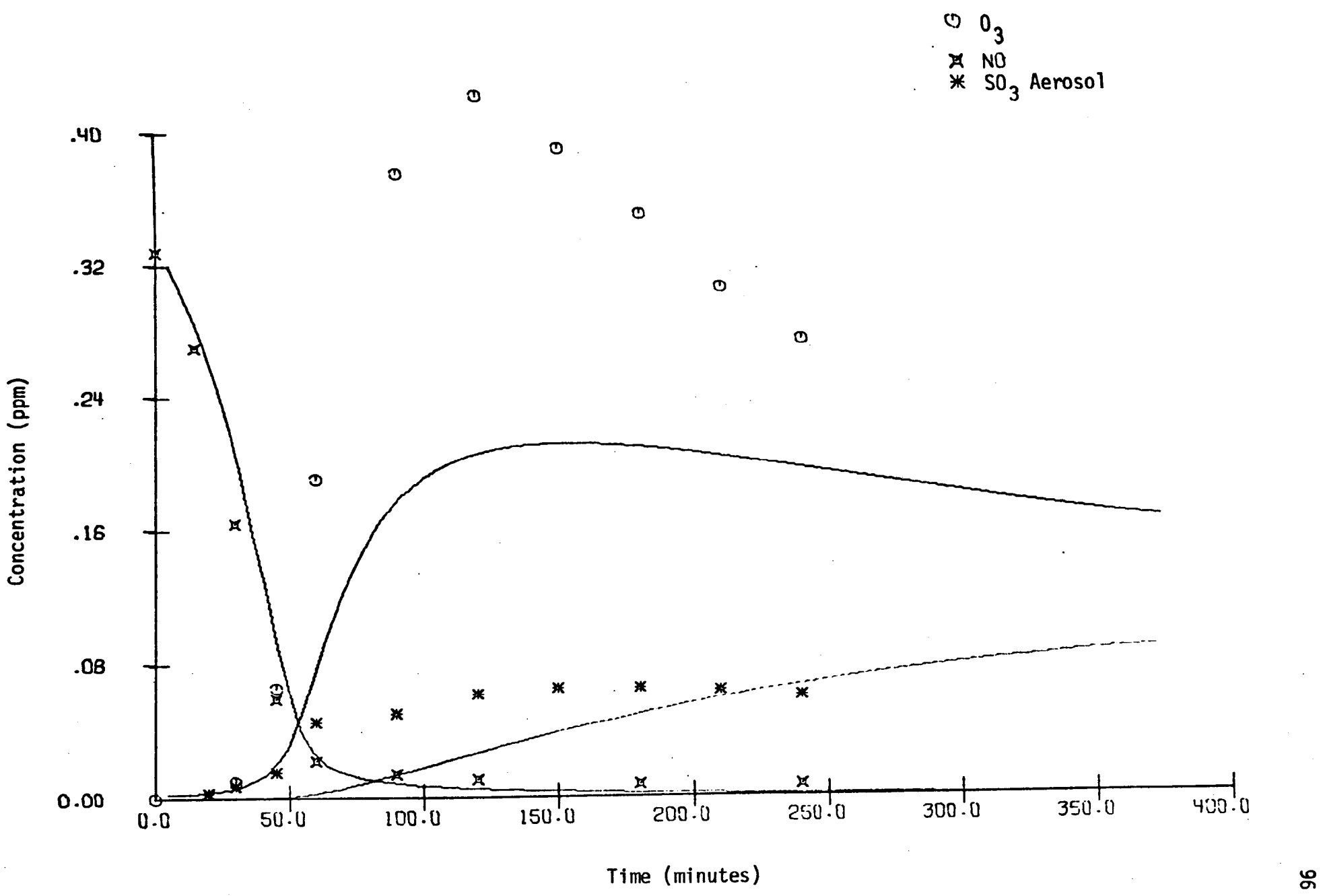

FIGURE 45. S-107 SIMULATION RESULTS AND BATTELLE LABS DATA FOR O_3, NO, AND SO_3 AEROSOL

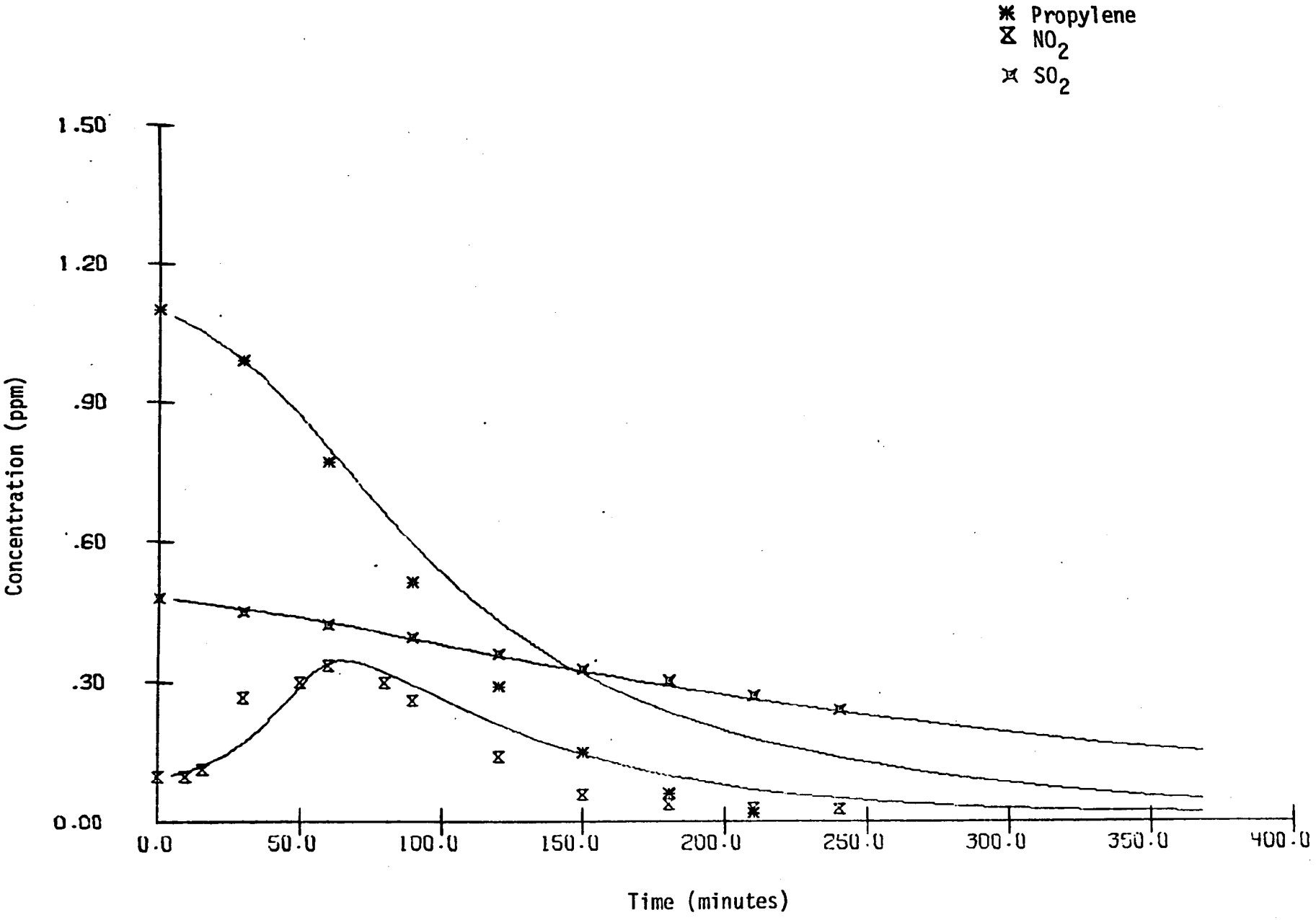

FIGURE 46. S-110 SIMULATION RESULTS AND BATTELLE LABS DATA FOR PROPYLENE, NO_2, AND SO_2

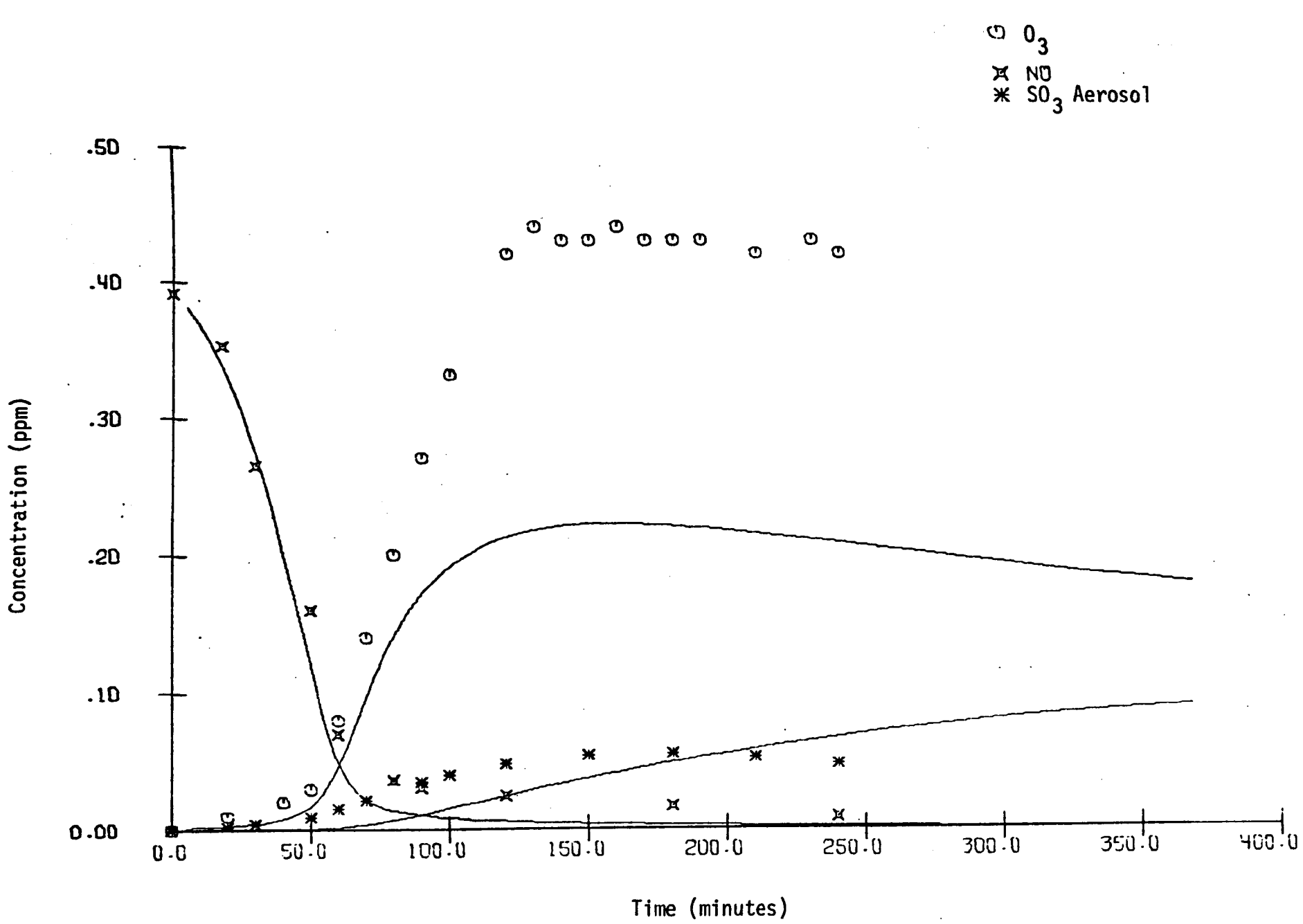

FIGURE 47. S-110 SIMULATION RESULTS AND BATTELLE LABS DATA FOR O_3, NO, AND SO_3 AEROSOL

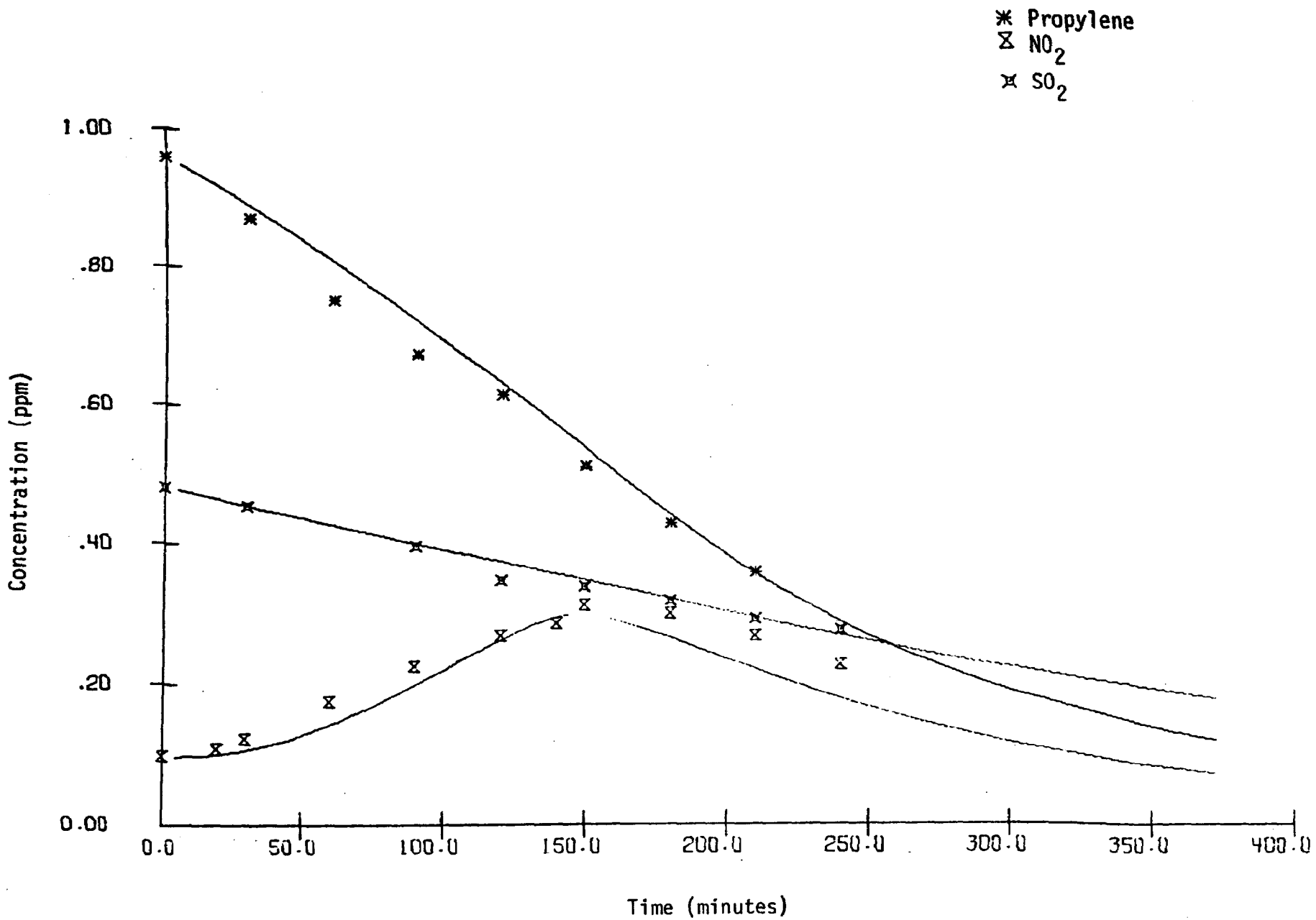

FIGURE 48. S-113 SIMULATION RESULTS AND BATTELLE LABS DATA FOR PROPYLENE, NO_2, AND SO_2
(This run was done with reduced light intensity)

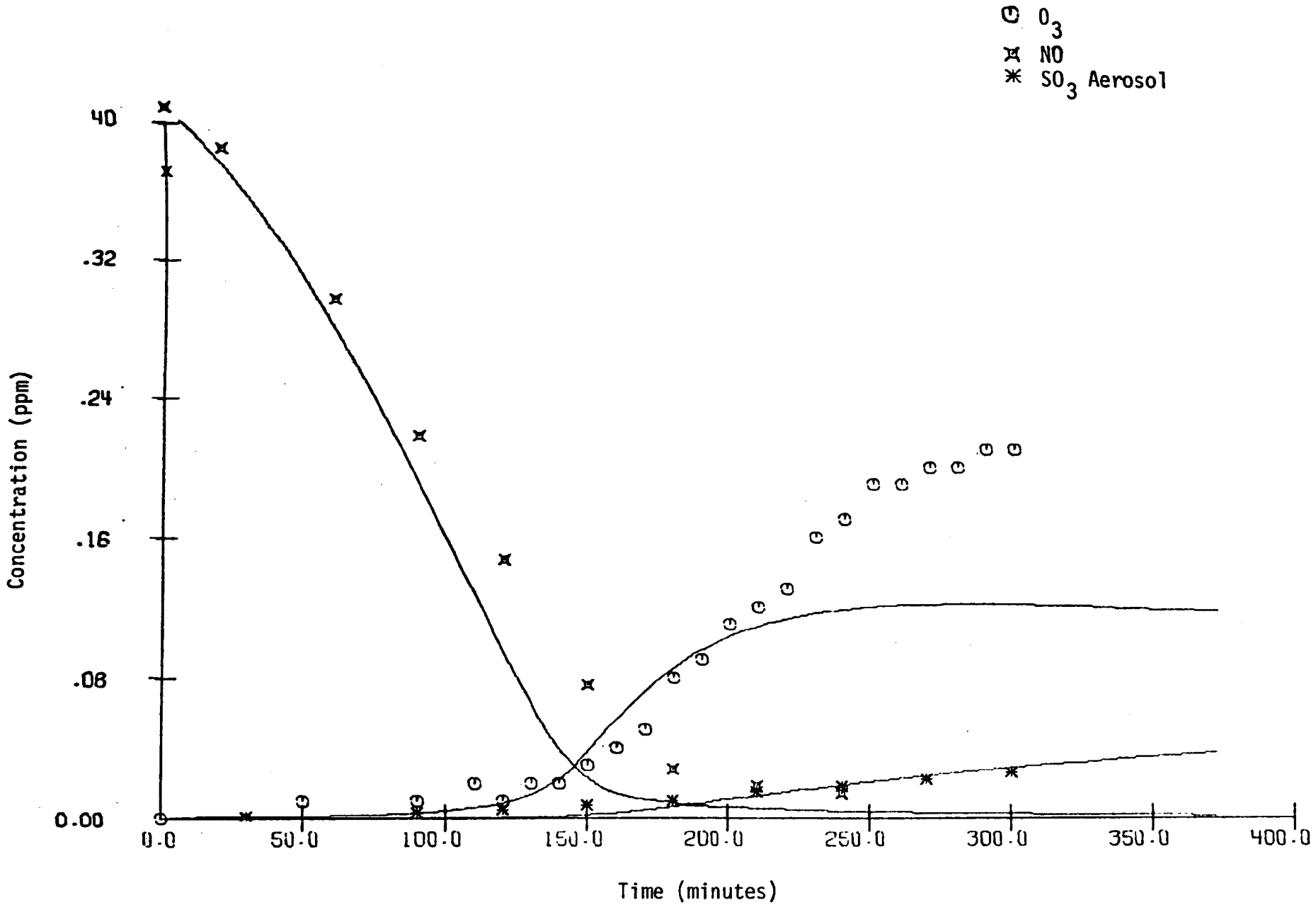

FIGURE 49. S -113 SIMULATION RESULTS AND BATTELLE LABS DATA FOR O_3, NO, AND SO_3 AEROSOL

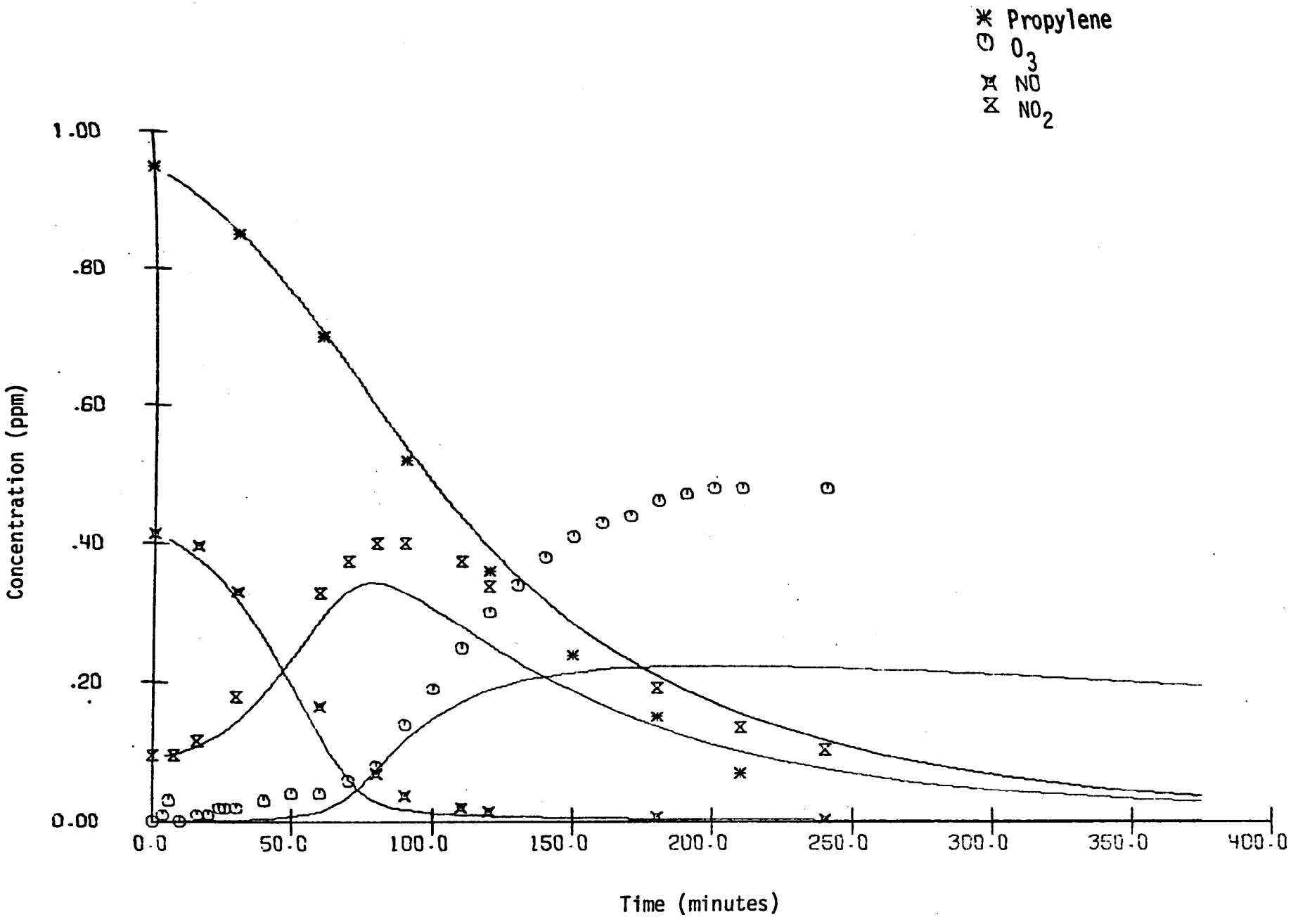

FIGURE 50. S-114 SIMULATION RESULTS AND BATTELLE LABS DATA FOR PROPYLENE, O_3, NO, AND NO_2

(This experiment was done without SO_2)

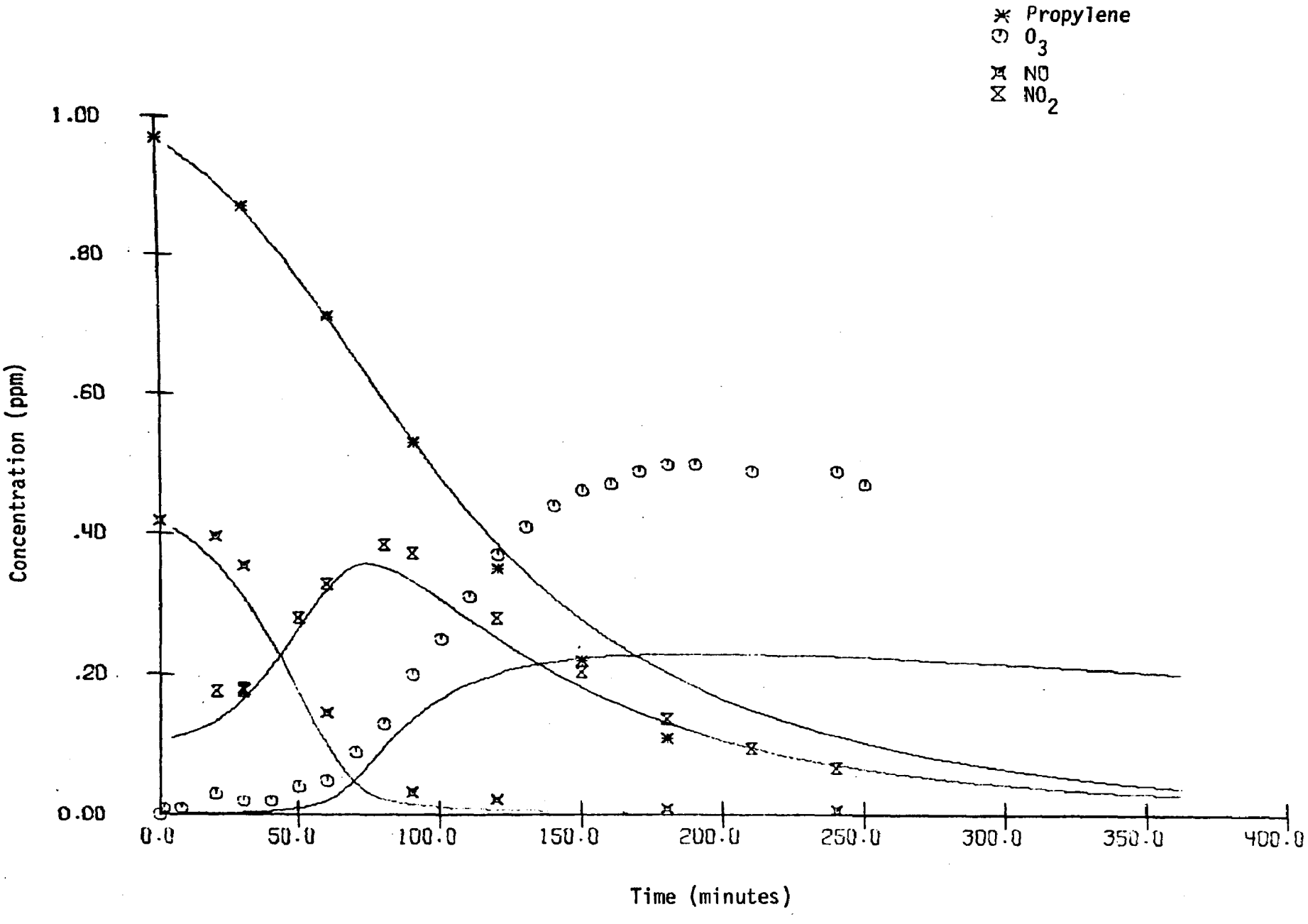

FIGURE 51. S-115 SIMULATION RESULTS AND BATTELLE LABS DATA FOR PROPYLENE, O_3, NO, AND NO_2
(This experiment was done without SO_2)

The NO_2 predictions are good, but it is only fair to reiterate that heterogeneous rate constants were "tuned" to this curve. It was impossible, however, to fit all the data by adjusting these reactions. In S-107 and S-110 post-peak NO_2 predictions are high, whereas in S-113, S-114, and S-115 they are low. O_3 is always low, usually by at least a factor of 2. This could be due simply to under-prediction of propylene oxidation (and consequently over-prediction of NO), though such a large difference is hard to explain. SO_3 appears too late and in too great a quantity, being about a factor of 2 too high in both S-107 and S-110. With proper propylene oxidation and O_3 production, the discrepancy in SO_3 yield would undoubtedly grow even worse, but the time delay would be shortened. One possible source of error could be an overestimate of the rate of reaction of NO_3 with SO_2. The rate constant of 14 ppm^{-1} min^{-1} is, after all, Davis' (1974) upper limit. Table 12 summarizes the magnitude of the various modes of SO_2 oxidation as a function of time. NO_3 does not account for more than 10 percent of the net oxidation rate until after 3 hours. Then it accounts for one-fourth to one-third of the total rate. Since the discrepancy between the data and predictions appears in the form of an overshoot late in the reaction, NO_3 is a likely culprit. Thus, a measurement of the NO_3 + SO_2 rate constant is needed.

Table 11

BATTELLE PROPYLENE-NO_x-SO_2 EXPERIMENTS

	Initial concentrations of Reactants (ppm)				
Run No.	NO	NO_2	SO_2	Propylene	k_1
S-107	0.328	0.113	0.474	1.03	0.175
S-110	0.392	0.099	0.480	1.10	0.177
S-113	0.409	0.099	0.482	0.96	0.079
S-114	0.414	0.095	0	0.95	0.172
S-115	0.417	0.108	0	0.97	0.176

Table 12

RATES OF SO_2 OXIDATION BY VARIOUS OXIDANTS
(From the S-107 Simulation)

Time (min)	Oxidant	Rate (ppm min^{-1})
60	OH·	8.8×10^{-5}
	$RO_2^·$	5.6×10^{-5}
	$RC(O)O_2^·$	6.1×10^{-6}
	$HO_2^·$	1.1×10^{-4}
	NO_3	7.2×10^{-6}
	Total	2.7×10^{-4}
120	OH·	4.5×10^{-5}
	$RO_2^·$	1.4×10^{-4}
	$RC(O)O_2^·$	1.8×10^{-5}
	$HO_2^·$	1.8×10^{-4}
	NO_3	3.2×10^{-5}
	Total	4.2×10^{-4}
180	OH·	2.1×10^{-5}
	$RO_2^·$	1.9×10^{-4}
	$RC(O)O_2^·$	3.8×10^{-5}
	$HO_2^·$	1.2×10^{-4}
	NO_3	4.9×10^{-5}
	Total	4.2×10^{-4}
240	OH·	1.1×10^{-5}
	$RO_2^·$	2.4×10^{-4}
	$RC(O)O_2^·$	8.0×10^{-5}
	$HO_2^·$	6.8×10^{-5}
	NO_3	1.2×10^{-4}
	Total	5.2×10^{-4}
300	OH·	7.1×10^{-6}
	$RO_2^·$	1.7×10^{-4}
	$RC(O)O_2^·$	2.1×10^{-5}
	$HO_2^·$	4.6×10^{-5}
	NO_3	9.5×10^{-5}
	Total	3.3×10^{-4}
360	OH·	5.4×10^{-6}
	$RO_2^·$	1.2×10^{-4}
	$RC(O)O_2^·$	2.3×10^{-5}
	$HO_2^·$	3.3×10^{-5}
	NO_3	6.6×10^{-5}
	Total	2.5×10^{-4}

Another possible source of the SO_3 discrepancy could be an unmeasured buildup of products on walls. Hence, not all SO_3 would be contained in gas phase aerosols. In the current mechanism, only the reaction $HSO_4^{\cdot} + NO_2 \rightarrow H_2SO_4 + NO_3$ (Reaction 56) was assumed to leave products on the walls.

C. SIMULATIONS OF THE NAPCA TOLUENE-NO_x DATA

The NAPCA data served as a base for our previous two years of mechanism development (Hecht et al., 1974b; Hecht et al., 1973). The latter reference describes the chamber and experimental techniques and discusses the data.

1. The Mechanism Used

The mechanism for toluene oxidation, described in Chapter II, is presented in Table 13. The inorganic reactions, not included there, are the same as those in Table 6. The formaldehyde chemistry was also taken from Table 6. The photolysis reactions were adjusted to $k_1 = 0.266$, and the following changes were made in heterogeneous HNO_x chemistry:

$$k_9 = 1 \times 10^{-3}$$
$$k_{10} = 3 \times 10^{-11}$$
$$k_{11} = 6 \times 10^{-1} \quad .$$

k_9 is now Jaffee and Ford's (1967) value, and k_{10} has been brought to within a factor of 3 of Noeh et al.'s (1974) value for a metal surface.

2. Results and Discussion

The results of three simulations are displayed in Figures 52 through 57. The NO_2 data for EPA-272 (Figures 54 and 55) between 100 and 300 minutes appear to be erroneous, probably as a result of instrument failure. The initial concentrations and values of k_1 are given in Table 14.

Table 13

TOLUENE OXIDATION MECHANISM

Reaction	Rate Constant ($ppm^{-1}\ min^{-1}$)
$C_6H_5CH_3 + OH\cdot \xrightarrow{O_2} C_6H_5CH_2O_2 + H_2O$	4.5×10^3
$C_6H_5CH_3 + OH\cdot \xrightarrow{O_2} C_6H_4(CH_3)(OH) + HO_2$	4.0×10^3
$C_6H_4(CH_3)(OH) + OH\cdot \xrightarrow{O_2} C_6H_4(CH_3)(O\cdot)(O_2) + H_2O$	3.0×10^4
$C_6H_5CH_3 + OH\cdot \xrightarrow{O_2} C_6H_5OH + CH_3O_2$	7.0×10^2
$C_6H_5OH + OH \xrightarrow{O_2} C_6H_5(O)O_2 + H_2O$	1.0×10^4
$C_6H_5CHO + OH\cdot \xrightarrow{O_2} C_6H_5C(O)O_2 + H_2O$	1.0×10^4
$C_6H_5CH_2O\cdot \xrightarrow{O_2} C_6H_5O_2 + H_2CO$	$1.5 \times 10^{4\dagger}$
$C_6H_5CH_2O\cdot + O_2 \rightarrow C_6H_5CHO + HO_2$	0.4
$C_6H_5CH_2O_2 + NO \rightarrow C_6H_5CH_2O\cdot + NO_2$	1.0×10^3
$C_6H_4(CH_3)(O)O_2 + NO \xrightarrow{O_2} NO_2 + C_6H_3(CH_3)(O)O + HO_2$ (Me-quinone)	1.0×10^3
$C_6H_5(O)O_2 + NO \xrightarrow{O_2} NO_2 + C_6H_4(O)O + HO_2$ (Quinone)	1.0×10^3
$C_6H_5O_2 + NO \rightarrow NO_2 + C_6H_5(O)O_2$	1.0×10^3
$C_6H_5C(O)O_2 + NO \xrightarrow{O_2} NO_2 + C_6H_5O_2 + CO_2$	1.0×10^3
$C_6H_5C(O)O_2 + NO_2 \rightarrow C_6H_5C(O)O_2NO_2(PB_2N)$	3.0×10^2
$C_6H_5C(O)O_2NO_2 \xrightarrow{O_2} C_6H_5O_2 + NO_3 + CO_2$	$3.0 \times 10^{-3\dagger}$
$HO_2 + C_6H_5C(O)O_2 \rightarrow C_6H_5C(O)O_2H$	3.0×10^3
$HO_2 + C_6H_5CH_2O_2 \rightarrow C_6H_5CH_2O_2H + O_2$	3.0×10^3
$HO_2 + C_6H_5O_2 \rightarrow C_6H_5O_2H + O_2$	3.0×10^3
$HO_2 + C_6H_5(O)O_2 \rightarrow C_6H_5(O)O_2H$	3.0×10^3
$HO_2 + C_6H_4(CH_3)(O)O_2 \rightarrow C_6H_4(OH_3)(O)O_2H$	3.0×10^3

$^{\dagger}min^{-1}$

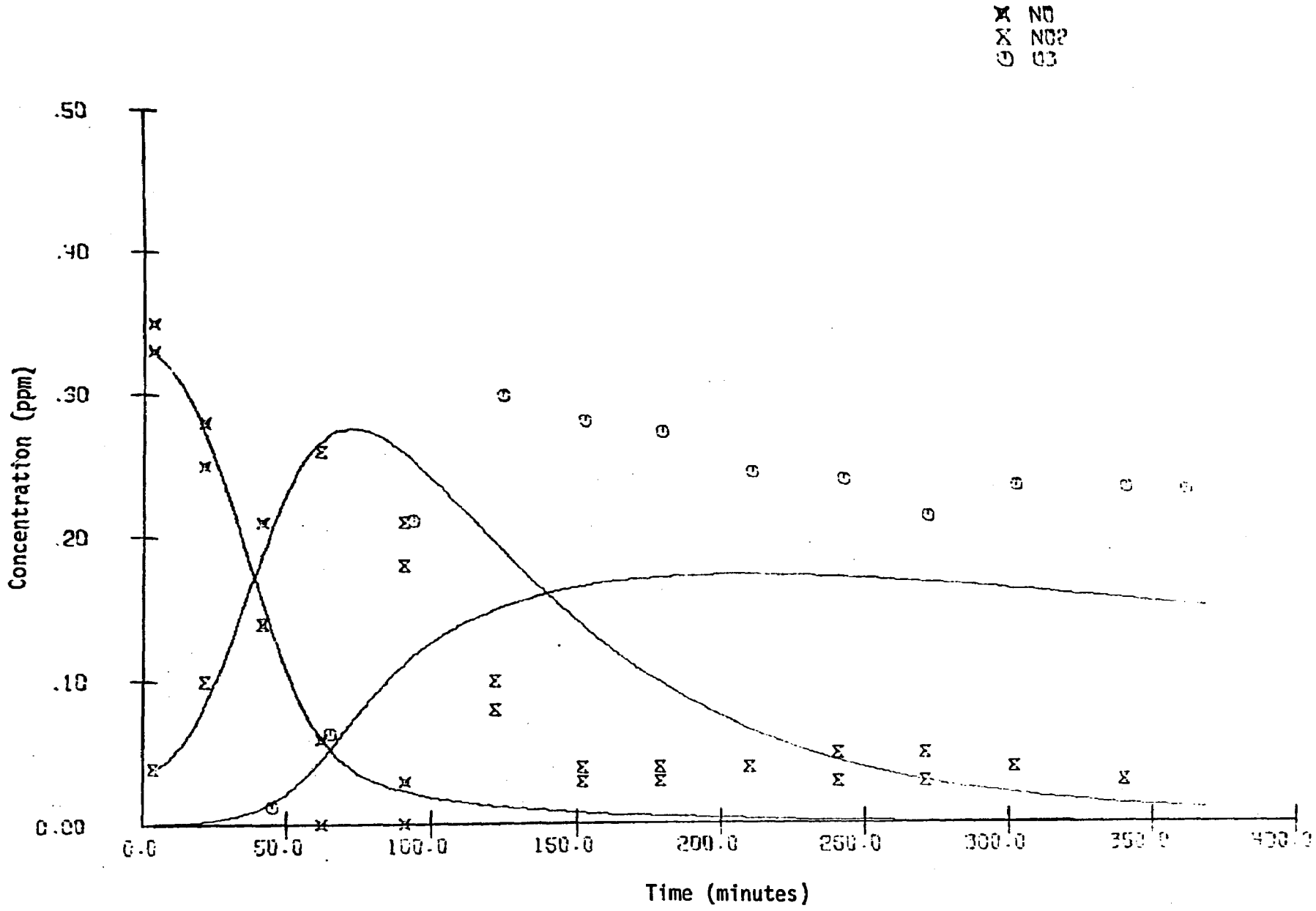

FIGURE 52. EPA-258 SIMULATION RESULTS AND NAPCA DATA FOR NO, NO_2, AND O_3

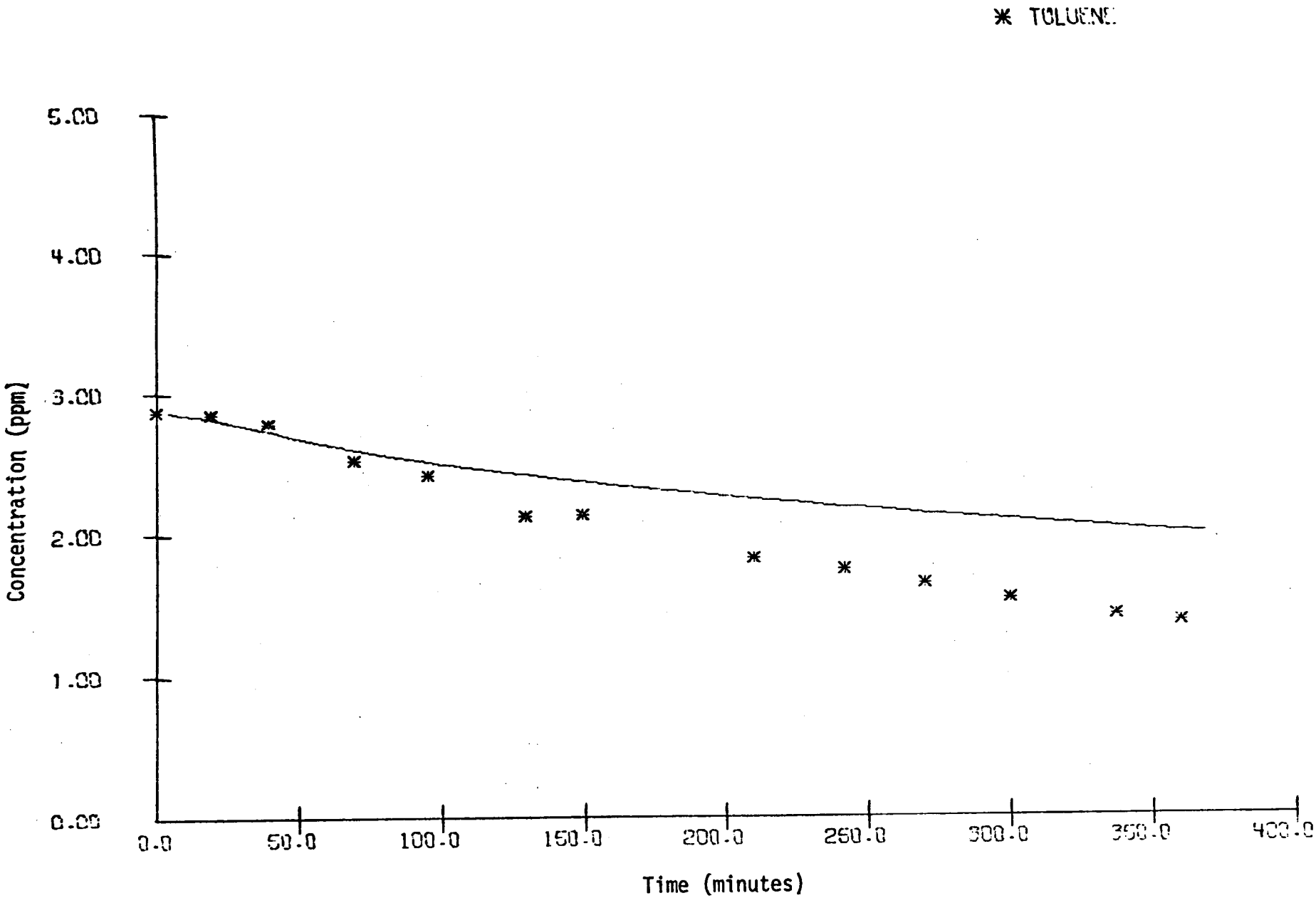

FIGURE 53. EPA-258 SIMULATION RESULTS AND NAPCA DATA FOR TOLUENE

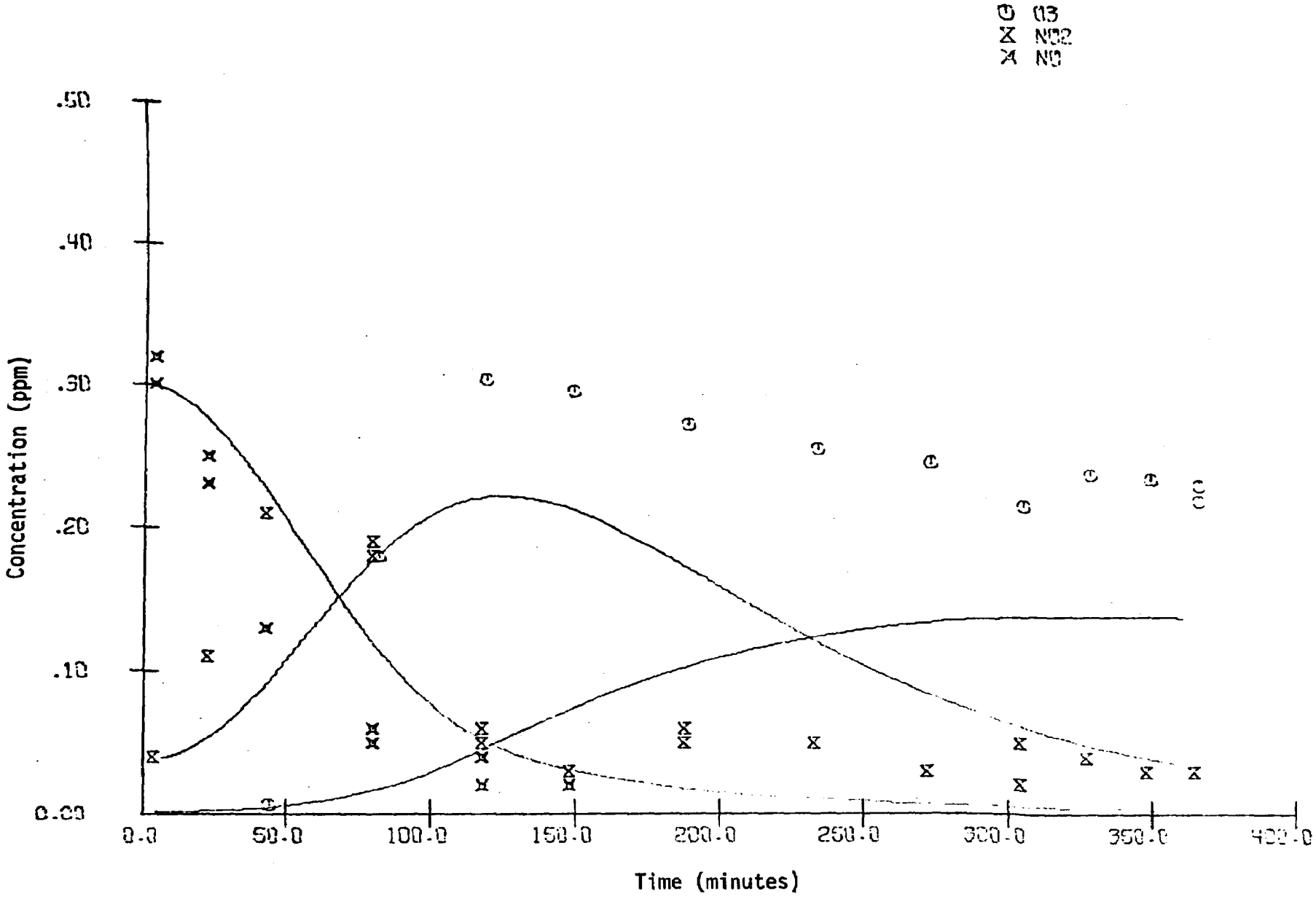

FIGURE 54. EPA-272 SIMULATION RESULTS AND NAPCA DATA FOR NO, NO_2, AND O_3

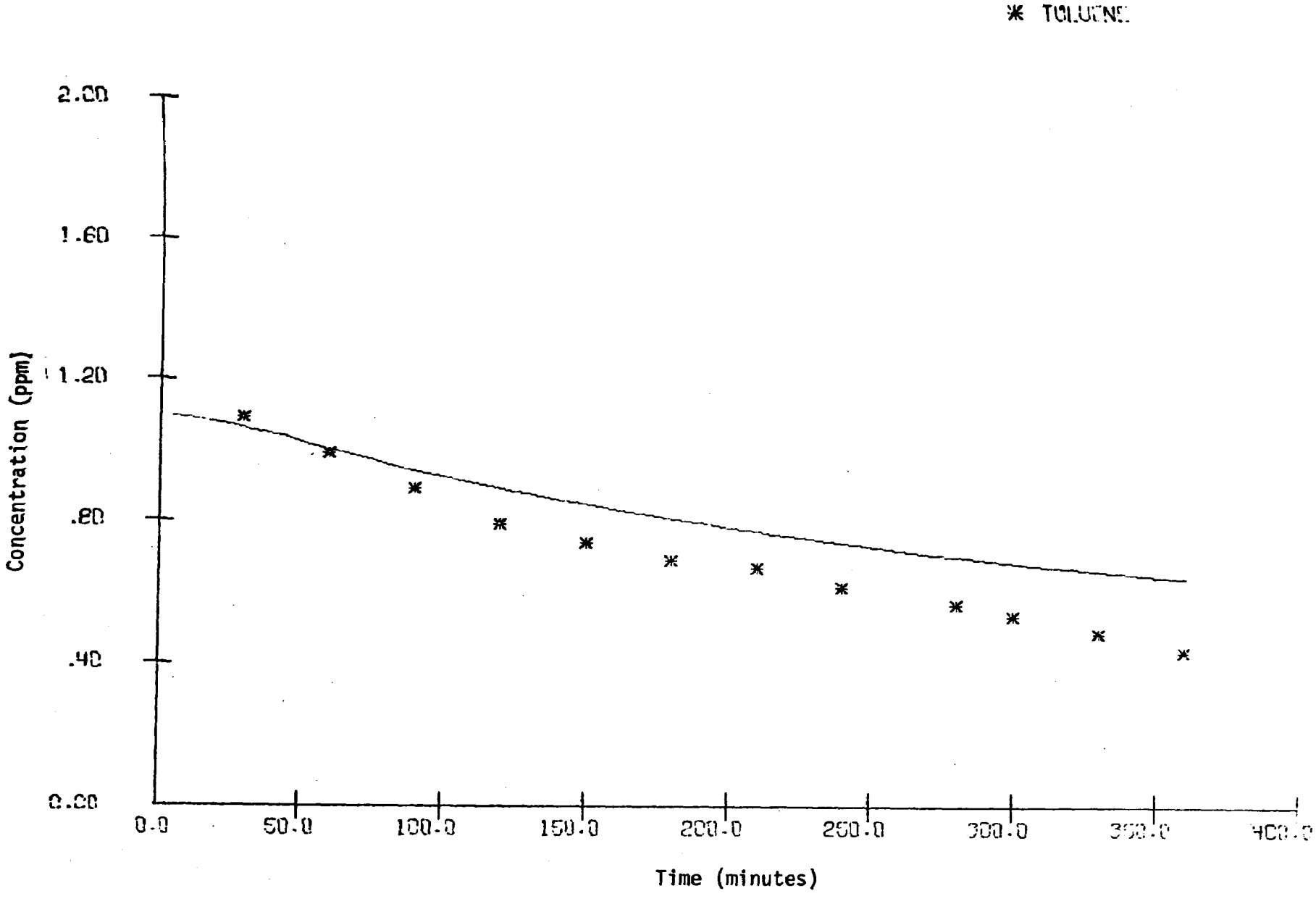

FIGURE 55. EPA-272 SIMULATION RESULTS AND NAPCA DATA FOR TOLUENE

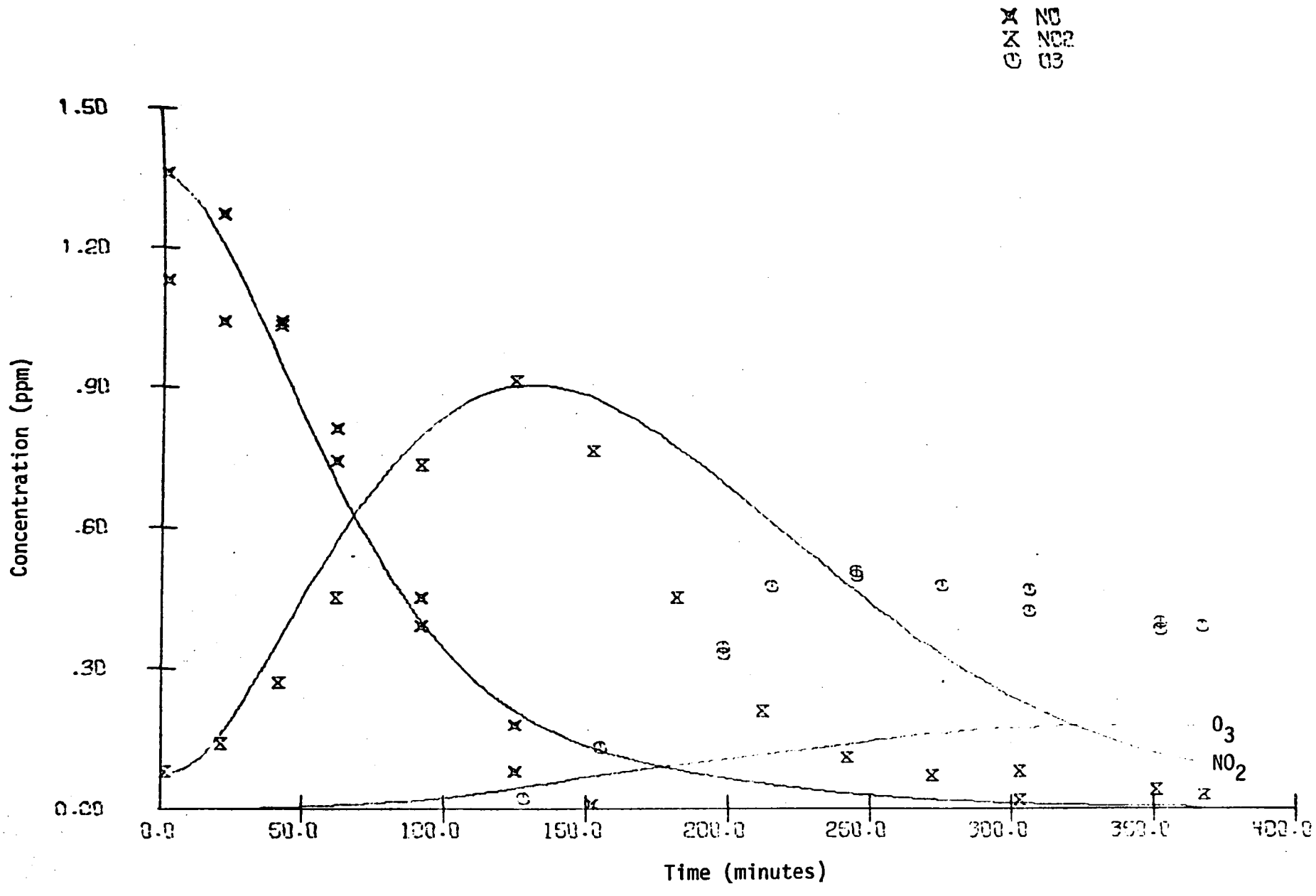

FIGURE 56. EPA-305 SIMULATION RESULTS AND NAPCA DATA FOR NO, NO_2, AND O_3

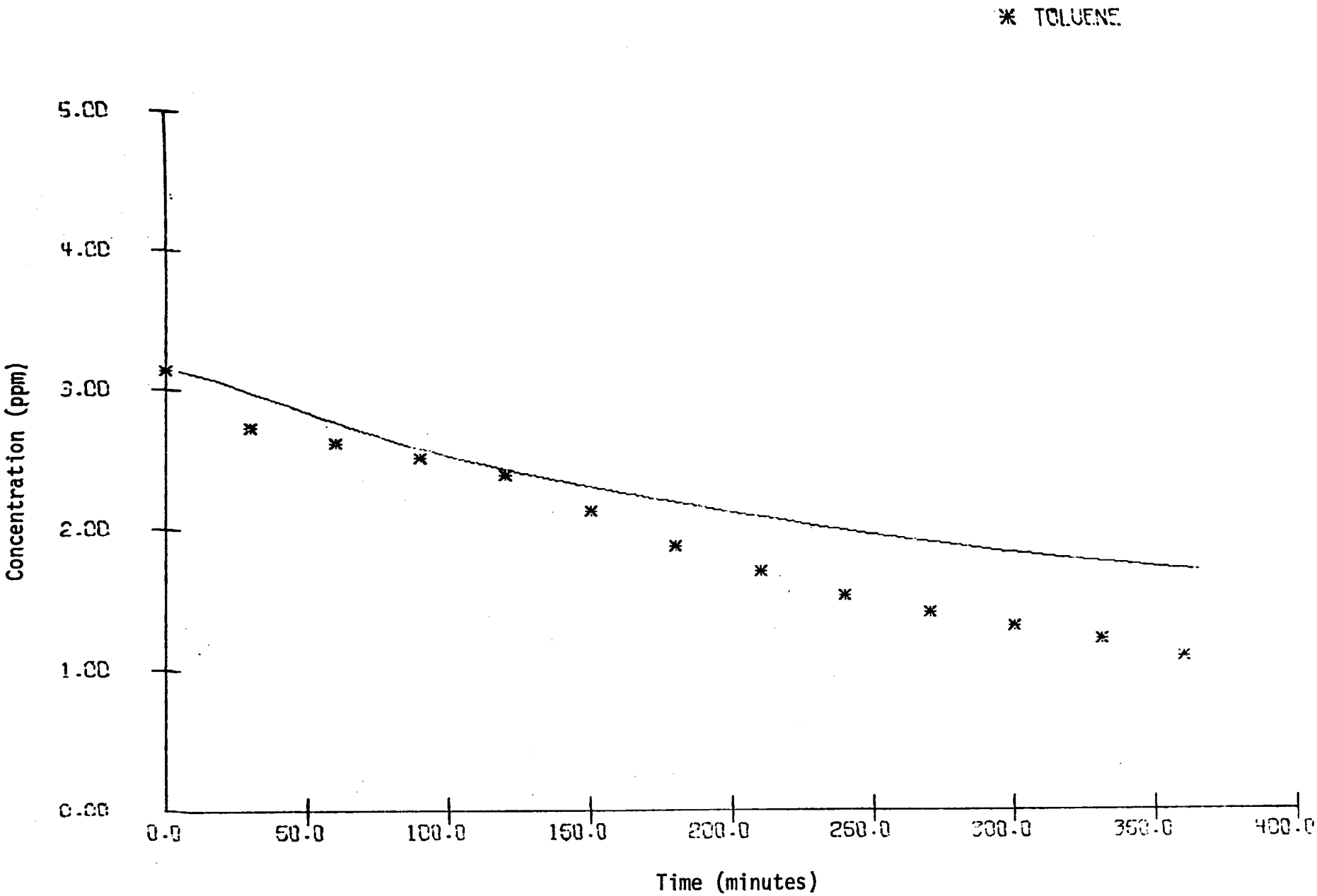

FIGURE 57. EPA-305 SIMULATION RESULTS AND NAPCA DATA FOR TOLUENE

Table 14

INITIAL CONCENTRATIONS AND VALUES OF k_1 FOR THE NAPCA TOLUENE-NO_x EXPERIMENTS

EPA Run No.	NO	NO_2	Toluene	k_1
258	0.33	0.04	2.88	0.266
272	0.30	0.04	1.10	0.266
305	1.36	0.08	3.14	0.266

The current mechanism cannot match the observed toluene oxidation rate, and, as a result, it under-predicts ozone yields. The hypothetical chain processes for ring oxidation to quinones and methyl group oxidation to benzaldehyde and PBzM are apparently too short. Product analyses currently being performed at UCR may help to clarify the true mechanism of toluene oxidation.

IV HYDROCARBON REACTIVITY

A. SURVEY OF REACTIVITY MEASURES

The concept of "reactivity" is familiar to every chemist, yet a precise definition of the term can often be very difficult. While one might intuitively feel that a given species is more reactive than another, quantification of reactivity requires careful definition of (1) the physical conditions of the system in which reactivity is being determined, (2) the concentrations of the reactants, and (3) the time scale of the reactions. If we restrict consideration to the photochemical reactions occurring in smog chamber experiments, the apparent reactivity of hydrocarbons will depend on the physical characteristics of the chamber system, e.g., light intensity, temperature, and surface-to-volume ratio. The rate of disappearance of the hydrocarbon (or the appearance rate of products) will also be a function of the concentrations of (1) the hydrocarbon, (2) the oxidants of the hydrocarbon, and (3) the other species that either react with or lead to the formation of the oxidants. And, since the chemical state of the system changes continuously, a measure of reactivity based on instantaneous rates of formation or disappearance of chemical species will consequently be a function of time.

We summarize below the criteria that have been used to quantify reactivity. In considering these measures, we assume that the physical state of the system, the initial concentrations of reactants, and the time scales are all suitably defined and controlled, so that a meaningful comparison of the reactivity values for different hydrocarbons can be made. The measures fall into three classifications based on the physical dependence of the index: temporal, concentration, or combined temporal and concentration criteria.

1. Temporal Measures

Many indices have been constructed to characterize reactivity in terms of the temporal occurrence of chemical or associated physiological events during the smog formation process.

The most common of these include:

> The time of the NO_2 peak (τ_{max}) (Altshuller and Cohen, 1963).
> τ_{max} for oxidant or ozone (Altshuller and Bufalini, 1971).
> The time required for one-half or one-quarter of the initial hydrocarbon to be oxidized (Altshuller and Bufalini, 1971).
> The threshold time for eye irritation (Heuss and Glasson, 1968).

Other criteria that might be considered are the threshold times for "harmful" effects measurable in terms of biological indicators (Feldstein, 1974). However, such effects--for example, the onset of eye irritation--are difficult to quantify.

2. Concentration Measures

The intensity of smog formation is often assessed in terms of the concentrations of major primary and secondary pollutants. As a result, some investigators have chosen to base hydrocarbon reactivity measures on the maximum concentrations of products that ultimately form. Their criteria include:

> Maximum (or asymptotic) oxidant (Heuss and Glasson, 1968; Altshuller and Bufalini, 1971; Dimitriades and Wesson, 1972).
> Maximum eye irritation*--a function of the concentrations of lachrymators and other irritants (Heuss and Glasson, 1968; Altshuller and Bufalini, 1971).

---

* Yeung and Phillips (1973) have attempted to relate reactivity to eye irritation through the use of a "biological effect factor":

$$\text{Relative Chemical Reactivity} = \frac{\text{Relative Eye Irritation Reactivity}}{\text{Biological Effect Factor}}$$

Because air pollution really consists of all the products listed above and more, a reactivity measure based on the concentrations of smog components might best be expressed in the form

$$R = \sum_i \alpha_i c_i \quad ,$$

where

R = reactivity measure,
i = an index of all harmful components in the system,
c_i = the maximum concentration of the i^{th} species,
α_i = a species weighting factor relating the toxicity (or other harmful effects) of c_i.

3. Combined Temporal and Concentration Measures

Investigators have also characterized reactivity using measures that depend on both concentration and time. The most common of these criteria are dosage (ppm-min), rate (ppm min^{-1}), rate constants (ppm^{-1} min^{-1}), and percentage of hydrocarbon or NO_x consumed at a fixed time (dimensionless).

a. Dosage

Dosage is defined as

$$\int_{t_0}^{t_f} c_i \, dt \quad .$$

Altshuller et al. (1970) and Dimitriades and Wesson (1972) have used NO_2, oxidant, PAN, and formaldehyde dosages as measures of hydrocarbon reactivity. The choice of t_f, the ending period of the integration, is important. One might wish to use the characteristic residence time of pollutants in major

air basins, the time to the NO_2 peak, or the time to the oxidant peak. The beginning time of the integration, t_0, is usually the initiation of irradiation, but some later time might also be chosen. In the case of oxidant dosage, for instance, it might be more practical to take t_0 as the time of the NO_2 peak. Consideration of maximum one-hour dosages (e.g., $t_f - t_0 = 60$ minutes) might also be appropriate in view of existing federal air quality standards.

b. Rate

The rates of the chemical transformations in polluted air change continuously, and both instantaneous and average rates have been used as measures of hydrocarbon reactivity. The instantaneous rate, $(dc_i/dt)_{t=t_I}$, has been considered by Altshuller and Cohen (1963), using NO_2 as c_i and $t_I = t(1/2\ NO_{2\ max})$ on both the ascending and descending portions of the NO_2 versus time profile. One could also evaluate the slopes at $t_I = 0$ or at the time of maximum slope. Average formation rates for NO_2 can be defined as $1/2(NO)_0/t(1/2$ NO conversion) or as $(NO_2)_{max}/t_{NO_2\ max}$. The former has been taken as a reactivity measure by Heuss and Glasson (1968) and Glasson and Tuesday (1970). Other average rate measures using oxidant rather than NO_2 have been reported by Heuss and Glasson (1968) and Altshuller and Bufalini (1971).

c. Rate Constants

Hydrocarbons in the atmosphere are oxidized principally through reactions with O, OH·, and O_3. Of these three species, OH· is thought to be the most important oxidant of all classes of hydrocarbons, and the rate constant for the OH-hydrocarbon reaction has been used by Niki et al. (1972) to characterize reactivity. They found that k_{OH} correlated much better with the reactivity measures of Glasson and Tuesday (1970) and Altshuller and Cohen (1963) than did k_O or k_{O_3}, the respective rate constants for the O and O_3 oxidation reactions of hydrocarbons.

d. Percent Hydrocarbon Oxidation

A final measure of reactivity is the percentage of initial hydrocarbon oxidized at a fixed time (Altshuller and Bufalini, 1971). As in the case of dosage, one might consider a time span equivalent to the residence time of an air mass in a polluted air basin, the time of the NO_2 peak, the time of the ozone peak, or some other relevant period.

B. MEASURE ASSESSMENT

Since an evaluation of all of the measures listed above would be impractical, this study has been limited to a group representative of the simplest and most practical of those proposed. The evaluation process is described in Section 2; the final selections are reported in Section 3.

A primary application of reactivity measures is the prediction of the smog formation potential of mixtures of hydrocarbons emitted as automobile exhaust and solvent fumes. Predictive ability is essential to effective control-strategy planning and evaluation (Dimitriades, 1973). As part of the present study, several smog simulations using mixtures of olefins and NO_x in air were performed to determine whether mixture reactivity can be predicted for these simple cases. The results of the mixture study appear in Section 4. A semi-theoretical justification for some experimental observations made during this study is presented in Section 5. The section immediately following describes experimental methods.

1. Scope and Procedure

a. Mathematical Simulation

The data used in this study were generated by the mathematical model for smog simulation presented in Table 8 of the Second Annual Report (Hecht et al., 1974b). The use of numerical rather than physical experiments is unusual, but it offers definite advantages. Initial concentrations can be

specified precisely; ambiguities due to chamber effects are absent; the concentrations of all species (including free radicals) are known at any given time; "experiments" are quick (a few seconds of computation), easy, and inexpensive to carry out; and instrumentation is not needed to measure species concentrations.

The principal drawback to modeling is its possible inaccuracy in representing reality. For the present purpose, which is the theoretical evaluation of reactivity measures, it is not mandatory that the kinetic mechanism be absolutely accurate, since all comparisons of measures are made between computed results. If the mechanism were infallible, reactivity could be evaluated directly by simulation. As an example of direct simulation, consider an industrial process that normally results in atmospheric concentrations of 1 ppm propylene, 0.2 ppm NO, and 0.02 ppm NO_2. Suppose, in addition, that at a slightly higher cost, about one-half this propylene could be oxidized to form aldehyde (and CO_2). Kopczynski et al. (1974) and Dimitriades and Wesson (1972) showed that aldehydes can be as reactive as olefins, so the effect of this partial oxidation is not, a priori, obvious. The utility of this proposed approach to hydrocarbon emissions reduction would therefore be of concern to control strategists. Figure 58 demonstrates how direct simulation can be used. As this figure shows, in this simple system the production of smog constituents (typified here by O_3) can be predicted quite easily and the cost-effectiveness of the proposed strategy thus evaluated. Unfortunately, obtaining a perfected mechanism for the entire spectrum of emitted pollutants would require an overwhelming validation effect. The present study requires only that the model suffice for the purpose of measure comparison. The model has been tested extensively and shown to be capable of providing reasonably accurate predictions of smog chamber data (see the Second Annual Report, Hecht et al., 1974b).

b. Purpose

The assessment of factors pertinent to reactivity determination can help in the planning of laboratory experiments, improve the efficiency of data

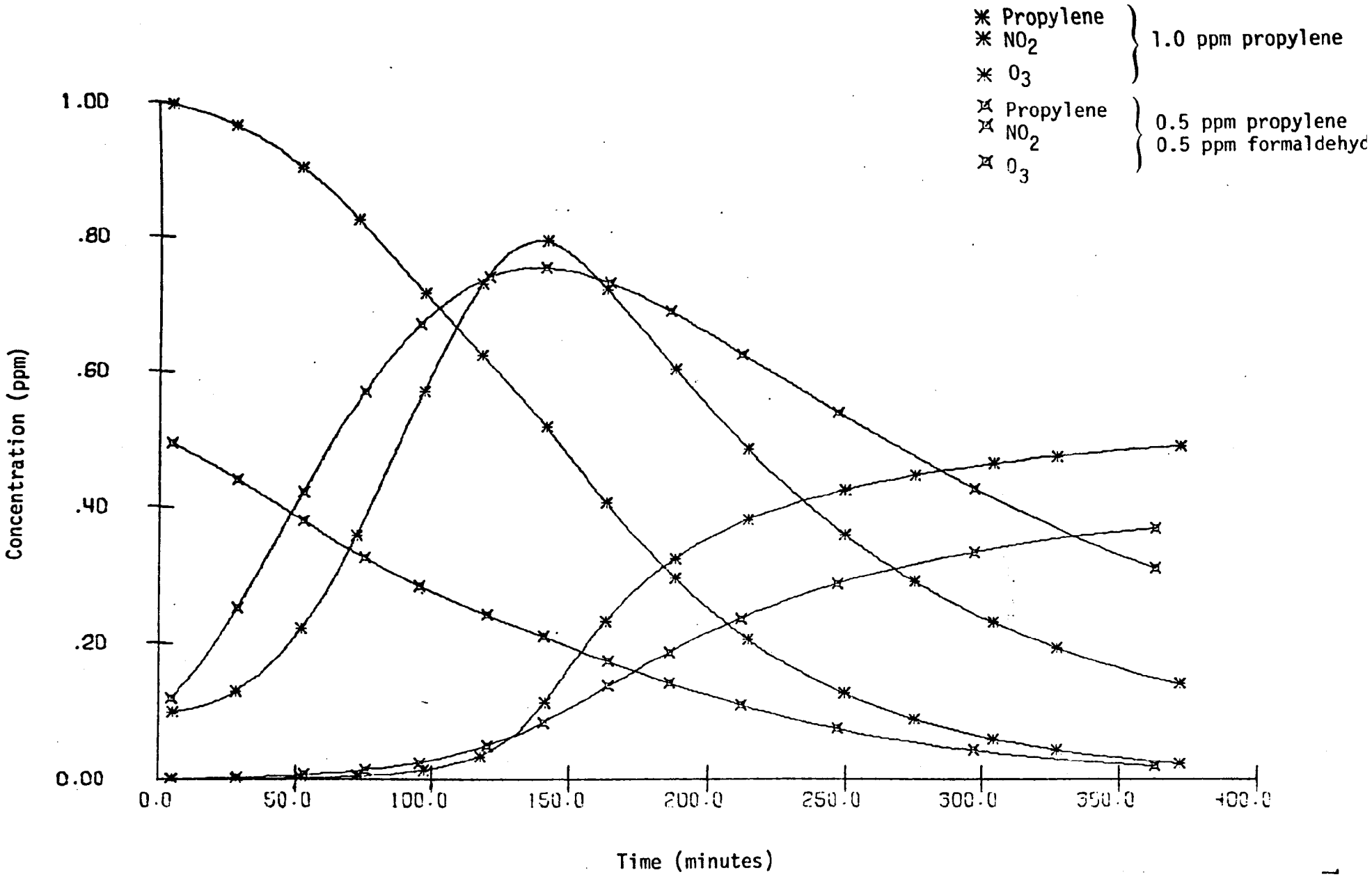

FIGURE 58. THE USE OF KINETIC SIMULATIONS TO ASSESS REACTIVITY

collection, and provide heuristic guidelines for impact evaluation. Toward this end, the kinetic mechanism provides a basis for conclusions, strengthens arguments, and tests hypotheses. Although the mechanism has been validated for a restricted number of hydrocarbons, by using it as a "laboratory" we have obtained results that hopefully have broad significance.

The purpose of this study was not to provide absolute quantification of hydrocarbon reactivity. Such quantification, if it is possible, must be obtained from well-controlled laboratory experiments. Extensive tabulations of laboratory results can be found in Heuss and Glasson (1968), Glasson and Tuesday (1970), and an MSA Research Corporation report (1972).

c. Procedure

By inputting desired initial conditions and integrating the appropriate kinetic equations, we obtained concentration-versus-time curves for a given hydrocarbon-NO_x-air system. It was then necessary to select the relevant points, such as peak concentrations or times of peaks, from the computer output to determine values for the various reactivity measures. More details on what these points were and how they were used are given in subsequent sections.

2. Measure Study

a. Criteria for the Evaluation of Measures

While criteria for a good measure are basically intuitive, it is worth mentioning a few of them here. Ideally, a measure of a given hydrocarbon's reactivity would be independent of initial reactant concentrations. Unfortunately, because of the complexity of smog systems, such independence is not realizable. However, some measures will show less variability than others. If the inevitable variations show a consistent trend, it may be possible to specify their functional dependence and, hence, to develop a very useful predictive ability. Within this report, a measure that shows a

small predictable trend is termed "self-consistent." Aside from being self-consistent, satisfactory measures must also be consistent with each other and not widely disparate with accepted reactivity values.

Three pragmatic requirements we have imposed are that the measure be (1) directly related to the production of harmful smog components, (2) clearly defined, and (3) easily and accurately measurable. Without these properties, the applicability of the measure would be severely limited. Other criteria will be developed as needed.

b. Normalization

The results from a study of the measures defined in Table 15 are tabulated in Table 16, and the initial conditions for the experiments reported are shown in Table 17. The entries in Table 16 were normalized by the reactivity of propylene; i.e., they are in units of propylene equivalents. Propylene simulations were carried out at initial NO, NO_2, and hydrocarbon concentrations corresponding to each row, and the times, concentrations, and rates corresponding to each column were determined. These were then used to normalize values obtained for other olefins. Since the rate constants are inversely proportional to time, for the time scales, an inverse ratio was used, in which the relative reactivity of a given hydrocarbon (HC) is given by the ratio $T_{propylene}/T_{HC}$, where T is the appropriate time scale. For other measures, a direct ratio was used.

c. The Elimination Process

The data in Table 16 do not provide a sufficient basis for choosing the best measure of reactivity without additional considerations. But an inspection of these data does permit a rapid elimination of three of the criteria. The $\%\ HC_{t=100}$ obviously fails the self-consistency test because it produces a wide range of values at various initial concentrations. While showing self-consistency, $NO_2(max)$ and $O_3(max)$ are quite inconsistent with other measures. In fact, they are so close to unity that, in light of model inaccuracy, the differences in reactivity between the various olefins

Table 15

DEFINITIONS OF REACTIVITY MEASURES*

Reactivity Measure	Definition
% $HC_{t=100}$	$100 \times HC_{(t=100\ min)}/HC_0$
$NO_2(max)$	Peak concentration of NO_2
$O_3(max)$	Peak O_3 concentration or asymptotic concentration
Scaling	Reciprocal of the HC concentration required to obtain a $T_{NO_2(max)}$ equal to that of 1 ppm C_3H_6
NO_2 rate	$NO_{2(max)}/T_{NO_2(max)}$
$T_{½}NO$ conversion	Time for the NO_2 concentration to reach the value $[NO_2]_0 + 1/2[NO]_0$
$T_{NO_2(max)}$ (or T_m)	Time to the NO_2 peak
$T_{¼}HC$ conversion (or $T_{¼}$)	Time when $[HC] = 0.75[HC]_0$

* Reactivities relative to C_3H_6 are given by the reciprocal ratio of time scales and direct ratio of all other measures.

Table 16

RESULTS OF THE MEASURE STUDY: REACTIVITIES* RELATIVE TO PROPYLENE

Experiment†	% HC_{100}	$NO_{2(max)}$	$O_{3(max)}$	Scaling	NO_2 rate	$T_{(½\ NO\ conversion)}$	$T_{NO_{2(max)}}$	$T_{¼\ HC}$
1	0.12	--	--	< 0.25	--	--	--	∿ 0.2
2	0.10	0.91	--	0.25	0.23	0.25	0.25	0.23
3	0.16	0.93	0.89		0.23	0.22	0.25	0.23
4	0.27	0.95	0.90		0.28	0.20	0.29	0.24
5	0.29	0.96	0.90		0.28	0.21	0.29	0.26
6	0.18	0.92	0.90		0.28	0.25	0.30	0.24
7	0.06	0.91	--		0.27	0.29	0.30	0.24
8	0.17	0.84	--	0.27	0.23	0.24	0.27	0.26
9			1.16				1.45	1.68
10			1.12				3.27	3.84
11			1.10				1.83	2.11
12			1.09				3.98	5.23
G&T§						0.49		
A&B**							0.36	0.48
A&C††							0.23,0.31	

* The reactivity measures are defined in Table 15.

** Altshuller and Bufalini (1970) values for ethylene.

† The initial concentrations are given in Table 16.

†† Altshuller and Cohen (1963) values for ethylene.

§ Glasson and Tuesday (1971) values for ethylene.

Table 17

INITIAL CONCENTRATIONS FOR EXPERIMENTS LISTED IN TABLES 16 AND 18

Experiment	$[NO]_0$	$[NO_2]_0$	$[HC]_0$	Initial HC Composition
1	0.4	0.1	0.5	HC_5*
2†	0.4	0.1	1.0	HC_5
3	0.4	0.1	2.0	HC_5
4	0.4	0.1	3.0	HC_5
5	0.4	0.1	4.0	HC_5
6	0.2	0.05	1.0	HC_5
7	0.48	0.02	1.0	HC_5
8	0.5	0.1	1.0	HC_5
9†	0.4	0.1	1.0	HC_1
10†	0.4	0.1	1.0	HC_2
11†	0.4	0.1	1.0	HC_3
12†	0.4	0.1	1.0	HC_4
13†	0.4	0.1	1.0	0.2 each HC_1, HC_2, HC_3, HC_4, and HC_6
14	0.3	0.075	1.0	0.2 each HC_1, HC_2, HC_3, HC_4, and HC_6
15	0.48	0.02	1.0	0.25 each HC_2, HC_4, HC_5, and HC_6
16†	0.4	0.1	1.0	0.25 each HC_2, HC_4, HC_5, and HC_6
17	0.4	0.1	0.6	0.15 each HC_2, HC_4, HC_5, and HC_6

* In this study HC_1 ≡ 1-butene; HC_2 ≡ cis-2-butene; HC_3 ≡ 2-me-1-butene; HC_4 ≡ 2-me-2-butene; HC_5 ≡ ethylene; HC_6 ≡ propylene.

† These initial conditions are defined as "standard." Experiments 2 and 9 through 13 provided data for the mixture study.

are insignificant when they are based on either NO_2(max) or O_3(max). The investigators who successfully used O_3(max) probably defined it either as a peak or, when no peak occurred, as the concentration of O_3 at the end of a time-limited experiment; they are usually not clear on this point. The entries omitted from Table 16 correspond to experiments in which O_3 had reached neither a peak nor an asymptotic value by the end of 400 minutes. In these omitted cases, the final value indicated a reactivity significantly less than one. Thus, the definition of O_3(max) varies, depending on whether a peak is reached. The values of reactivity obtained will thus depend on the length of the experiment; they are neither clearly defined nor consistent. We surmise that O_3(max) and NO_2(max) are insufficient measures.

As shown in Section 5, scaling can be demonstrated to be equivalent to T_m. Their theoretical equivalence is borne out by experimental evidence, as shown in Table 16.

Relative reactivity based on the NO_2 rate is defined as NO_2(max) times T_m (it is multiplicative because of the inverse normalization of time scales). Since the NO_2(max) values are all close to unity, the difference between T_m and the NO_2 rate should be small. The added complexity in rate determination hardly seems worthwhile. Because it is a "combined spatio-temporal" measure, the error in determination of the NO_2 rate is the sum of errors of its component parts. Clearly, if one of these components is a good measure, accuracy as well as simplicity can be gained by using it alone. A last, and possibly undesirable, property of the NO_2 rate is that it is a difference approximation to the rate of NO_2 formation. Therefore, it does not represent the actual rate at any point on the NO_2 curve; it is instead an average value.

$T_{½NO\ conversion}$ is a widely used measure, usually appearing in the guise of "NO photooxidation rate," defined as $NO_0/2T_{½}$ (c.f., Glasson and Tuesday, 1970). Since, in the present study, relative reactivities were computed at a given NO_0, this column in Table 16 could just as easily have been labeled "$R_{(NO\ photooxidation)}$". Interpreted as such, $T_{½}$ also has the possible shortcoming of being a difference approximation, although it is a

very good one when the induction period is negligibly short. $T_{\frac{1}{2}}NO$ conversion, as defined in Table 15, is not the half-time for NO_2 formation, rather it falls somewhere between the half-time and peak time of NO_2. Its location relative to the time of product formation is therefore ill defined. Thus, the most objectionable quality of $T_{\frac{1}{2}}$ is its lack of direct correlation with O_3 production or other harmful smog constituents. In the application of reactivity criteria to pollution control, this is indeed a serious shortcoming.

$T_{NO_2(max)}$ and $T_{\frac{1}{4}}HC$ conversion, the only measures left, are the measures we have selected for use. Because of their importance to the present study, they are discussed in detail in Section 3.

The results of other investigations are also included in Table 17 for the purpose of indicating the need to eventually combine the work contained in this report with laboratory investigations. Meaningful comparisons of our values with those of the other investigators cannot be made now because experimental conditions generally differ considerably.

3. The Measures Selected

a. Practicality

The measures found to be most conducive to the quantification of smog effects are the time of the NO_2 peak, $T_{NO_2(max)}$ (hereafter denoted as T_m), and the time required for one-quarter of the initial hydrocarbon to be oxidized ($T_{\frac{1}{4}}$). In the terminology introduced in Section A, these are temporal measures. By being one dimensional, they avoid the increased measurement error inherent in the combined concentration and temporal measures. Both are simply and clearly defined. Although the NO_2 peak may not be sharply resolved in practice, interpolation methods along with extremum theory provide for its accurate determination. A parabolic curve fit can be used for this purpose.

As shown by the results of Experiments 1 through 5 in Table 16, the relative reactivity of ethylene based on T_m (hereafter abbreviated RR_{T_m}) varies by about 15 percent as the initial hydrocarbon concentration (HC_0) is changed by a factor of 4. There is a visible trend toward increasing RR_{T_m} with increasing HC_0. Although any variability is undesirable, the fact that it is small indicates that the RR_{T_m}, measured as a single HC_0, may be applicable throughout a wide range of HC_0's (at fixed NO_0 and $NO2_0$). It may even be possible to capitalize on the consistency of the trend to estimate the accuracy of a constant value in this range.

At fixed HC_0, increasing $NO_0/NO2_0$ by a factor of 6 caused an increase in RR_{T_m} of almost 20 percent (see Experiments 2 and 7). In Section 5, this behavior is shown to be attributable to induction period effects. Because of its role in determining RR_{T_m}, further study of the induction period would be useful.

As shown by the data in Table 17, $RR_{T_{1/4}}$ exhibits the same trend with increasing HC_0 as that observed for RR_{T_m}. But variability with $NO_0/NO2_0$ is almost absent. An increase in this ratio by a factor of 6 caused virtually no change in $RR_{T_{1/4}}$. The slightly erratic behavior shown in Experiment 8 is most probably caused by inaccuracy in this experiment. (Unfortunately, the need to incorporate an interpolation scheme did not become apparent until the late stages of this study.) $T_{1/4}$ is therefore partially inconsistent with T_m. The apparent absence of induction period effects on $RR_{T_{1/4}}$ is interesting and deserves further investigation. It is probably due to the smaller initial slope of the hydrocarbon curve.

b. Usefulness

Aside from considerations of simplicity and consistency, a useful measure must ultimately be related to objectionable pollution effects. Dimitriades et al. (1970) have discussed this issue and concluded that, while no one index is fully satisfactory, "...there is evidence that the over-all [sic] level of activity in the photosimulated hydrocarbon/NO_x

system is reflected in the pattern of NO_2 formation." It is well known that the NO_2 peak is correlated with the formation of O_3 and PAN, two hazardous components of smog. In any "time-limited" system, such as an urban airshed with a characteristic residence time, the amount of O_3 present due to chemical reaction is directly related to T_m. Aldehydes also contribute to the deleterious effects of smog. Because aldehyde appearance is complementary to hydrocarbon disappearance, $T_{\frac{1}{4}}$ is an indication of their importance in a time-limited system. $T_{\frac{1}{4}}$ is also useful for evaluating the magnitude of synergistic effects in mixture reactions. Altshuller and Bufalini (1971) define a synergistic effect as "...one in which the reactivity or the amount of product produced by a given compound is affected by the presence of a second." Since, in general, the oxidation of several hydrocarbons in a particular mixture will lead to the same or similar products, synergism is not easily determined from product measures. A much simpler means, particularly when using a numerical model, is to monitor the rate of hydrocarbon disappearance. For a given hydrocarbon, the change in $T_{\frac{1}{4}}$ from its value in an individual hydrocarbon-NO_x reaction system to that in a multihydrocarbon-NO_x reaction system provides an indication of interactive effects.

c. Measurability

Because laboratory techniques must ultimately be used either to measure reactivity or to obtain empirical constants needed for its prediction, a satisfactory measure must have the additional property that accurate and reliable instrumentation be available for its determination. NO_2 and hydrocarbon concentrations are routinely monitored in smog chamber experiments with reasonable accuracy. Hydrocarbon concentration can be measured with as little as 1 percent error by gas chromatographic methods. In contrast, NO_2 is obtained from the difference between NO_x (after conversion to NO) and NO concentrations. These are measured by chemiluminesence with about 95 percent accuracy. When NO_2 concentrations are low, the percentage error in the difference of these values may be large. When $[NO_2]$ is at its peak and, consequently, [NO] is low, the error in the difference will be at a minimum. The accuracy in $[NO_2]$ at the peak should therefore be close to 95 percent.

Of course, only the temporal location (T_m), not the peak value itself is used. The cycling time for NO measurement is only a minute or two; so a high density of points and, hence, sharp resolution of T_m can be obtained. With reasonably accurate values of concentration and the time of measurement of each point well known, an accurate determination of T_m should be possible.

4. Mixture Study

a. Mixtures Used

Reactivities were computed for five different olefin-NO_x mixtures at the initial concentrations indicated in Table 16. Experimental and predicted results are shown in Table 18. The reactivities are all relative to that of propylene at standard initial conditions (NO_0=0.4, $NO2_0$=0.1, HC_0=1.0). The olefin mixture used in Experiments 13 and 14 is composed of the five most reactive olefins studied and is a typical "highly reactive" mixture. A second mixture, used in Experiments 15 through 17, contains the two most reactive and the two least reactive olefins and is characteristic of a wide reactivity range mixture.

b. Results

The first row of entries for each experiment in Table 18 is labeled "mixture." In Columns 3 and 5 (T_m and $T_{¼}$ measured) of this row, relative reactivities of the olefin mixtures are measured. T_m, as before, is the time of the NO_2 peak. $T_{¼}$ is now the time required for the total olefin concentration to drop by 25 percent. Below the $T_{¼}$ entry are the time for each component olefin to reach 75 percent of its initial concentration. As before, all results are normalized by propylene experiments at the given initial concentrations.

c. Predictions

There are also three prediction columns in Table 18. These are predictions of mixture reactivity computed by the "linear summation" method, defined by:

Table 18

RESULTS OF THE MIXTURE STUDY: MIXTURE REACTIVITIES RELATIVE TO PROPYLENE

		T_m		T_{t_5}			
Experiment	Hydrocarbons	Simulated	LSM	Simulated	LSM Uncorrected Prediction	Simulated Reactivity of Hydrocarbons in Mixture	Prediction Corrected for Synergism
13	Mixture	2.42	2.31	2.86	2.77		2.81
	HC_1*			2.30		1.68	
	HC_2			3.42		3.84	
	HC_3			2.71		2.11	
	HC_4			4.27		5.23	
	HC_6			1.37		1.0	
14	Mixture	2.64	--	2.71	--		2.76
	HC_1			2.15		1.68	
	HC_2			3.39		3.84	
	HC_3			2.53		2.11	
	HC_4			4.44		5.23	
	HC_6			1.21		1.0	
15	Mixture	1.54	--	1.94	--		1.70
	HC_2			2.33		3.84	
	HC_4			2.83		5.23	
	HC_5			0.44		0.23	
	HC_6			1.20		1.0	
16	Mixture	2.16	2.13	2.58	2.56		2.73
	HC_2			3.58		3.84	
	HC_4			4.31		5.23	
	HC_5			0.47		0.23	
	HC_6			2.58		1.0	
17	Mixture	1.26	1.28	1.98	1.54		1.83
	HC_2			2.52		3.84	
	HC_4			3.15		5.23	
	HC_5			0.44		0.23	
	HC_6			1.20		1.0	

* In this study, HC_1 = 1-butene; HC_2 = cis-2-butene; HC_3 = 2-me-1-butene; HC_4 = 2-me-2-butene; HC_5 = ethylene; HC_6 = propylene.

$$R_{LS} = \sum_{i=1}^{n} c_i R_i \quad ,$$

where

R_{LS} = mixture reactivity by linear summation,
n = number of organic mixture components,
c_i = initial concentration of the i^{th} hydrocarbon,
R_i = reactivity of the i^{th} hydrocarbon.

The linear summation technique has been discussed by Glasson and Tuesday (1971) and Dimitriades et al. (1970).

The values of R_i, based on either T_m or $T_{¼}$, were obtained from the experiments in Table 16 as follows: R_1 comes from Experiment 9, R_2 from Experiment 10, R_3 from Experiment 11, R_4 from Experiment 12, R_5 from Experiment 2, HC_6 is the reference olefin (propylene) with a reactivity defined to be 1. (Note, from the definitions of HCs 1 through 6 in the footnote to Table 17, that R_i increases with increased substitution at the double bond.

Column 4 of Table 18 gives the mixture reactivity based on T_m as computed by the linear summation method. The values shown agree very well with observations. Experiments 14 and 15 were done under nonstandard initial NO and NO_2 values, and, therefore, no predictions could be made. Although the initial olefin concentration in Experiment 17 was not the standard value of 1 ppm, prediction could be made by "scaling." This procedure consists simply of multiplying R_{LS} by the ratio of the initial hydrocarbon concentration to its standard value (in this case the RR_{LS} of Experiment 16 times 0.6). Hence, the slower rate at lower hydrocarbon concentrations is compensated for multiplicatively. Justification for the application of the scaling technique to RR_{T_m} is given in Section 5. Its application to $RR_{T_{¼}}$ is not really justifiable because the approximately exponential hydrocarbon decay rate indicates a nonlinear dependence of $T_{¼}$ on HC_0. This explains the low value listed.

d. Synergism

Columns 6 and 7 of Table 18 show both the linearly predicted reactivity of the mixtures and the standard reactivities of their components. The latter were copied from Table 16. Comparison of the standard reactivities in Column 7 with the observed values in Column 5 indicates the presence of synergistic effects. It is evident that in all cases the two most reactive olefins, HC_2 and HC_4, experienced a decrease in relative reactivity, whereas the less reactive olefins experienced an increase. This behavior can be explained qualitatively in the following manner. The competition for available oxidant between higher and lower reactivity olefins depressed the reaction rate of the former. At the same time, the high rate of oxidant production by HC_2 and HC_4 accelerated the consumption of less reactive olefins.

Linear summation was also applied to the synergistically modified values of $T_{\frac{1}{4}}$ ($T_{\frac{1}{4}}$ measured). The resulting mixture reactivities are listed in the last column of Table 18. Although these predictions are close to observed values, we cannot state that they are always an improvement over the unmodified predictions.

Another inconsistency between T_m and $T_{\frac{1}{4}}$ is contained in Table 18. Whereas decreasing NO_{x0} from Experiment 13 to the value used in Experiment 14 increased RR_{T_m}, it decreased $RR_{T_{\frac{1}{4}}}$. Many explanations of this behavior can be offered, including the changed O_3 production and the radical-scavenging ability of NO_2. It is the complex interaction of all these effects that leads to the discrepant behavior.

5. Derivation of Some Properties of T_m

a. Derivation

In this section, the analytical solution for the dependency of T_m on initial hydrocarbon and NO concentrations is obtained through a consideration of simplistic photochemical smog kinetics. Kinetic equations and empiricism based on the observed shape of smog profiles are used toward this end.

O'Brien (1974) has demonstrated that, except in the late stages of the photolytic hydrocarbon-NO_x-air reaction, the concentrations of NO, O_3, and NO_2 are related by the approximation

$$[NO_2] \approx \frac{k_3}{k_1}[NO][O_3] \quad , \qquad \text{(IV-1)}$$

where k_1 and k_3 are rate constants for the reactions

$$NO_2 + h\nu \xrightarrow{k_1} NO + O \quad , \qquad (1)$$

$$NO + O_3 \xrightarrow{k_3} NO_2 + O_2 \quad . \qquad (3)$$

Existence of the photostationary state, expressed by Eq. (IV-1), in smog profiles computed using the Hecht-Seinfeld-Dodge kinetic model has been demonstrated by Liu (1974).

In addition to Reaction (3), the conversion of NO to NO_2 is accomplished through the reaction

$$RO_2\cdot + NO \xrightarrow{k_{42}} RO\cdot + NO_2 \quad , \qquad (42)$$

where R is usually an alkyl group or hydrogen atom. Hence, in the period before the NO_2 peak, the rate of NO production and consumption is governed by Reactions (1), (3), and (42). Thus,

$$\frac{d[NO]}{dt} = k_1[NO_2] - k_3[NO][O_3] - k_{42}[RO_2\cdot][NO] \qquad \text{(IV-2)}$$

Equation (IV-1) can be used to simplify Eq. (IV-2):

$$\frac{d[NO]}{dt} = -k_{42}[RO_2^{\cdot}][NO] \qquad \text{(IV-3)}$$

This expression represents the perturbation to photostationarity introduced by free radical oxidation.

In a completely generalized mechanism, $RO_2^{\cdot}$ includes all free radical oxidation products of hydrocarbons. It is formed in the following reaction:

$$HC_i + O_x \xrightarrow{k_{ox_i}} \alpha_i\, RO_2^{\cdot} \quad , \qquad \text{(IV-4)}$$

where O_x represents a general oxidant (primarily OH· in the time prior to the NO_2 peak), HC_i a hydrocarbon, and α_i an appropriate stoichiometric coefficient (see Hecht and Seinfeld, 1972).

Using Reactions (IV-4), (42), and the steady-state assumption for $RO_2^{\cdot}$* leads to the following equation:

$$[RO_2^{\cdot}] = \frac{k_{ox_i}\alpha_i[HC_i][O_x]}{k_{42}[NO]}$$

Substituting for $RO_2^{\cdot}$ in Eq. (IV-3) and using Reaction (IV-4) gives

$$\frac{d[NO]}{dt} = -k_{ox}\alpha_i[HC_i][O_x] = \alpha_i \frac{d[HC_i]}{dt} \quad . \qquad \text{(IV-5)}$$

The rate terms in Eq. (IV-5) can be used to relate T_m to HC_0 and NO_0 through the use of empirical observation. Figure 59 is an illustration of a typical, through idealized smog profile at initial NO and NO_2 concentrations for which there is a very short induction period. It is apparent that the curves labeled NO and hydrocarbon are approximately linear during the early stages of the reaction. Good approximations in this linear period are

---

* Liu (1974) has demonstrated that this assumption becomes valid within a few seconds of reaction initiation. The neglect of termination reactions in the steady-state expression is valid early in the reaction.

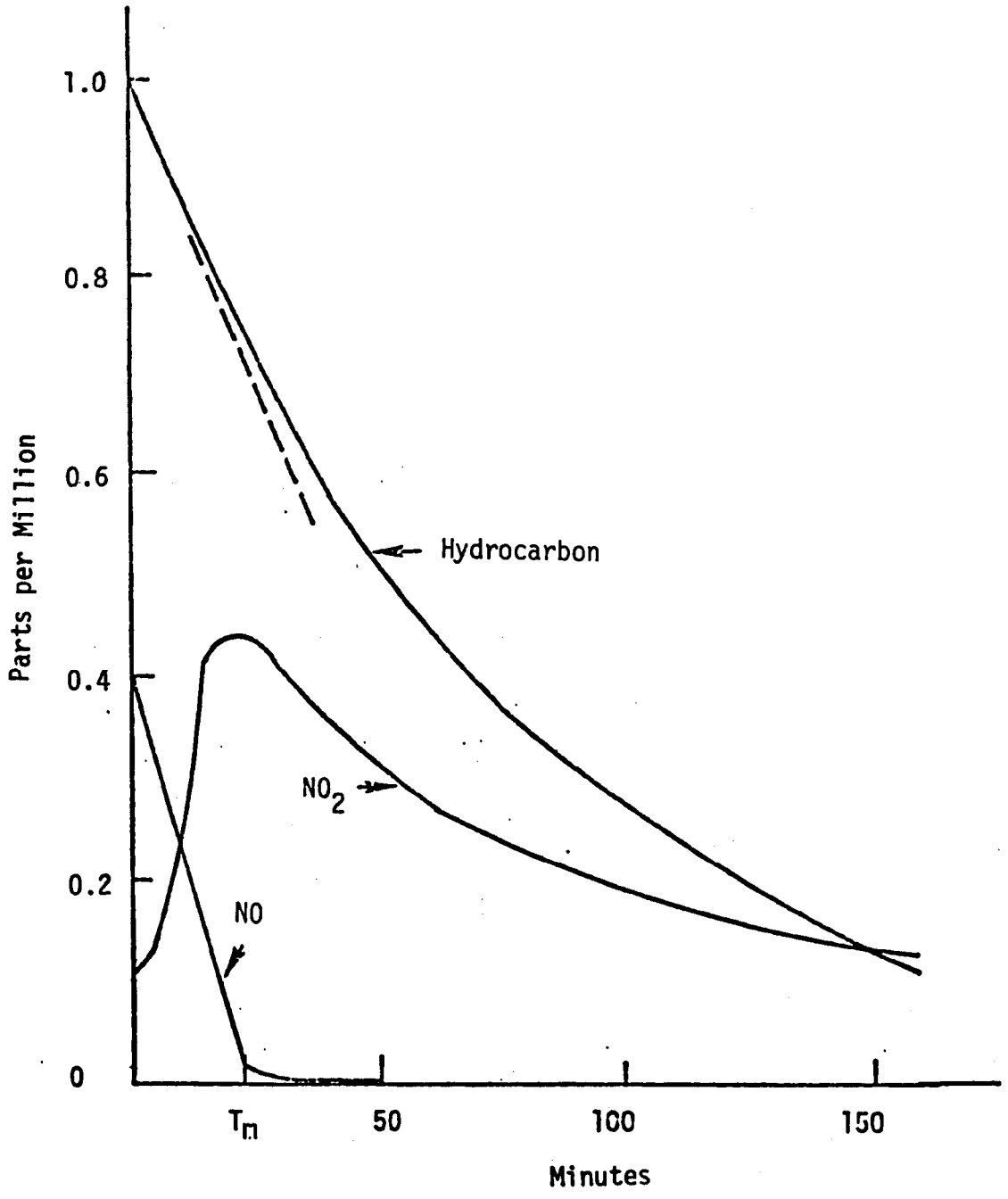

FIGURE 59. TYPICAL SMOG PROFILE

$$\frac{d[NO]}{dt} \approx - \frac{[NO]_0}{T_m} \qquad \text{(IV-6)}$$

and

$$[HC_i] \simeq [HC_i]_0 \ (1 - b_i t) \quad , \qquad \text{(IV-7)}$$

where b_i is a constant related to the slope.

The introduction of HC_{0_i} as a multiplicative factor can be justified by a direct integration of the hydrocarbon rate equation derived from Reaction (IV-4):

$$[HC_i] = [HC_i]_0 \exp\left[- \int k_{0_{x_i}} [O_x] \, dt \right] \approx [HC_i]_0 \left(1 - \int k_{0_{x_i}} [O_x] \, dt\right) \quad ; \quad t < t_m$$

(IV-8)

Comparison of Eq. (IV-8) with Eq. (IV-7) shows that b_i can be related to the average oxidant concentration,

$$b_i t \simeq \int k_{0_{x_i}} [O_x] \, dt \simeq k_{0_{x_i}} [O_x] \, t \quad , \qquad \text{(IV-9)}$$

but such an interpretation is not essential to this derivation. There is no reason to believe that b_i will be independent of NO_0, NO_{2_0}, or HC_{i_0}. Furthermore, the evidence indicates that b_i is proportional to light intensity (Niki et al., 1972; Glasson and Tuesday, 1970). Other factors not considered may also influence b_i. However, the dependence on NO_{x_0} and HC_0 is assumed to be negligible.

Substituting Eqs. (IV-6) and (IV-7) in Eq. (IV-5) and rearranging gives

$$T_m \simeq \frac{[NO]_0}{b_i' [HC_i]_0} \quad ; \quad b_i' \equiv \alpha_i b_i \quad . \qquad \text{(IV-10)}$$

b. Verification and Application

At a fixed initial NO concentration, Eq. (IV-10) states that the time to the NO_2 peak should be inversely proportional to the initial hydrocarbon concentration. In Figure 60, the observed values of T_m are plotted as a function of HC_{i_0} for HC_i = propylene at one NO_0 value and HC_i = ethylene at two values of NO_0. All curves can be fit by the form α/HC_0. From Eq. (IV-10), $\alpha = NO_0/b_i'$. For propylene, the curve fit has been drawn in, whereas for the two ethylene curves it has only been indicated. When the two values of α for ethylene are divided by the corresponding values of NO_0, the results are: $\alpha/NO_0 = 500$ and $\alpha/NO_0 = 496$. Therefore, b_i' for ethylene is 2×10^{-3}.* The data presented in Figure 60 thus confirm Eq. (IV-10).

Equation (IV-10) can be used to predict reactivity relative to propylene (RR_{T_m}):

$$RR_{T_m} \equiv \frac{T_{m\ prop}}{T_{m\ HC_i}} = \frac{b_i'}{b'_{prop}} \frac{HC_{i_0}}{[prop]_0} \quad . \qquad \text{(IV-11)}$$

Once RR_{T_m} has been determined at one HC_{i_0}, it can be predicted at other HC_{i_0}'s by applying Eq. (IV-11). Recall that this is exactly the procedure (called "scaling") used to predict the mixture reactivity in Experiment 17.

The equivalence of scaling and T_m as reactivity measures can be shown as follows: Equation (IV-11), with $T_{m\ HC_i} = T_{m\ propylene}$ and $[prop]_0 = 1$ ppm, states that

$$\left(HC_{i_0}\right)^{-1} = \frac{b_i'}{b'_{prop}} \quad . \qquad \text{(IV-12)}$$

---

* As an order of magnitude check using Eq. (IV-9) and taking O_x as OH·, $k_{OH} = 0.75 \times 10^4$ ppm^{-1} min^{-1}, $\overline{OH}\cdot = 1.5 \times 10^{-7}$ ppm; thus $b_i \sim 1 \times 10^{-3}$ min^{-1} (α_i is then 2).

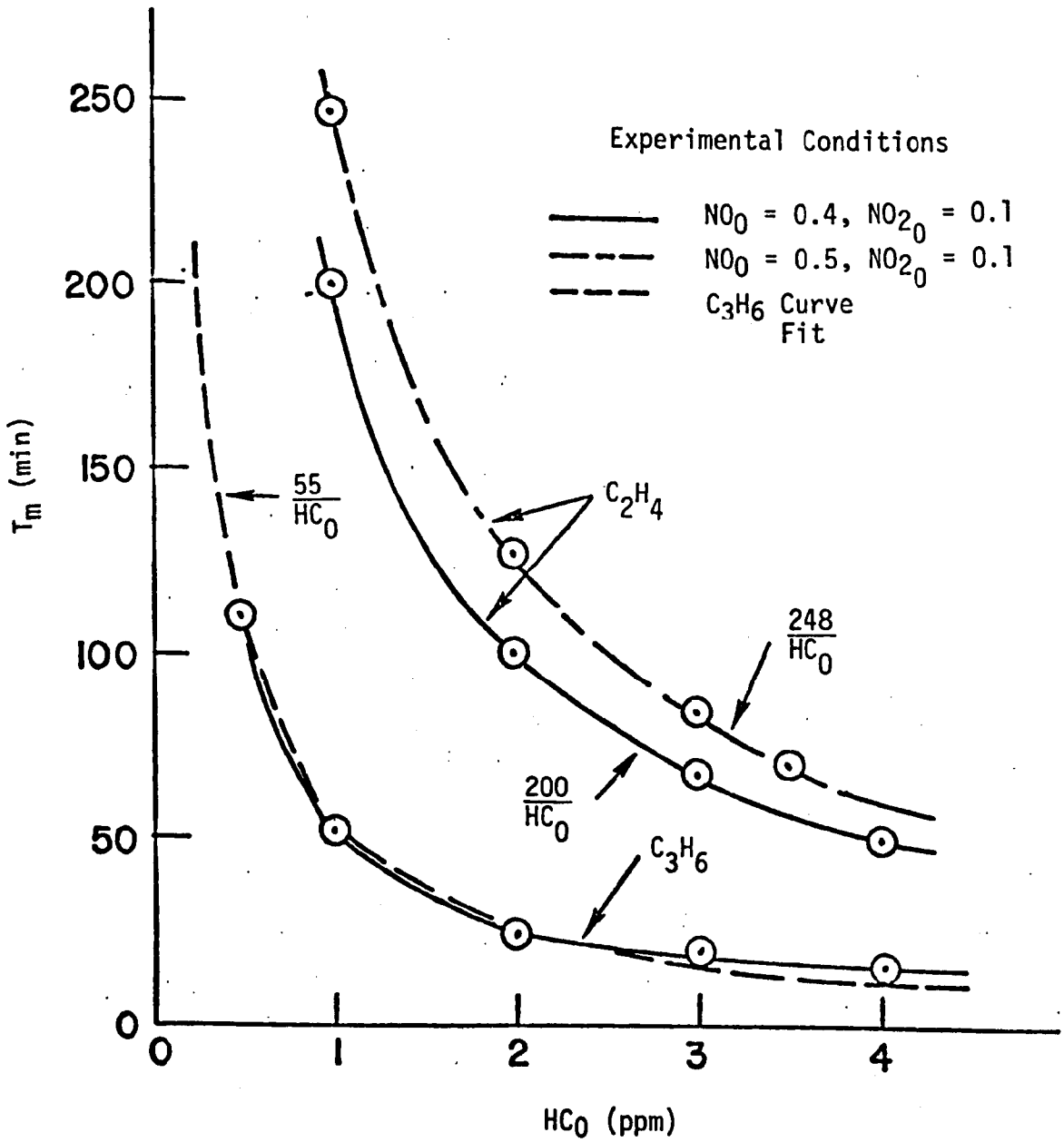

FIGURE 60. T_m AS A FUNCTION OF INITIAL HYDROCARBON CONCENTRATION

This, by definition (Table 15), is the scaling reactivity of HC_i. Because RR_{T_m} is normalized, $HC_{i_0} = [prop]_0$. Thus, from Eq. (IV-11),

$$RR_{T_m} = \frac{b_i'}{b'_{prop}} \quad . \tag{IV-13}$$

The equivalence of RR_{T_m} and scaling follows directly.

The derivation of Eq. (IV-10) can be extended to multihydrocarbon smog systems by summing over the index i from Eq. (IV-4) onward. Equation (IV-10) then becomes (upon inversion)

$$\frac{1}{T_m} \approx \sum_{i=1}^{n} \frac{HC_{i_0} b_i'}{NO_0} \quad , \tag{IV-14}$$

where n is the number of hydrocarbons. Assuming the values of b_i' are those obtained in individual hydrocarbon simulations, the linear summation method results directly. In light of this required assumption, it is surprising that synergistically modified predictions (Table 18) are not better than unmodified values. However, the modified values were based on $RR_{T_{1/4}}$, whereas the above derivation is based on T_m and is not rigorously applicable to $T_{1/4}$.

c. The Induction Period

It is worth reiterating that Eqs. (IV-6) and (IV-7) are valid only if induction period effects are negligible. For this condition to hold, the initial HC/NO_x and NO_2/NO ratios must be relatively high (lower bounds have not been established but 2 and 0.1, respectively, seem reasonable). In addition, the individual values of HC_0, NO_0, and NO_{2_0} may themselves be important.

A striking, and possibly disconcerting, feature of Eq. (IV-10) is the absence of explicit dependence on NO_{2_0}. Dimitriades (1972) found that, for irradiated auto exhaust with an NO_{2_0}/NO_0 ratio of about 0.1, the rate of NO photooxidation was independent of NO_{2_0} as long as NO_{2_0} was above 0.03 ppm. The major effect of low values of NO_{2_0} is to cause a nonnegligible induction period. It seems reasonable to speculate that an induction period of length T_I will simply cause a shift in the start of the "linear period" by T_I. T_m can then be replaced by

$$T'_m = T^0_m + T_I \quad , \tag{IV-14}$$

where T^0_m is given by Eq. (IV-10). $RR_{T'_m}$ is defined as follows:

$$RR_{T'_m} \equiv \frac{T'_{m\ prop}}{T'_{m_i}} = \frac{T^0_{m\ prop} + T_{I\ prop}}{T^0_{m_i} + T_{I_i}} \tag{IV-16}$$

$$\approx RR_{T^0_m} + \frac{T_{I\ prop}}{T^0_{m_i}} - RR_{T^0_m} \frac{T_{I_i}}{T^0_{m_i}} \tag{IV-17}$$

where $T_I/T^0_m << 1$ has been assumed. If hydrocarbon i is less reactive than propylene ($RR^0_{T_m} < 1$) and has an induction period about equal to that of propylene, the correction to $RR_{T^0_m}$ will be positive.* Conversely, for more reactive hydrocarbons ($RR_{T^0_m} > 1$), the correction will be negative. The induction period, therefore, always has the effect of shifting the relative reactivity toward unity. The increase in RR_{T_m} with decreasing initial $[NO_2]$ from a value of 0.25 in Experiment 2 (Table 17) to 0.30 in Experiment 7 can be cited as evidence of this tendency.

Since atmospheric concentrations include the range of NO_{0}, NO_{2_0}, and HC_0 for which there is an induction period, methods for predicting T_I are needed. Apparently, an inverse dependence on NO_{2_0} is indicated.

---

* Under these conditions, $RR_{T'_m} \approx RR_{T_{m_0}} + \left(T_I/T^0_{m_i}\right)\left(1 - RR_{T^0_m}\right)$.

C. RELATION OF THE ABOVE CONSIDERATIONS TO OZONE PRODUCTION

The preceding discussion of the issue of relative hydrocarbon reactivity has shown that indices directly related to ozone production are inadequate for reactivity assessment. The production of ozone entered only indirectly through its relation to T_m. In the following discussion, this relationship is explored in greater detail. As a prefacing note, the distinction between individual hydrocarbon reactivity (at a fixed NO_x concentration) and hydrocarbon-NO_x system reactivity (with both hydrocarbon and NO_x being variable) should be emphasized. From a control strategist's point of view, this distinction is between emissions composition and total emissions. For the former, which was the topic of the previous section, net ozone production is not a sufficient characterization, whereas for the latter, ozone production (as shown below) is a distinct characteristic.

1. Ozone Isopleths

Isopleths relating the concentration of O_3 and the time of the NO_2 peak, T_m, to initial hydrocarbon and NO concentrations at various reaction times are shown in Figures 61 through 66.* These figures are based on the same computer output used to generate the isopleths contained in the final report for the first contract year (Hecht et al., 1973). The initial conditions were as follows:

- $[HC]_0$ = 75 percent n-C_4H_{10} and 25 percent C_3H_6
- $[NO]_0$ = as stated on each figure
- $[NO_2]_0 = 0.1\ [NO_x]_0$
- $k_1 = 0.35\ min^{-1}$.

As might be expected from the derivation in the preceding section of this report, the lines of constant T_m (Figure 66) are nearly straight, and their slope increases as T_m decreases.

---

* The dashed portions of these figures have been obtained by extrapolation.

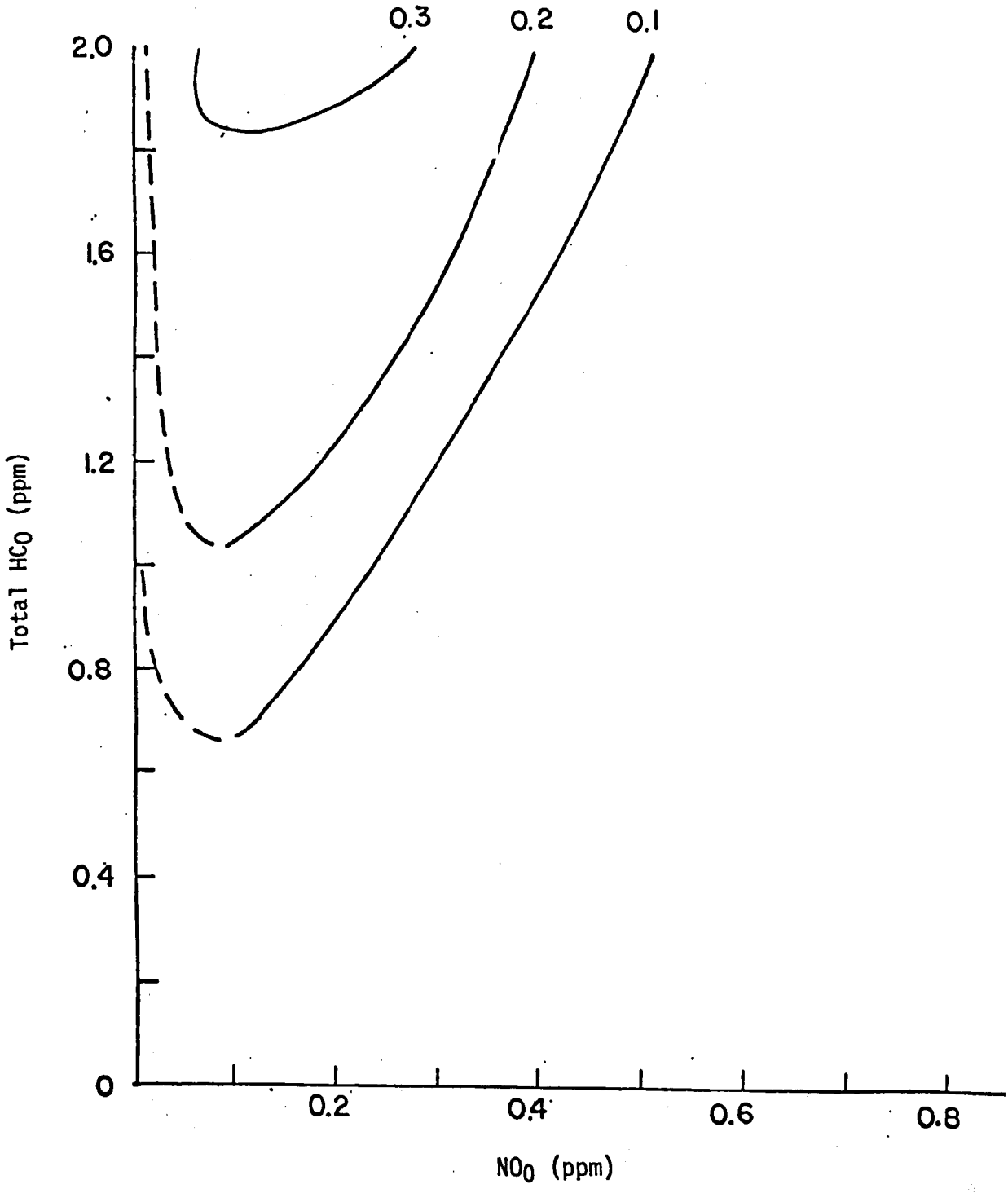

FIGURE 61. LINES OF CONSTANT O_3 (IN PPM) AFTER 1 HOUR OF SIMULATION

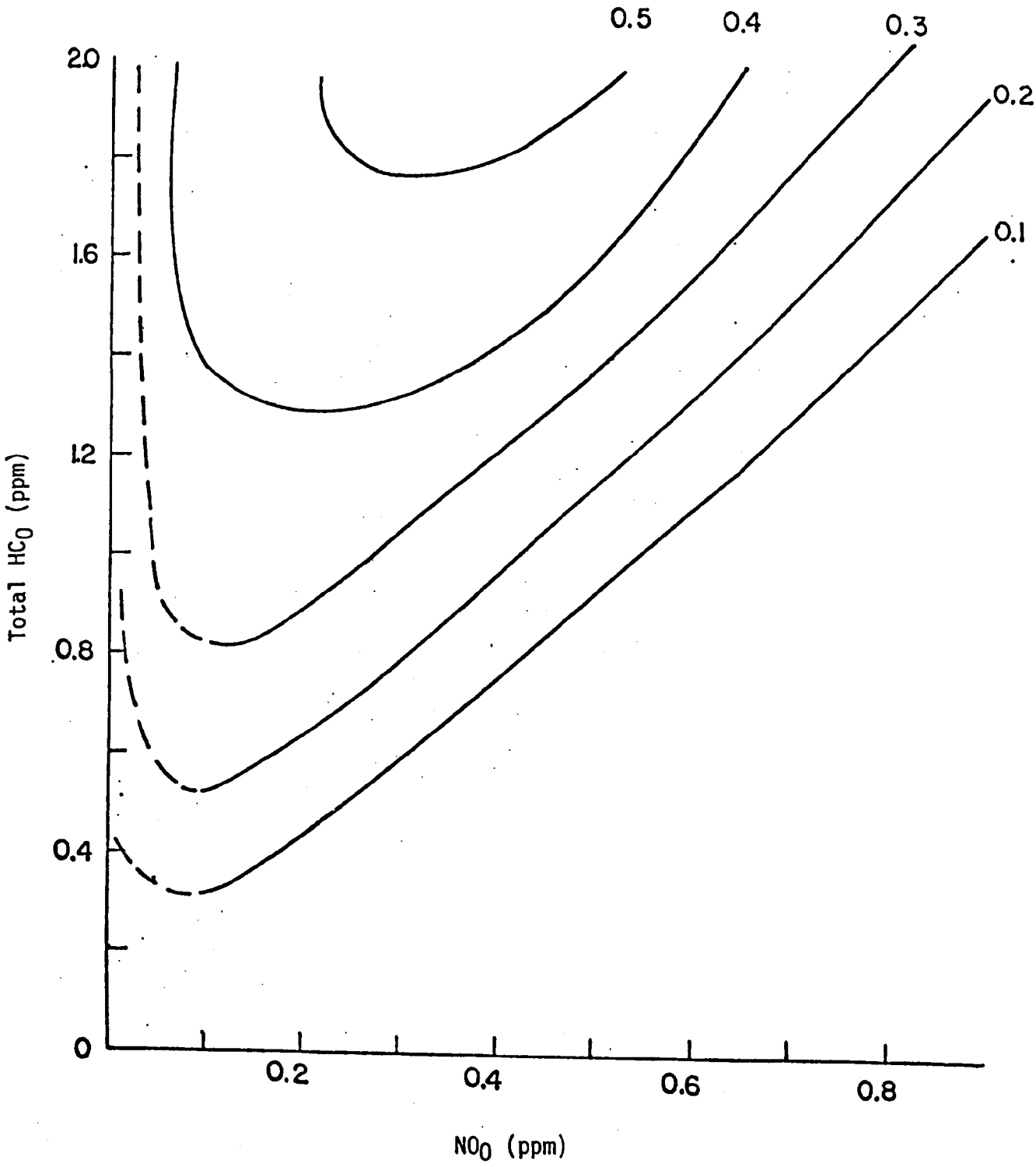

FIGURE 62. LINES OF CONSTANT O_3 (IN PPM) AFTER 2 HOURS OF SIMULATION

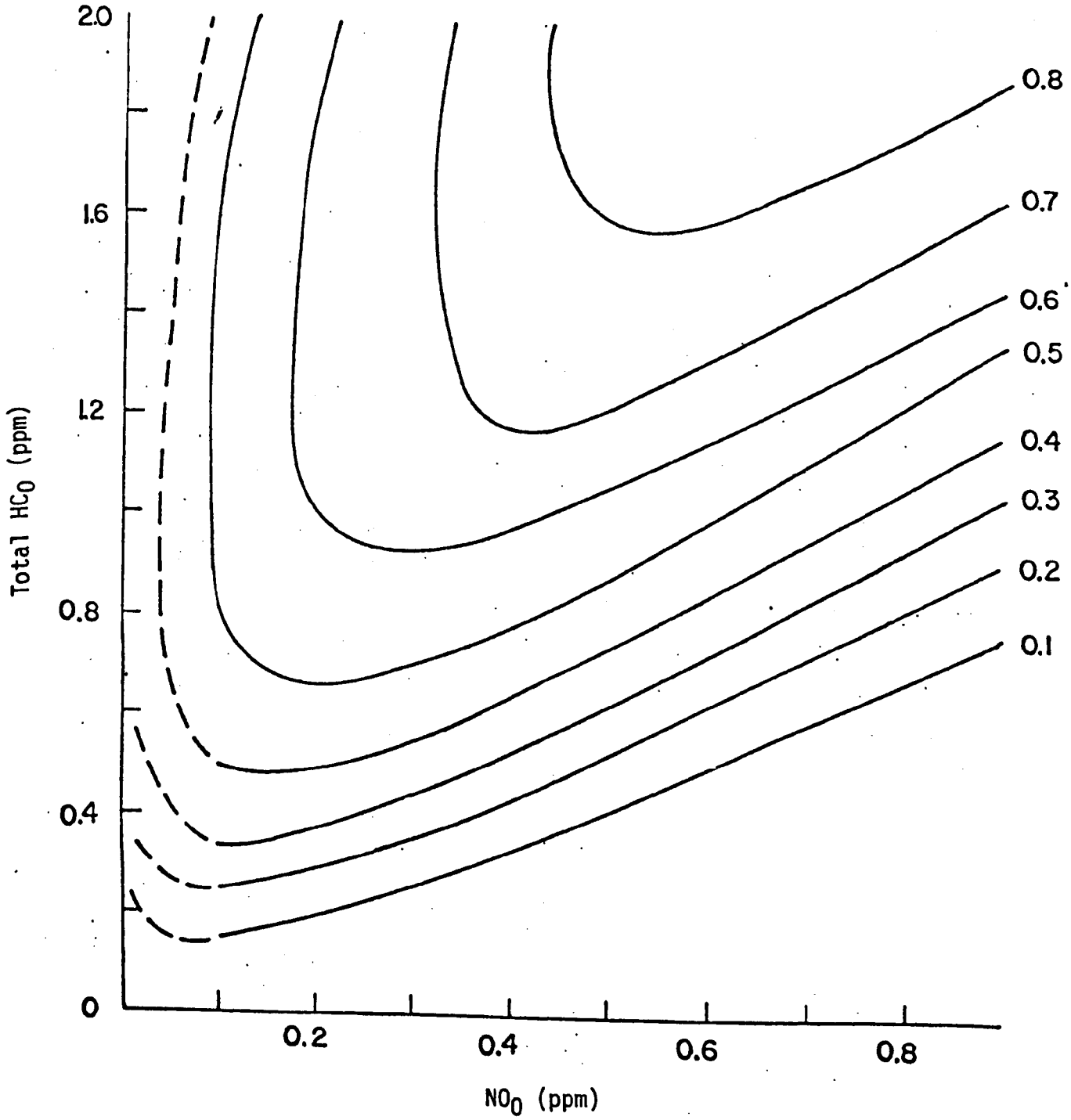

FIGURE 63. LINES OF CONSTANT O_3 (IN PPM) AFTER 5 HOURS OF SIMULATION

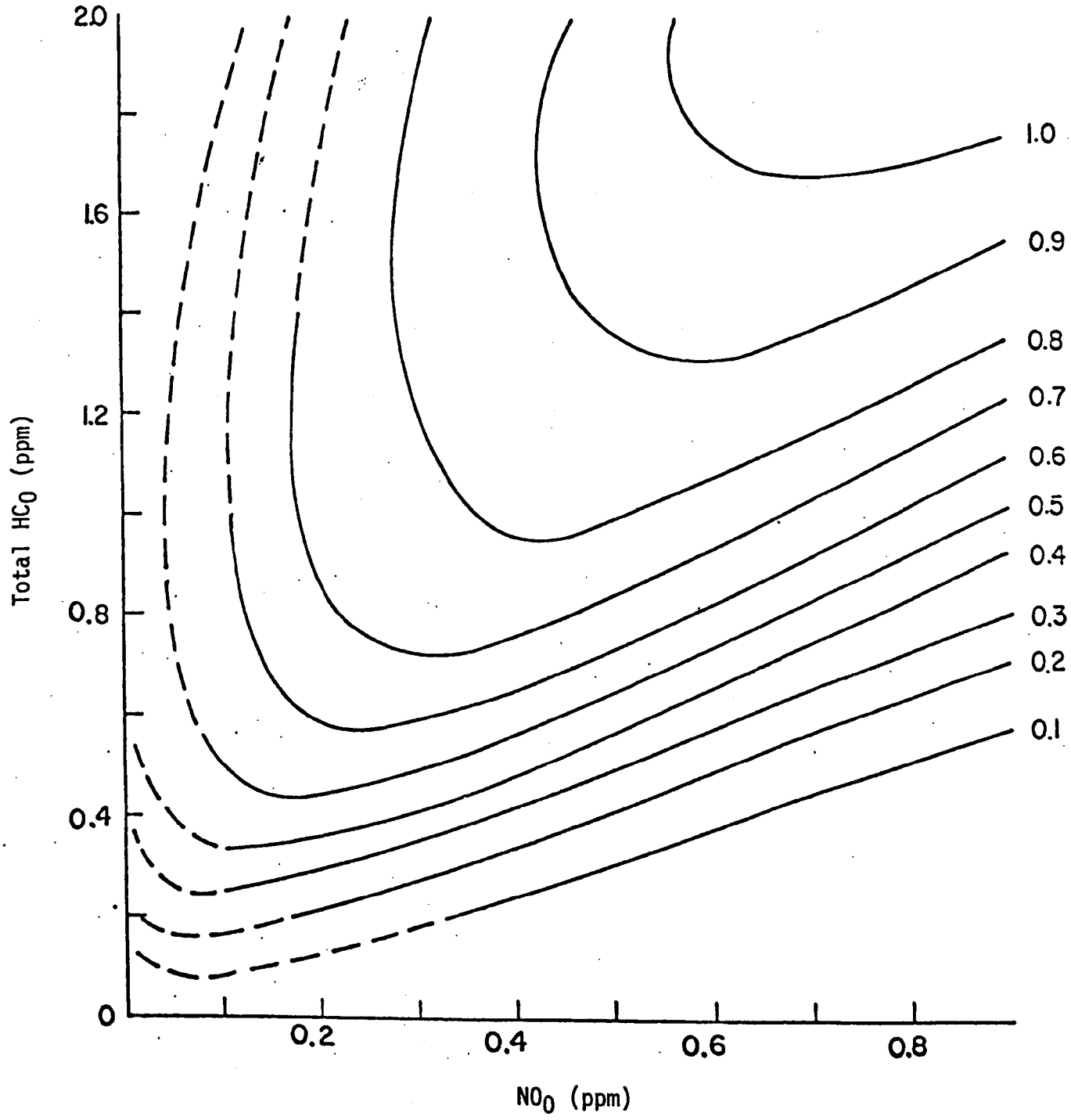

FIGURE 64. LINES OF CONSTANT O_3 (IN PPM) AFTER 8 HOURS OF SIMULATION

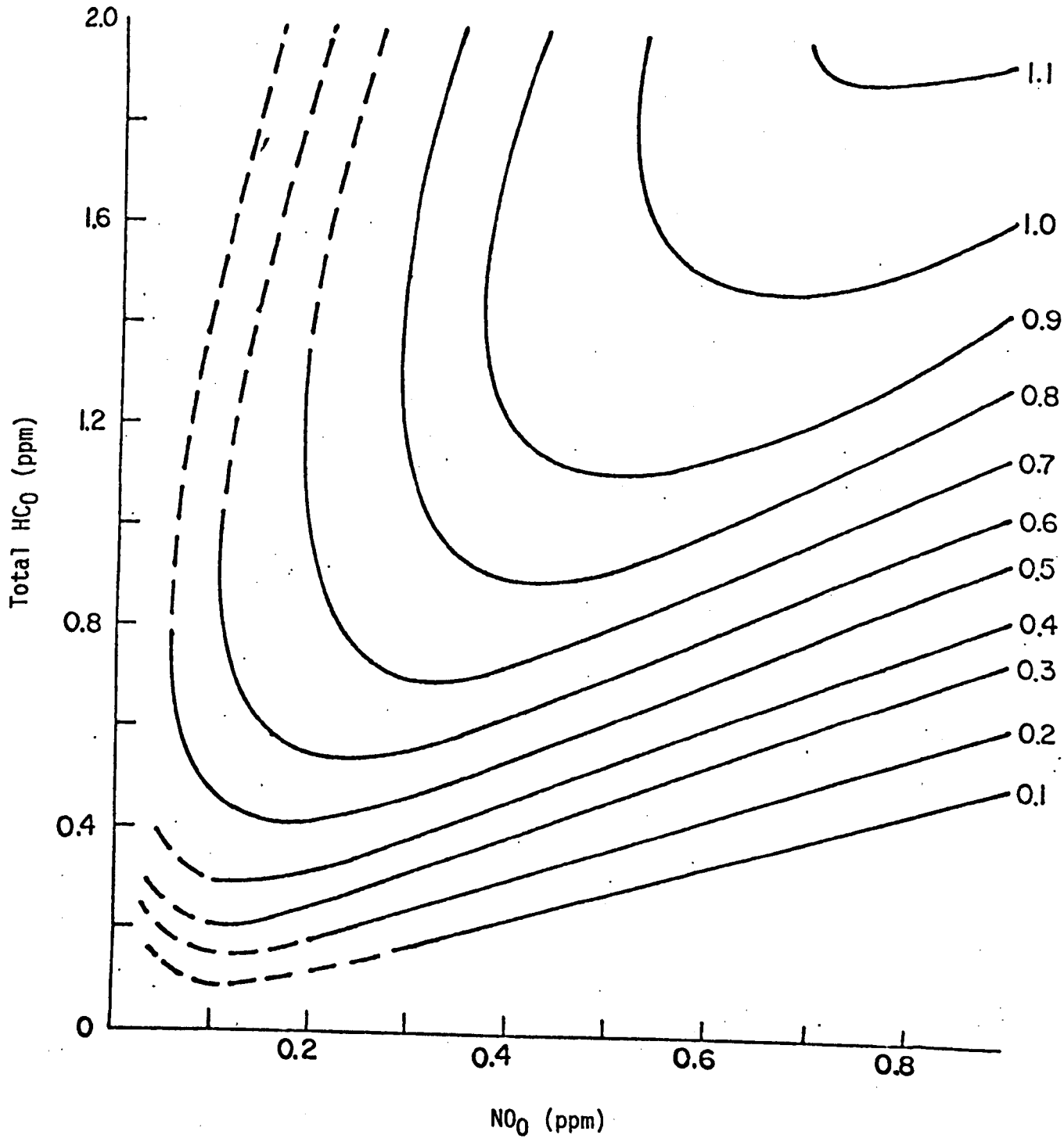

FIGURE 65. LINES OF CONSTANT O_3 (IN PPM) AFTER 9 HOURS OF SIMULATION

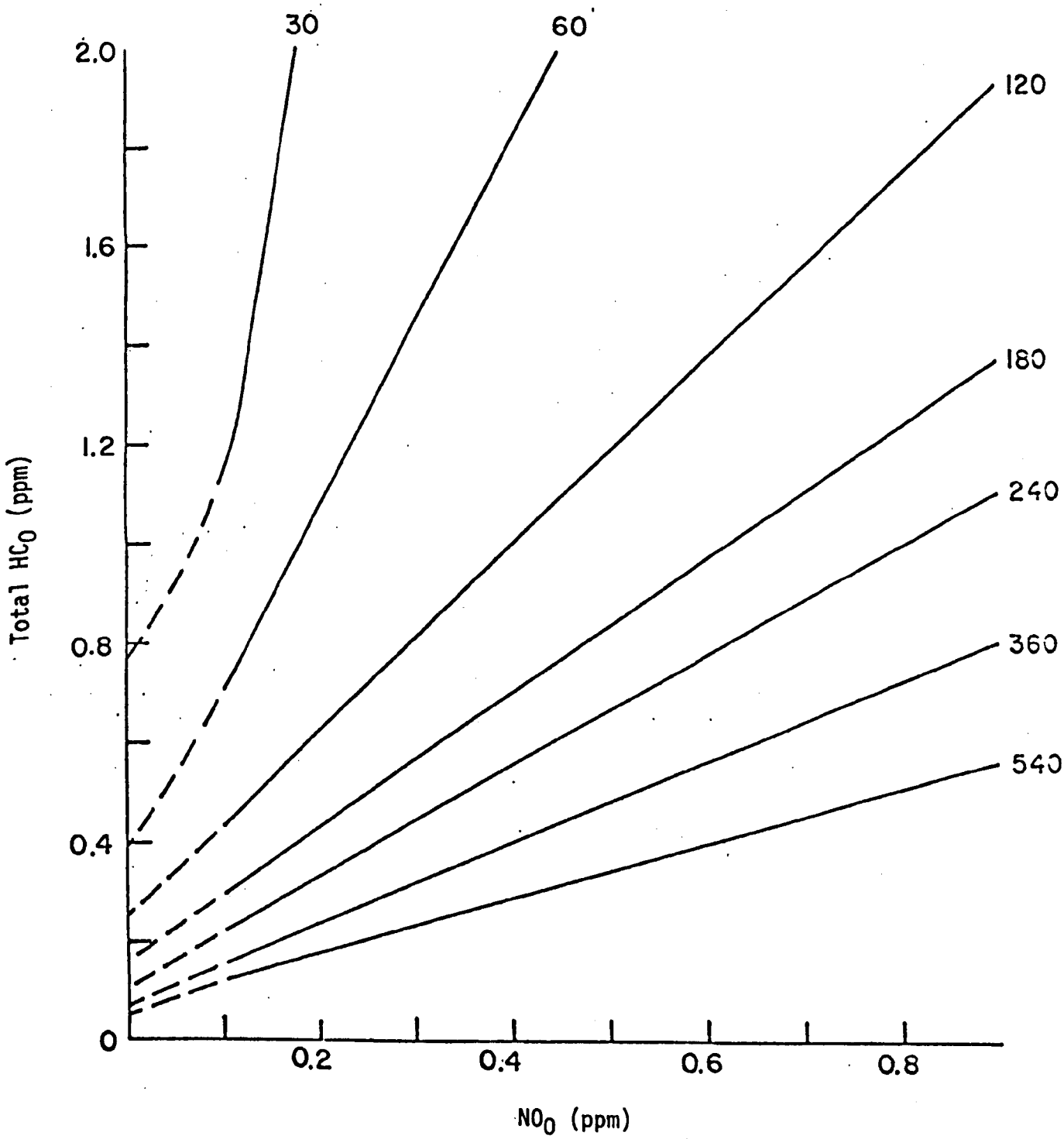

FIGURE 66. TIME OF THE NO_2 PEAK (IN MINUTES)

In Figures 61 through 65, there are two characteristic regions. A line drawn along the ridge line of the surface represented by the set of isopleths in each of these figures would divide these regions. In the region to the right of the ridge line, the isopleths are fairly straight, and the superimposition of Figure 66 would indicate that, especially at earlier times, they are nearly parallel to the lines of constant T_m. The line dividing the regions is also nearly a line of constant T_m. The region to the left is characterized by almost vertical isopleths, though in Figures 64 and 65 they curve back on themselves noticeably.

The features of these figures are not at all surprising; they simply reflect the characteristics of O_3-versus-time profiles observed in smog chambers (see, for example, the UCR profiles contained in this report). The empty space in the lower right-hand corner of Figures 61 through 65 (O_3 < 0.1 ppm) reflects the finite time that elapses before O_3 begins to build up. At T_m, O_3 begins to accumulate almost linearly with time--hence, the closely spaced isopleths that parallel lines of T_m = constant (Figure 66). Eventually, $[O_3]$ approaches an asymptotic level. Correspondingly, the spacing of isopleths widens, and they turn to the vertical. The reactions

$$NO_2 + O_3 \rightarrow NO_3 + O_2 \quad , \qquad (5)$$

$$NO_3 + NO_2 \rightleftharpoons N_2O_5 \quad , \qquad (7)$$

$$N_2O_5 + H_2O \rightarrow 2HNO_3 \quad , \qquad (9)$$

and

$$O_3 + HC \rightarrow \text{Products} \quad ,$$

along with photolysis and destruction on surfaces, cause O_3 depletion late in the reaction, resulting in the backward curvature of the isopleths.

2. Chemical Dynamics

These observations indicate that the characteristics of Figures 61 through 65 are prescribed by the chemical dynamics of smog formation. In the atmosphere, where chemistry interacts with the mechanical processes of dispersion and transport, a consideration of dynamics is essential to control strategy planning. For example, consider the upper region in the 8-hour isopleths (Figure 64). Figure 62 indicates that, at a fixed level of NO, a reduction in $[HC]_0$ would have very little effect on O_3 production. The results presented previously show that maximum O_3 levels (at fixed NO_x concentrations) are also almost independent of hydrocarbon reactivity (for a set of olefins). However, an examination of Figure 66 (and the data in Section B above) shows that a reduction in $[HC]_0$ (or HC reactivity) has a significant effect on increasing T_m. Thus, a reduction in $[HC]_0$ could slow down O_3 production, even though this decrease may have little effect on the expected net yield. In the atmosphere, where pollutants can be rapidly dispersed, the predicted maximum yield, based on simulations of smog chamber experiments, may never be realized. The peak O_3 level achieved is therefore closely related to the expected T_m.

From the preceding results, one can conclude that both HC and NO must be taken into account when attempting to select optimum O_3 abatement strategies. However, because of the complex interaction of mechanical and chemical processes in the atmosphere, it is difficult to extrapolate such results as those presented in this report directly to atmospheric emissions. To evaluate the effect of control strategies directly, one would need to imbed the kinetic mechanism in an airshed model that takes atmospheric conditions into consideration. In isolation, the kinetic mechanism can only provide "rules of thumb."

V CONCLUDING REMARKS

In closing, some mention should be made of the implications of our findings on air pollution modeling. First, we briefly summarize these findings.

Kinetic mechanisms for the chemical transformations occurring in irradiated propylene, butane, toluene-NO_x, and propylene-NO_x-SO_2 systems were postulated and used to simulate smog chamber data. Varying degrees of correspondence between predicted and observed profiles were obtained. In general, the propylene-NO_x and propylene-NO_x-SO_2 mechanisms were the most successful. For the most part, their predictions of propylene, O_3, NO, NO_2, and SO_2 were reasonably good. Although the accuracy was not very good, the propylene mechanisms were still able to follow the behavior of each species. The butane mechanism predicted too rapid NO oxidation and the toluene mechanism predicted insufficient oxidation of toluene. Butane oxidation products containing structures of two or more carbon atoms were apparently produced in greater quantity than the mechanism indicated; the low carbon recoveries in the UCR butane runs support this conclusion. However, more kinetic and smog chamber data are needed before the toluene mechanism can be assessed and revised.

We demonstrated that uncertainty in the magnitude of surface reactions and light source spectrum decay, as well as other chamber effects, could account for a great deal of the discrepancy between data and theory, although erroneous rate constants and reaction mechanisms contributed also. Instrument error, a topic barely touched upon here, is another ever-present source of ambiguity.

Unlike purely gas-phase thermal reactions, surface and photolytic reactions are chamber-dependent; furthermore, for a given chamber they may vary from experiment to experiment. Their proper treatment would require a considerable and continuous effort toward chamber characterization. Thus, smog

chamber experiments, which are meant to clarify the kinetics by eliminating some of the complexities present in the atmosphere, have introduced their own problems, although they are not as complex as those in the atmosphere. We are not denying the value of smog chamber experiments; instead, we are emphasizing the intricacy of this analysis.

Upon being confronted with the important role chamber effects play in the laboratory, one cannot help wondering whether atmospheric counterparts exist, and if so, how to incorporate them into an airshed model. Heterogeneous (pseudo-gas-phase) rate constants are functions of surface-to-volume ratio, as well as the surface's catalytic efficiency, both of which are not known for the urban environment. Solar irradiation depends on the state of the upper atmosphere, as well as on meteorological conditions, and has a diurnal and seasonal periodic variation. Hopefully, parametric representation of the variability of the solar spectrum will make the characterization of the spectrum feasible. Clearly, the spectrum itself affects numerous reactions, and the variation of a single rate constant (such as k_1) cannot adequately account for the effects of spectrum variability.

The approach to modeling heterogeneous chemistry used in the present work was to represent local surface reactions as pseudo-gas-phase reactions. The pattern of NO_2 formation was shown to reflect the value assigned to rate constants for heterogeneous (HNO_x) chemistry. Capitalizing on this relationship, we determined heterogeneous rate constants by "tuning" to the NO_2 curve. When applying the mechanism to the atmosphere, one can take a similar approach. In the absence of requisite kinetic data, tuning to atmospheric NO_2 data may be possible. Assuming gas phase kinetics are accurately represented, this approach would provide a practical means of evaluating the heterogeneous reactions.

The mechanism's applied utility was demonstrated, in Chapter IV, in a study of hydrocarbon reactivity and ozone formation.* Thus, the kinetic mechanism can be a useful tool to investigators of photochemical air pollution, either in the explicit form or in the streamlined, generalized format.

* There the issue of chamber effects was avoided by presenting results on a relative basis.

REFERENCES

Altshuller, A. P., and J. Bufalini (1971), Environ. Sci. Technol., Vol. 5, p. 39.

Altshuller, A. P., and I. R. Cohen (1963), Int. J. Air Water Pollut., Vol. 7, p. 787.

Altshuller, A. P., S. L. Kopczynski, W. A. Lonneman, T. L. Becker, and D. L. Wilson (1968), Environ. Sci. Technol., Vol. 2, pp. 696-698.

Altshuller, A. P., S. L. Kopczynski, W. A. Lonneman, F. D. Sutterfield, and D. L. Wilson (1970), Environ. Sci. Technol., Vol. 4, pp. 44-49.

Atkinson, R. (1975), unpublished.

Atkinson, R., and J. N. Pitts, Jr. (1975), J. Phys. Chem., Vol. 79, pp. 295-298.

Badcock, C. C., H. W. Sidebotton, J. G. Calvert, G. W. Reinhardt, and E. K. Darmon (1971), J. Am. Chem. Soc., Vol. 93, pp. 3115=3121.

Batt, L., R. D. McCulloch, and R. T. Milne (1974), "Thermochemical and Kinetic Studies of Alkyl Nitrites (RONO)," Department of Chemistry, University of Meston Walk, Aberdeen, Scotland.

Becker, K. H., V. Schurath, and H. Seitz (1974), Int. J. Chem. Kinet., Vol. 6, pp. 725-739.

Benson, S. W. (1968), Thermochemical Kinetics (John Wiley & Sons, New York).

Bufalini, M. (1971), Environ. Sci. Technol., Vol. 8, pp. 685-700.

Burton, S. (1974), private communication.

Calvert, J. G., and R. D. McQuigg (1975), Int. J. Chem. Kinet., to be published.

Calvert, J. G., and J. N. Pitts, Jr. (1967), Photochemistry (John Wiley & Sons, New York).

Castleman, A. W., Jr., R. E. Davis, H. R. Munkelwitz, I. N. Tang, and W. P. Wood (1974), "Abstracts of Symp. on Chem. Data for the Lower and Upper Atmos.," Warrenton, Virginia.

Chung, K., J. G. Calvert, and J. W. Bottenheim (1975), Int. J. Chem. Kinet., Vol. 7, pp. 161-182.

Cox, R. A. (1972), J. Phys. Chem., Vol. 76, p. 814.

_____ (1972), J. photo. Chem., Vol. 3, pp. 291-304.

Cox, R. A., and S. A. Penkett (1972), J. Chem. Soc., Faraday Trans. I, Vol. 68, pp. 1736-1753.

Darnell, K. (1974), private communication.

Davis, D. D. (1974), "Absolute Rate Constants for Elementary Reactions of Atmospheric Importance: Results from the University of Maryland's Gas Kinetics Laboratory," Chemistry Department, University of Maryland, College Park, Maryland.

Davis, D. D., W. Bollinger, and S. Fischer (1975), J. Phys. Chem., Vol. 79, pp. 293-294.

Davis, D. P., G. Smith, and G. Klauber (1974), Science, Vol. 179, p. 280.

Demerjian, K. L., A. J. Kerr, and J. G. Calvert (1974a), "The Mechanism of Photochemical Smog Formation," in Advances in Environmental Science Technology, J. N. Pitts and R. L. Metcalf, eds., John Wiley & Sons, New York.

Demerjian, K. L., J. G. Calvert, and D. L. Thorsell (1974b), Int. J. Chem. Kinet., Vol. 6, pp. 829-848.

Dimitriades, B. (1973), draft for EPA policy paper.

_____ (1972), Environ. Sci. Technol., Vol. 6, p. 253.

Demitriades, B., B. H. Eccleston, and R. W. Hurn (1970), J. Air Pollut. Contr. Assoc., Vol. 20, p. 150.

Dimitriades, B., and T. C. Wesson (1972), J. Air Pollut. Contr. Assoc., Vol. 22, p. 33.

Domalski, E. S. (1971), Environ. Sci. Technol., Vol. 5, pp. 443-444.

Doyle, G. T., A. C. Lloyd, K. R. Darnall, A. M. Winer, and J. N. Pitts, Jr. (1975), Environ. Sci. Technol., Vol. 3, pp. 237-241.

Feldstein, M. (1974), J. Air Pollut. Contr. Assoc., Vol. 24, p. 469.

Filby, W. G., and H. D. Penzhorn (1974), "Kinetics of the Photoreaction of SO_2 with Alkanes--The Diversion of Intermediate Radicals by Oxygen," in "Abstracts of Symposium on Chemical Data for the Lower and Upper Atmosphere," Warrenton, Virginia.

Finlayson, B. J., J. N. Pitts, Jr., and R. Atkinson (1974), Contribution #IGPP-UCR-74-3, from Department of Chemistry and Statewide Air Pollution Research Center, University of California, Riverside, California.

Garvin, D., and R. F. Hampson (1974), "Chemical Kinetics Data Survey VII: Tables of Rate and Photochemical Data for Modeling of the Stratosphere," NBSIR 74-430, National Bureau of Standards, Washington, D. C.

Gitchell, A., R. Simonaitis, and J. Heicklen (1974), JAPCA, Vol. 24, pp. 357-361.

Glasson, W., and C. Tuesday (1970), Environ. Sci. Technol., Vol. 4, p. 916.

_____ (1971), Environ. Sci. Technol., Vol. 5, p. 155.

Hecht, T. A., and J. H. Seinfeld (1972), Environ. Sci. Technol., Vol. 6, p. 47.

Hecht, T. A., P. M. Roth, and J. H. Seinfeld (1973), "Mathematical Simulation of Atmospheric Photochemical Reactions," Report R73-28, Systems Applications, Incorporated, San Rafael, California.

Hecht, T. A., M. K. Liu, and D. C. Whitney (1974a), "Mathematical Simulation of Smog Chamber Photochemical Experiments," Report R74-9, Systems Applications, Incorporated, San Rafael, California.

Hecht, T. A., J. H. Seinfeld, and M. C. Dodge (1974b), Environ. Sci. Technol., Vol. 8, p. 327.

Hefter, J. H., T. A. Hecht, and G. S. Hammond (1972), J. Am. Chem. Soc., Vol. 94, pp. 2793-2797.

Heuss, J. M., and W. A. Glasson (1968), Environ. Sci. Technol., Vol. 2, pp. 1109-1116.

Jaffee, S., and H. W. Ford (1967), J. Phys. Chem., Vol. 71, p. 1832.

Jaffee, R. J., and F. C. Smith, Jr. (1974), Presentation at 67th Annual Meeting of the Air Pollution Control Association, Denver, Colorado.

Johnston, H. S., and R. Graham (1974), Canad. J. Chem., Vol. 52, pp. 1415-1423.

Johnston, H. S., J. N. Pitts, Jr., J. Lewis, L. Bufonte, and T. Mottershead (1970), "Project Clean Air," University of California Task Force Assignments, Vol. 4.

Jones, G.R.H., and R. J. Cvetanovic (1961), Canad. J. Chem., Vol. 39, pp. 2444-2451.

Kopczynski, S. L., A. P. Altshuller, and F. D. Sutterfield (1974), Environ. Sci. Technol., Vol. 8, pp. 909-918.

Leighton, P. A. (1961), Photochemistry of Air Pollution (Academic Press, New York).

Liu, M. K. (1974), private communication.

Mabely, W. R., and A. G. Hendry (1974), Stanford Research Institute, Menlo Park, California.

Mendenhall, G. D., D. W. Golden, and S. W. Benson (1974), "The Very Low-Pressure Pyrolysis (VLPP) of n-Propyl Nitrite, tert-Butyl Nitrite and Methyl Nitrite--Rate Constants for Some Alkoxy Radical Reactions," Department of Thermochemistry and Chemical Kinetics, Stanford Research Institute, Menlo Park, California.

Miller, D. F. (1975), private communication.

Morris, E. D., Jr., and H. Niki (1971), J. Phys. Chem., Vol. 75, pp. 3640-3641.

_____ (1973), J. Phys. Chem., Vol. 77, pp. 1929-1932.

Morris, E. D., Jr., D. H. Stedman, and H. Niki (1971), J. Am. Chem. Soc., Vol. 93, pp. 3570-3572.

Morrison, R. T., and R. N. Boyd (1971), Organic Chemistry, Second Edition (Allyn and Bacon, Incorporated, Boston, Massachusetts).

MSA Research Corporation (1972), "Hydrocarbon Pollutant Systems Study," Vol. I, EPA Contract EHSD 71-72.

Mulcahy, M.F.R., J. R. Stephen, and J. C. Ward (1967), J. Phys. Chem., Vol. 71, pp. 2124-2131.

Niki, H., E. E. Daby, and B. Weinstock (1972), "Photochemical Smog and Ozone Reactions," American Chemical Society, Washington, D. C.

Noeh, S., B. H. Nordstrom, and H. S. Johnson (1974), "Kinetic Study of the Gas-Phase Formation of Nitrous Acid,", Department of Chemistry, University of California, Berkeley, California.

O'Brien, R. J. (1974), Environ. Sci. Technol., Vol. 8, p. 579.

O'Neal, H. E., and C. Blumstein (1973), Int. J. Chem. Kinet., Vol. 5, pp. 397-413.

Reynolds, S. D., M. K. Liu, T. A. Hecht, P. M. Roth, and J. H. Seinfeld (1974), Atmos. Environ., Vol. 8, pp. 563-596.

Schuck, E. A., E. R. Stephens, M. A. Price, and K. R. Darnall (1972), "Reaction of Peroxyacetyl Nitrate with Nitric Oxide," Statewide Air Pollution Research Center, University of California at Riverside.

Schulten, H. R., and U. Schurath (1975), J. Phys. Chem., Vol. 79, pp. 51-57.

Seinfeld, J. H., T. A. Hecht, and P. M. Roth (1973), "Existing Needs in the Experimental and Observational Study of Atmospheric Chemical Reactions," GPA Report EPA-R4-73-031, Systems Applications, Incorporated, San Rafael, California.

Sidebottom, H. W., C. C. Badcock, J. G. Calvert, B. R. Rabe, and E. K. Damon (1971), J. Am. Chem. Soc., Vol. 93, pp. 3121-3128.

Sidebottom, H. W., C. C. Badcock, G. W. Jackson, J. G. Calvert, G. W. Reinhardt, and E. K. Damon (1972), Environ. Sci. Technol., Vol. 6, pp. 72-79.

Slagle, I. R., J. R. Gilbert, R. E. Grahm, and D. Gutman (1974), "Direct Identification of Reactive Channels in the Reactions of Hydroxyl Radicals with Allene, Propylene, and 2-Butene," Department of Chemistry, Illinois Institute of Technology, Chicago, Illinois.

Smith, J. P., and P. Urone (1974), Environ. Sci. Technol., Vol. 8, pp. 742-746.

Spicer, C. W., and D. F. Miller (1974), "Nitrogen Balance in Smog Chamber Studies," presented at the 67th Annual Meeting of the Air Pollution Control Association, Denver, Colorado.

Stedman. D. H., C. H. Wu, and H. Niki (1973), J. Phys. Chem., Vol. 77, pp. 2511-2514.

UCR Monthly Report No. 4 (1974), "A Systematic Investigation of Varibles in Photochemical Systems in Smog Chamber: An Experimental Basis for Modeling Photochemical Air Pollution, " Statewide Air Pollution Research Center, University of Calfornia, Riverside, California.

Wilson, W. E., Jr., and A. Levy (1969), "A Study of Sulfur Dioxide in Photochemical Smog II," 2nd Annual Progress Report to American Petroleum Institute, Project S-11.

_____ (1970), JAPCA, Vol. 20, pp. 385-390.

Winer, A. (1975), private communication.

Wu, C. H., and H. Niki (1975), Environ. Sci. Technol., Vol. 9, pp. 46-52

Yeung, C.K.K., and C. R. Phillips (1973), Atmos. Environ., Vol. 7, p. 551.

TECHNICAL REPORT DATA

(Please read Instructions on the reverse before completing)

1. REPORT NO.	2.	3. RECIPIENT'S ACCESSION NO.
EPA-650/4-75-026		

4. TITLE AND SUBTITLE
Mathematical Modeling of Simulated Photochemical Smog

5. REPORT DATE
June 1975

6. PERFORMING ORGANIZATION CODE

7. AUTHOR(S)
Paul A. Durbin, Thomas A. Hecht, and Gary Z. Whitten

8. PERFORMING ORGANIZATION REPORT NO.
EF75-62

9. PERFORMING ORGANIZATION NAME AND ADDRESS
Systems Applications, Inc.
950 Northgate Drive
San Rafael, CA 94903

10. PROGRAM ELEMENT NO.
1A1008

11. CONTRACT/GRANT NO.
68-02-0580

12. SPONSORING AGENCY NAME AND ADDRESS
U. S. EPA
Office of Research And Development
National Environmental Research Center
Research Triangle Park, N. C. 27711

13. TYPE OF REPORT AND PERIOD COVERED
Final (June '74 - June '75)

14. SPONSORING AGENCY CODE

15. SUPPLEMENTARY NOTES

16. ABSTRACT

The continued development and testing of a kinetic mechanism for photochemical smog formation is described. Detailed mechanisms containing the individual chemical reactions occurring in irradiated propylene, n-butane, toluene-NO_x, and propylene-NO_x-SO_2 systems were postulated and used to simulate smog chamber data. A theoretical evaluation was made of the contribution of such chamber effects as light source spectrum decay and surface reactions to the reactivity of the chamber mixture. The application of kinetic simulation to a study of hydrocarbon reactivity and ozone production in smog systems is also discussed.

17. KEY WORDS AND DOCUMENT ANALYSIS

a. DESCRIPTORS	b. IDENTIFIERS/OPEN ENDED TERMS	c. COSATI Field/Group
Photochemical Modeling Chemical Kinetics Atmospheric Chemistry		

18. DISTRIBUTION STATEMENT	19. SECURITY CLASS *(This Report)*	21. NO. OF PAGES
Unlimited	Unclassified	160
	20. SECURITY CLASS *(This page)*	22. PRICE
	Unclassified	

EPA Form 2220-1 (9-73)